

Manyfield Inflation in Random Potentials

Theodor Bjorkmo and M.C. David Marsh

Department of Applied Mathematics and Theoretical Physics, University of Cambridge
Wilberforce Road, Cambridge, UK

E-mail: t.bjorkmo@damtp.cam.ac.uk, m.c.d.marsh@damtp.cam.ac.uk

Abstract. We construct models of inflation with many randomly interacting fields and use these to study the generation of cosmological observables. We model the potentials as multi-dimensional Gaussian random fields (GRFs) and identify powerful algebraic simplifications that, for the first time, make it possible to access the manyfield limit of inflation in GRF potentials. Focussing on small-field, slow-roll, approximate saddle-point inflation in potentials with structure on sub-Planckian scales, we construct explicit examples involving up to 100 fields and generate statistical ensembles comprising of 164,000 models involving 5 to 50 fields. For the subset of these that support at least sixty e-folds of inflation, we use the ‘transport method’ and δN formalism to determine the predictions for cosmological observables at the end of inflation, including the power spectrum and the local non-Gaussianities of the primordial perturbations. We find three key results: i) Planck compatibility is not rare, but future experiments may rule out this class of models; ii) In the manyfield limit, the predictions from these models agree well with, but are sharper than, previous results derived using potentials constructed through non-equilibrium Random Matrix Theory; iii) Despite substantial multi-field effects, non-Gaussianities are typically very small: $f_{\text{NL}}^{\text{loc}} \ll 1$. We conclude that many of the ‘generic predictions’ of single-field inflation can be emergent features of complex inflation models.

Contents

1	Introduction	2
2	Gaussian random fields for inflation	5
2.1	High-dimensional GRFs as random multifield scalar potentials	5
2.2	A new, efficient, local construction of GRFs	8
2.3	Physical properties of GRF potentials	10
2.3.1	Distributions of the parameters of the potential	10
2.3.2	GRF potentials and physical effective field theories	14
2.4	The statistical ensembles of models	16
2.5	Method: background	17
2.6	Method: perturbations	18
3	Result I: Planck compatibility is not rare, but future experiments may rule out this class of models	21
3.1	Background evolution in GRF inflation	21
3.1.1	The ‘straying’ smallest mass-squared	22
3.2	Smooth and simple power spectra from complex inflationary models	23
3.3	Distributions of n_s and α_s	25
3.4	Substantial superhorizon evolution, but also decaying isocurvature	29
4	Result II: At large N_f, GRF and RMT models largely agree	32
4.1	Comparison of DBM and GRF potentials	33
4.2	Comparison of DBM and GRF predictions	34
5	Result III: $f_{\text{NL}} \sim \mathcal{O}(1)$ is very rare in manyfield inflation	37
5.1	Why so small?	39
6	Conclusions	41
A	Formulae for the covariance matrices	44
B	Numerical method	45
C	Ensembles of models	46
D	A single-field toy model	47
E	The DBM construction of random manyfield potentials	49
F	Case studies and a modified GRF potential	51
F.1	A 100-field model	52
F.2	A 25-field model giving large non-Gaussianity	52
F.3	Manyfield inflation in uplifted potentials	52

1 Introduction

Inflation provides a rather simple explanation of the origin of the primordial density perturbations and successfully resolves the flatness and homogeneity problems of the standard hot big bang cosmology. However, little is known about the microscopic origin of inflation and, in particular, what degrees of freedom it involved. Inflation may have probed energies far above those accessible by terrestrial experiments, and is sensitive to physics beyond the Standard Model of particle physics. Models of inflation with only a single additional scalar field can be compatible with all current observations, but so may models with multiple fields. Additional scalar fields are common in extensions of the Standard Model that address the gauge hierarchy problem, and ubiquitous in ultraviolet completions realised in string theory. Determining the field content relevant in the early universe is a fundamental challenge of modern cosmology.

Primordial non-Gaussianity of the local type has been proposed as a key observable to observationally distinguish between multifield and single-field models of inflation. In single-field inflation, the levels of local non-Gaussianity can be related to the deviation from scale invariance of the primordial power spectrum [1, 2],¹ which is very small [5]. Multiple-field effects can significantly enhance the levels of non-Gaussianity, and amplitudes of the order of $f_{\text{NL}} \sim 1$ are realised in some models.² Current constraints from Planck observations of the Cosmic Microwave Background give $f_{\text{NL}} = 0.8 \pm 5.0$ (68% c.l.) [6], and future surveys of the Large-Scale Structure of the universe are expected to reach a sensitivity of $\sigma(f_{\text{NL}}) \sim \mathcal{O}(1)$ [7–13], probing some subset of models of multiple-field inflation. It is now pressing to assess what we realistically can hope to learn about fundamental physics from these experiments.

The conditions under which large non-Gaussianity is generated during and after inflation have been studied before by many authors (for a review, see [14]). However, direct investigations tend to be hampered by the computational complexity of multi-field systems, and most studies have been restricted to models with two or a few fields, or models with greatly restricting symmetry structures [15–21]. For a more complete understanding of multifield inflation, it is necessary to go beyond these simplifying assumptions, and allow both for more fields and for non-trivial interactions. This is crucial for understanding what models of inflation can be ruled out if f_{NL} is constrained to be less than one, or what types of inflationary models are favoured if f_{NL} of order one is measured. Addressing this question is one of the main aims of this paper.

Multifield inflation models with generic interactions between the fields have large numbers of free parameters. In a low-energy effective theory for N_f fields valid below the cut-off scale Λ , these are the Wilson coefficients, $c_{a_1 \dots a_n}$, of all operators that may be important during inflation, e.g.

$$V(\phi_1, \dots, \phi_{N_f}) = \Lambda^4 \sum_{n=0}^{n_{\text{max}}} c_{a_1 \dots a_n} \frac{\phi^{a_1}}{\Lambda} \dots \frac{\phi^{a_n}}{\Lambda}. \quad (1.1)$$

Unfortunately, the relevant values (or distribution of values) of these parameters are not known from fundamental physics. One approach, pursued here, is then to search for properties that are rather insensitive to the details of the parameter distribution, and that depend only on a few effective parameters. The widespread appearance of emergent universality in complex physical and mathematical systems suggests that such robustness may be found as the number

¹This rule applies under some assumptions, which can be violated in special models [3, 4].

²In this paper, we focus on non-Gaussianities of the local type, and denote $f_{\text{NL}}^{\text{loc}} = f_{\text{NL}}$ without superscript.

of fields, N_f , becomes large [22–25]. Motivated by this, we pursue a statistical approach: we generate ensembles of multifield scalar potentials $V(\phi_1, \dots, \phi_{N_f})$ randomly, and determine the distribution of observables as $N_f \gg 1$.

To access the interesting regime of multiple light fields with non-trivial interactions, the potentials need to be mathematically simple enough to be computationally tractable. One such class of potentials, recently studied in [26–32], can be constructed using non-equilibrium random matrix theory techniques. According to the prescription of [26], the computational difficulties of multifield inflation can be substantially mitigated by realising $V(\phi_1, \dots, \phi_{N_f})$ only locally along the field trajectory (while being undetermined elsewhere in field space), and by postulating that the Hessian matrix evolves according to Dyson Brownian motion (DBM) along the inflationary path. The local Taylor coefficients to quadratic order, defined patch-wise along the path, evolve non-trivially during inflation and implicitly capture the effects of higher-order interaction terms. This method remains computationally efficient up to very large N_f , making it possible to determine the observational predictions³ in models of inflation with up to a hundred interacting fields [27, 28]. In reference [27], it was shown that the predictions of these ‘DBM models’ become simpler and sharper as the number of fields is increases, and very complicated models with many fields are commonly compatible with Planck constraints on the primordial power spectrum [28].

However, the random matrix theory method of [26] is not suitable to investigate the generation of primordial non-Gaussianities during inflation: the Brownian motion of the eigenvalues of the Hessian matrix is continuous but not differentiable, and the third derivatives of the potential, required for the computation of the three-point correlation function, are not well-defined in the continuum limit.⁴

Manyfield inflation from Gaussian random fields

An alternative approach is to generate random multifield potentials using Gaussian random fields (GRFs). This first was done in [33, 34] by expanding $V(\phi_1, \dots, \phi_{N_f})$ in a set of Fourier modes for potentials with $N_f \leq 6$ and $\Lambda > M_{\text{Pl}}$ (see also [35] for $N_f = 1$). However, the interesting regime of multiple-field inflation in potentials with structure on sub-Planckian distances in field space remained intractable.

To access the regime with $\Lambda < M_{\text{Pl}}$, reference [36] proposed to generate the potential only locally in field space, e.g. by gluing together multiple patches along a path in field space, or by generating the Taylor coefficients of the potential to a sufficiently high order at a single point. These models have well-defined higher derivatives and are arguably simpler than the DBM potentials, but a significant limitation arises from the need to explicitly specify a very large number of Taylor coefficients, which are not statistically independent. For example, a model with $N_f = 100$ fields and the potential expanded up to fifth order around a single point involves 96,560,546 independent Taylor coefficients. The probability distribution of these coefficients involves the inverse covariance matrix which has 4.7×10^{15} independent, and in general non-vanishing, elements. Naively generating such a matrix numerically is computationally prohibitive, making explicit studies impractical or impossible.

³This method is limited to observables that can be inferred from information about the potential up to second order in derivatives as expanded around any point along the field trajectory. As we will review in section 2.6, this includes quantities computed from the two-field correlators such as the primordial power spectrum, including its spectral index and its running.

⁴This obstacle may be overcome by regularisation, or by modifying the rules governing the stochastic evolution (cf. [29] for one suggestion).

In this paper, we, for the first time, overcome these obstacles and generate multifield GRFs to explicitly study the manyfield limit of inflation in general potentials. We construct models with up to 100 fields by generating the potential locally around an ‘approximate saddle-point’ up to fifth order in the fields, and we use an adaption of the ‘transport method’ [37–40] to compute cosmological observables from the two-field and three-field correlation functions. To make this possible, we identify drastic algebraic simplifications for GRFs with a Gaussian covariance function, and we use these to obviate the need for extremely heavy numerics. This key advance allows us to study the generation of local non-Gaussianities in random manyfield models of inflation, and assess what levels of f_{NL} are generated.

There are three particularly important results in this paper:

1. Planck compatible power spectra are not rare for these models: even for highly complicated manyfield models with millions of non-vanishing interaction terms, the spectral index commonly falls within the observationally allowed range. Interestingly, these models make a sharp statistical prediction for the running of the spectral index, $\alpha_s = dn_s/d \ln k$, which can be ruled out by future experiments.
2. At large N_f , the observational predictions of our GRF models agree well with, but are sharper than, recent predictions derived from DBM potentials. As these two constructions are fundamentally different and independent, this indicates the existence of a ‘universality class’ of large- N_f models for which the observables are largely insensitive to the details of the underlying potential.
3. The amplitude of local non-Gaussianities is typically very small, $|f_{\text{NL}}| \ll 1$. Even when the power spectrum undergoes significant superhorizon evolution, indicative of multifield effects being important, f_{NL} is typically highly suppressed, and even approximately follows the single-field consistency relation: $f_{\text{NL}} = \frac{5}{12}(n_s - 1)$. Moreover, in the rare cases where $f_{\text{NL}} \sim \mathcal{O}(1)$, isocurvature modes remain unsuppressed at the end of inflation, and a detailed modelling of the reheating dynamics is required to extract reliable predictions. We conclude that constraining f_{NL} to be smaller than order unity would not rule out manyfield inflation, but a measurement of a large value for f_{NL} would point to rather special inflationary dynamics.

We expect that the predictions of this class of models may extend also to other constructions of small-field, slow-roll models of approximate saddle-point inflation. However, distinct classes of multifield models (such as large-field models, or models with sharp features in the potential) may well lead to different predictions for some observables.

This paper is organised as follows: in section 2, we review how GRFs can be used as models for multifield inflationary potentials, and we illustrate the key simplifications that allow us to access the manyfield regime. We furthermore discuss the natural energy scales intrinsic to GRF potentials, their possible interpretation as physical effective field theory potentials, and we critically discuss the tuning required to use these potentials to study multifield inflation. We finally present the ensembles of potentials that we study explicitly, and our method for computing cosmological observables. In sections 3–5 we discuss the three main results of this paper. We conclude and discuss further directions in section 6. A number of additional details, including illustrative case studies, can be found in the appendices.

Throughout this paper we set the reduced Planck mass to one, $M_{\text{Pl}} = 2.4 \times 10^{18} \text{ GeV} = 1$, but we occasionally reinstate factors of M_{Pl} for clarity.

2 Gaussian random fields for inflation

In this section we explain how we use Gaussian random fields (GRFs) to study random multi-field inflation.⁵ The basic idea is to construct the potential locally in field-space as a truncated Taylor series with randomly generated coefficients. By going to sufficiently high order in the Taylor expansion, one can obtain a well-approximated potential in a domain containing the inflaton trajectory. This makes GRFs a powerful tool for studying the observational signatures of generic large- N_f inflation models.

We begin by briefly reviewing the statistical properties of Gaussian random fields and how the probability distribution function (PDF) for the Taylor coefficients is obtained. This PDF involves the inverse of the covariance matrix and is unfortunately of very limited practical use when N_f is large. However, we find that for a Gaussian covariance function for the random field, there is a drastic simplification which allows us to generate explicit potentials even when $N_f \gg 1$.

We go on to present the class of random inflation models discussed in this paper. Specifically, we discuss the relevant mass-scales of the potentials, and how the GRFs under certain conditions admit an interpretation as proxies for physical effective field theories (EFTs). However, we also point out a challenge for using GRFs to study multifield inflation: the typical mass-splitting of the fields tend to exceed the Hubble parameter, leading to single-field dynamics. We then describe how we choose the initial conditions to generate large ensembles of potentials with multifield dynamics during inflation. We close this section by briefly explaining the methods used to calculate the background trajectory and the superhorizon evolution of the field perturbations.

2.1 High-dimensional GRFs as random multifield scalar potentials

A Gaussian random field has a mean value \bar{V} and a covariance function,

$$\langle (V(\phi_1) - \bar{V})(V(\phi_2) - \bar{V}) \rangle = C(\phi_1, \phi_2), \quad (2.1)$$

where the ϕ_i are position vectors in field space (with components ϕ_i^a), which we take to be flat \mathbb{R}^N . Furthermore, we take the GRF to be stationary and isotropic with mean zero⁶ so that,

$$C(\phi_1, \phi_2) = C(\phi_1 - \phi_2) = C(|\phi_1 - \phi_2|). \quad (2.2)$$

The covariances for the derivatives are given by the derivatives of the covariance function:

$$\left\langle \frac{\partial^{n_1} V(\phi_1)}{\partial \phi_1^{a_1} \dots \partial \phi_1^{a_{n_1}}} \frac{\partial^{n_2} V(\phi_2)}{\partial \phi_2^{b_1} \dots \partial \phi_2^{b_{n_2}}} \right\rangle = \frac{\partial^{n_1+n_2} C(\phi_1, \phi_2)}{\partial \phi_1^{a_1} \dots \partial \phi_1^{a_{n_1}} \partial \phi_2^{b_1} \dots \partial \phi_2^{b_{n_2}}}. \quad (2.3)$$

All non-vanishing elements have either n_1 and n_2 both odd, or both even. To simplify notation, we will from now on write derivatives as,

$$\frac{\partial^n V(\phi)}{\partial \phi_1^{a_1} \dots \partial \phi_1^{a_n}} \equiv V_{a_1 \dots a_n}(\phi). \quad (2.4)$$

⁵Previous work on inflation in random potentials include [33–35, 41–55]. References [56–58] studied the impact of randomness on particle production during inflation, and references [59–61] investigated random compactification effects in brane inflation in string theory.

⁶In the bulk of this paper, we focus exclusively on this simplest class of GRFs. However, in Appendix F we briefly discuss a modified GRF that includes a large field-independent cosmological constant, cf. $\bar{V} \gg 1$.

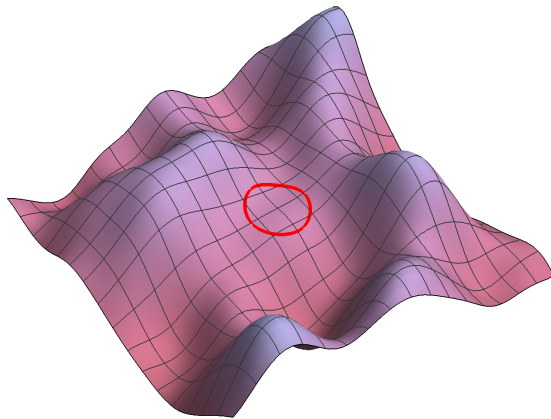


Figure 1: An example of a GRF potential with $N_f = 2$ and $n_{\max} = 175$. Here $\phi \in [-4\Lambda_h, 4\Lambda_h]^2$ and inflation is supported near $\phi = 0$. The red circle delineates the region in which a potential truncated at fifth order approximates the full potential to per cent level accuracy.

In this paper, we create random multifield potentials by generating Taylor coefficients at a single point in field space. The joint probability distribution of the Taylor coefficients is a multivariate normal distribution with a covariance matrix given by the derivatives of the covariance function at $\phi_1 = \phi_2$. Of course, not all the derivatives are independent, so we only generate the derivatives $V_{abc\dots}$ with indices ordered such that $a \geq b \geq c$ et cetera. This ensures that all the unique, independent derivatives are included exactly once. If we collectively denote the independent Taylor coefficients of the potential (which includes V , V_a , V_{ab} et cetera) by V_α , where α runs over all the ordered sets of indices for the derivatives we include, the multivariate probability distribution function is given by,

$$P(V_\alpha) = \frac{\exp\left(-\frac{1}{2}(V_\alpha - \mu_\alpha)(\Sigma^{-1})_{\alpha\beta}(V_\beta - \mu_\beta)\right)}{\sqrt{\det(2\pi\Sigma)}}, \quad (2.5)$$

where $\mu_\alpha = \langle V_\alpha \rangle$ is the expectation value vector and $\Sigma_{\alpha\beta} = \langle V_\alpha V_\beta \rangle$ is the covariance matrix.

Throughout this paper (and just as in [36]), we will be working with a Gaussian covariance function,

$$C(\phi_1, \phi_2) = \Lambda_v^8 e^{-(\phi_1 - \phi_2)^2 / 2\Lambda_h^2}. \quad (2.6)$$

Here Λ_v sets the ‘vertical energy scale’ of the potential and the ‘horizontal scale’, Λ_h , sets the correlation length of the potential. We are interested in studying models in which the potentials have structure on sub-Planckian scales, so we take $\Lambda_h < M_{\text{Pl}}$. In section 2.3.2, we will discuss the physical interpretation of Λ_v and Λ_h , and how potentials with the covariance function (2.6) may be regarded as proxies for Wilsonian effective field theories.

Schematically, our procedure for studying manyfield inflation in GRF potentials is as follows: we generate the potential locally in a domain of size Λ_h around $\phi = 0$,

$$V(\phi) = \sum_{n=0}^{n_{\max}} V_{a_1\dots a_n} \frac{1}{n!} \phi^{a_1} \dots \phi^{a_n} = \sum_{n=0}^{n_{\max}} \Lambda_v^4 \tilde{V}_{a_1\dots a_n} \frac{1}{n!} \frac{\phi^{a_1}}{\Lambda_h} \dots \frac{\phi^{a_n}}{\Lambda_h}, \quad (2.7)$$

up to some order n_{\max} . Throughout this paper we take $n_{\max} = 5$, unless otherwise specified. This ensures that the third derivatives of the potential, which are required to compute non-Gaussianities, are well-approximated and non-trivial within the domain.⁷

If all Taylor coefficients are chosen randomly according to the PDF of equation (2.5), the potential is typically much too steep to support inflation. However, by choosing a subset of the Taylor coefficients, V, V_{a_1} and $V_{a_1 a_2}$, by hand and generating the remaining coefficients through the corresponding conditional PDF, we can construct multifield scalar potentials that are suitable for slow-roll inflation around $\phi = 0$, but have the random structure of a Gaussian random field away from this point. For example, with $N_f = 100$ and $n_{\max} = 5$, we specify the $1 + 100 + 5,050 = 5,151$ first Taylor coefficients by hand, and generate the remaining 96,555,395 coefficients randomly by using the constrained PDF obtained from equation (2.5). We will refer to scalar potentials generated by this method as ‘GRF potentials’.⁸

As we will discuss in detail in section 2.4, we choose the parameters V, V_{a_1} and $V_{a_1 a_2}$ so that $\phi = 0$ is an approximately saddle-point of the potential with multiple fields with $m^2 \leq H^2$. The ‘horizontal scale’, Λ_h , and the number of fields, N_f , both have important effects on the generated model. Finally, Λ_v can be fixed from the normalisation of the primordial perturbations for each model. We will refer collectively to the set $(V, V_{a_1}, V_{a_1 a_2}, N_f, \Lambda_h)$ as the ‘hyperparameters’ of the GRF potentials.

For each of the potentials that we construct, we study how the fields evolve from the approximate saddle-point, assuming that the field initially ‘rolls’ slowly. Due to the randomness of the potentials, models with the same hyperparameters but different higher-order Taylor coefficients give rise to different inflationary trajectories, and consequently different numbers of e-folds of inflation. For models supporting at least 60 e-folds of inflation, we compute the evolution of the two-field and three-field correlation functions for the perturbations during inflation using the ‘transport method’ [37–40], and we evaluate the predictions for observables of the models at the end of inflation (for the two-point statistics, our approach is exactly that of [27]).

By generating large numbers of inflationary models for each fixed set of hyperparameters that we are interested in, we can study the statistical predictions for the generation of cosmological observables in manyfield models of inflation. In particular, we compute the power spectrum of the primordial curvature perturbation, and, upon finding that it is typically well-fitted by a power-law over the scales that are constrained by observations of the Cosmic Microwave Background (CMB), we compute the values of the spectral index n_s and its running $\alpha_s = dn_s/d \ln k$, and in addition, the tensor-to-scalar ratio, r . Furthermore, from the two-field correlators, we study the co-evolution of the isocurvature and curvature perturbations during inflation. Finally, using the standard δN formula [15, 16, 62–64] and the three-point function of the fields, we compute the local non-Gaussianity parameter $f_{\text{NL}} = f_{\text{NL}}^{\text{loc}}$.

We emphasise that we only study the generation of observables *during* the inflationary period, and we defer the study of the post-inflationary approach to the final vacuum and the reheating process to future studies.

⁷With the covariance function given in (2.6), the dimensionless coefficients \tilde{V}_α at order n have rms-values ranging between 1 (all indices different) and $\sqrt{(2n-1)!!}$ (all indices the same). Since these increase slower than $n!$, the Taylor series convergences as $n_{\max} \rightarrow \infty$. By going to high orders in the series, one can therefore construct a large potential landscape, cf. Figure 1. In this paper, we focus on the inflationary phase in models with small field excursions (see below), for which an expansion to $n_{\max} = 5$ suffices.

⁸By the use of this phrase, we do not suggest that our class of models is unique: other covariance functions or field space geometries can lead to distinct ensembles of models. For the ease of presentation however, we will in this paper refer to our models as ‘the’ GRF models.

2.2 A new, efficient, local construction of GRFs

Given the probability distribution function of equation (2.5), it might seem straightforward to just start generating the Taylor coefficients. However, the appearance of the inverse covariance matrix presents a significant complication which has curtailed previous attempts to the single-field or effectively single-field regimes [36, 52, 55]. Even with a sparse covariance matrix, as it is in our case, the inverse covariance matrix is in general hard to diagonalise, and grows rapidly in size as the number of fields is increased.

We here identify an algebraic property of the covariance matrix which allows us to circumvent this computational hurdle: Gaussian random fields with a Gaussian covariance function have the elegant property that if we know all the derivatives of the same type (even or odd) to some order, then the conditional covariance matrix for the Taylor coefficients at the next order of the same type is diagonal. This result holds to all orders and for any number of fields. This means that all the Taylor coefficients can be generated in a step-by-step fashion as a set of *independent* Gaussian random variables, without inverting or diagonalising any matrices at all. In practice, the only large matrices that need to be constructed explicitly are those that are used to calculate shifts in the expectation values of higher-order derivatives, caused by fixing the lower-order derivatives. These matrices are sparse and require little memory to be used. All together, this makes it rather easy to construct the GRF potentials even for a very large number of fields, e.g. $N_f = 100$. In fact, this method shifts the computational bottle-neck for studying manyfield inflation in GRF potentials from generating the potential to solving the equations of motions during inflation.

To provide some practical intuition for this method, we here illustrate it by looking at the covariance matrices in the case of $N_f = 2$. It is straightforward to check that the covariances vanish between odd and even derivatives for any stationary, isotropic covariance function. The covariance matrix then becomes block diagonal, and we can treat the odd and even derivatives separately. We will therefore look at the potential, Hessian, and fourth derivatives in this case, which is the simplest non-trivial example.

Suppose we have a collection of non-independently distributed Gaussian random variables, Z . If we split them into two parts, they follow the distribution,

$$\begin{bmatrix} Z_1 \\ Z_2 \end{bmatrix} \sim N \left(\begin{bmatrix} \mu_1 \\ \mu_2 \end{bmatrix}, \begin{bmatrix} \Sigma_{11} & \Sigma_{12} \\ \Sigma_{21} & \Sigma_{22} \end{bmatrix} \right), \quad (2.8)$$

where (μ_1, μ_2) is the mean vector and Σ_{ij} are block components of the covariance matrix. In our construction, Z_1 will correspond to lower-order Taylor coefficients, and Z_2 to higher-order coefficients in an iterative way which we will make clear below. We may fix the lower-order coefficients by hand (as we will do for the hyperparameters \tilde{V} , \tilde{V}_{a_1} and $\tilde{V}_{a_1 a_2}$ in our construction of inflationary potentials), or by randomly generating them from their marginal probability distribution (as we will do for Taylor coefficients of order three or more). The latter case is greatly simplified by the Gaussianity of the distribution: the marginal probability distribution of a subsystem of Gaussian variables (cf. the lower-order coefficients) is simply obtained by truncating the full covariance matrix and mean vector to the variables of the subsystem. For example, the marginal probability distribution of Z_1 obtained from equation (2.8) is simply $Z_1 \sim N(\mu_1, \Sigma_{11})$. If we then fix $Z_1 = z_1$, the conditional probability distribution for the remaining variables Z_2 is another multivariate Gaussian distribution given by,

$$Z_2 \sim N \left(\mu_2 + \Sigma_{21} \Sigma_{11}^{-1} (z_1 - \mu_1), \Sigma_{22} - \Sigma_{21} \Sigma_{11}^{-1} \Sigma_{12} \right). \quad (2.9)$$

We now want to write down the covariance matrices for the potential and its second and fourth derivatives at $\phi = 0$. For convenience, we here work with the dimensionless fields, ϕ/Λ_{h} , and the dimensionless potential, V/Λ_{v}^4 . By taking the appropriate derivatives of the covariance function, we find that the covariance matrix for the potential, second and fourth derivatives is given by,

$$\Sigma = \begin{pmatrix} 1 & -1 & 0 & -1 & 3 & 0 & 1 & 0 & 3 \\ -1 & 3 & 0 & 1 & -15 & 0 & -3 & 0 & -3 \\ 0 & 0 & 1 & 0 & 0 & -3 & 0 & -3 & 0 \\ -1 & 1 & 0 & 3 & -3 & 0 & -3 & 0 & -15 \\ 3 & -15 & 0 & -3 & 105 & 0 & 15 & 0 & 9 \\ 0 & 0 & -3 & 0 & 0 & 15 & 0 & 9 & 0 \\ 1 & -3 & 0 & -3 & 15 & 0 & 9 & 0 & 15 \\ 0 & 0 & -3 & 0 & 0 & 9 & 0 & 15 & 0 \\ 3 & -3 & 0 & -15 & 9 & 0 & 15 & 0 & 105 \end{pmatrix}, \quad (2.10)$$

where the first row/column is for the potential, the following three are for the (1,1), (2,1) and (2,2) components of the Hessian, and the final five are for the components of the fourth derivatives in the order (1,1,1,1), (2,1,1,1), et cetera.

Fixing the zeroth order Taylor coefficient \tilde{V} and using equation (2.9), the covariance matrix for the remaining variables becomes,

$$\Sigma' = \begin{pmatrix} 2 & 0 & 0 & -12 & 0 & -2 & 0 & 0 \\ 0 & 1 & 0 & 0 & -3 & 0 & -3 & 0 \\ 0 & 0 & 2 & 0 & 0 & -2 & 0 & -12 \\ -12 & 0 & 0 & 96 & 0 & 12 & 0 & 0 \\ 0 & -3 & 0 & 0 & 15 & 0 & 9 & 0 \\ -2 & 0 & -2 & 12 & 0 & 8 & 0 & 12 \\ 0 & -3 & 0 & 0 & 9 & 0 & 15 & 0 \\ 0 & 0 & -12 & 0 & 0 & 12 & 0 & 96 \end{pmatrix}, \quad (2.11)$$

where we note that the 3-by-3 block matrix in the upper-left corner, corresponding to the three independent components of $\tilde{V}_{a_1 a_2}$, has become diagonal. This is the conditional covariance matrix for the second derivatives. Fixing \tilde{V}_{ab} (either by hand or randomly, by generating three independent Gaussian variables) in addition to \tilde{V} , we find that the covariance matrix for the fourth derivatives is given by,

$$\Sigma'' = \begin{pmatrix} 24 & 0 & 0 & 0 & 0 \\ 0 & 6 & 0 & 0 & 0 \\ 0 & 0 & 4 & 0 & 0 \\ 0 & 0 & 0 & 6 & 0 \\ 0 & 0 & 0 & 0 & 24 \end{pmatrix}, \quad (2.12)$$

which again is diagonal. Generating the fourth derivatives randomly now simply involves generating five independent Gaussian random numbers. Note in particular that to construct the Taylor coefficients up to fourth order, we are never required to invert or diagonalise the full covariance matrix. This is the key realisation that allows us to commence the study of manyfield inflation in GRF potentials.

The method illustrated here extends to arbitrary N_f and to all orders in the Taylor expansion. The general formulae for these covariance matrices and the matrices that shift

the expectation values can be found in Appendix A. The details and a general proof of this method will be presented separately in [65].

2.3 Physical properties of GRF potentials

It is important to note that physical effective field theories supporting manyfield inflation may differ substantially in many details from the mathematically simple GRF models that we study. For example, EFTs with many light fields may reflect the imprints of broken symmetries, such as supersymmetry or axionic shift symmetries for some of the fields. It then appears reasonable to expect that some of the GRF estimates (e.g. of the fine-tuning of manyfield inflationary models) may differ from that of a physically motivated manyfield theory. However, it is still possible for GRF models of manyfield inflation to be sufficiently complex to capture non-trivial multifield dynamics, and can provide access to ‘universal’ or robust aspects of manyfield models, if they exist. Motivated by this, our approach here is to engineer manyfield models of slow-roll saddle-point inflation using GRFs, and to search for mechanism that determine the distribution of observables.

To understand the properties of the class of potentials that we study, it is important to characterise the various energy scales that are associated with them. In this subsection, we discuss the distribution of the slow-roll parameters and the typical scale of higher-order terms in the potential. We furthermore discuss the conditions under which GRF potentials may be interpreted as proxies for physical effective field theories. Finally, we point out that the mass distribution of GRF potentials is broad compared to the Hubble scale. This raises an additional challenge for using these potentials to study multifield inflation.

2.3.1 Distributions of the parameters of the potential

The value of the potential:

The GRF potentials have mean zero and typically takes values in the 1σ range between $-\Lambda_v^4$ and Λ_v^4 . For the models of inflation that we consider in the bulk of this paper, we take the dimensionless parameter $\tilde{V} = 1$, so that $V = \Lambda_v^4 (1 + \mathcal{O}(\phi/\Lambda_h))$. The hyperparameter Λ_v then sets the energy scale of inflation. During slow-roll inflation close to the approximate saddle-point at $\phi = 0$, the square of the Hubble parameter is then given by,

$$H^2 = \frac{1}{3} \frac{\Lambda_v^4}{M_{\text{Pl}}^2}. \quad (2.13)$$

The gradient:

The typical magnitude of the gradient vector is most easily characterised in terms of the inflationary slow-roll parameter,

$$\epsilon_V = \frac{M_{\text{Pl}}^2}{2} \frac{\partial_a V \partial_a V}{V^2} = \frac{1}{2} \frac{M_{\text{Pl}}^2}{\Lambda_h^2} \tilde{V}_a \tilde{V}_a. \quad (2.14)$$

For the theory defined by equation (2.6), the covariance of the dimensionless Taylor coefficients \tilde{V}_a is given by,

$$\langle \tilde{V}_a \tilde{V}_b \rangle = \delta_{ab}, \quad (2.15)$$

so the typical value of the slow-roll parameter ϵ_V is given by,

$$\langle \epsilon_V \rangle = 2N_f \left(\frac{M_{\text{Pl}}}{\Lambda_h} \right)^2 \gg 1. \quad (2.16)$$

At a typical point in field space, the potential is then too steep to support inflation. Since the Taylor coefficients \tilde{V}_a are N_f independent Gaussian variables, the probability of ϵ_V being no larger than some value ϵ_* is given by [36],

$$P(\epsilon_V \leq \epsilon_*) = \frac{1}{(\sqrt{2\pi})^{N_f}} \int_{|\mathbf{x}| \leq \sqrt{2\epsilon_*} \Lambda_h / M_{\text{Pl}}} d^{N_f} x e^{-x^2/2} \simeq \frac{2}{N_f \Gamma(\frac{N_f}{2})} \left(\sqrt{\epsilon_*} \frac{\Lambda_h}{M_{\text{Pl}}} \right)^{N_f}. \quad (2.17)$$

Obtaining a small ϵ_V parameter requires tuning of the slope of the potential, and this tuning becomes more severe as Λ_h is decreased from M_{Pl} . Note however that equation (2.17) gives the probability of a randomly chosen point having a small ϵ_V parameter, not the probability that a point with a small ϵ_V parameter exists in the field space. The latter probability depends on the volume of field space, which we do not model in this paper.

The Hessian matrix:

The Hessian matrix, V_{ab} , determines the curvature of the potential and its eigenvalues are the squared masses of the fields. From the covariance function (2.6) it is easy to see that the dimensionless Hessian has zero mean and a covariance given by,

$$\langle \tilde{V}_{ab} \tilde{V}_{cd} \rangle = \left(\delta_{ab} \delta_{cd} + \delta_{ac} \delta_{bd} + \delta_{ad} \delta_{bc} \right). \quad (2.18)$$

The probability distribution for the Hessian (with all other Taylor coefficients marginalised over), can then be obtained by inverting the covariance matrix $\Sigma_{(ab)(cd)} \equiv \langle \tilde{V}_{ab} \tilde{V}_{cd} \rangle$ to find,

$$(\Sigma^{-1})_{(ab)(cd)} = -\frac{1}{2(N_f + 2)} \delta_{ab} \delta_{cd} + \delta_{ac} \delta_{bd} - \frac{1}{2} \delta_{ad} \delta_{bc}. \quad (2.19)$$

The marginal probability distribution is then given by [66],

$$P(\tilde{V}_{ab}) = C_n \exp \left(-\frac{1}{4} \left(\tilde{V}_{ab} \tilde{V}_{ba} - \frac{1}{N_f + 2} (\tilde{V}_{aa})^2 \right) \right). \quad (2.20)$$

Here C_n is a normalisation factor.

To elucidate the consequences of this probability distribution, it is useful to consider the large- N_f limit in which an eigenvalue density can easily be derived. We will denote the physical squared masses by m_a^2 and work with the dimensionless eigenvalues λ_a of \tilde{V}_{ab} :

$$m_a^2 = \frac{\Lambda_v^4}{\Lambda_h^2} \lambda_a. \quad (2.21)$$

To derive the eigenvalue density, we change variables from \tilde{V}_{ab} to its eigenvalues and eigenvectors, and integrate out the latter. Importantly, the probability distribution of the eigenvalues involves the Vandermonde determinant arising from the change of measure,

$$\prod_{a < b} d\tilde{V}_{ab} \sim \prod_{a < b} |\lambda_a - \lambda_b| \prod_{a=1}^{N_f} d\lambda_a. \quad (2.22)$$

The Vandermonde determinant encodes the ‘eigenvalue repulsion’ which is the key driver behind the large- N_f universality encountered in random matrix theory (see e.g. [23–25]). The appearance of the Vandermonde determinant in the probability distribution for the Hessian

matrix of GRF potentials is indicative of the close connection between random function theory and random matrix theory. We will return to this connection towards the end of this section, and then again in section 4.

By using the eigenvalue density function,

$$\rho(\lambda) = \frac{1}{N_f} \sum_a^{N_f} \delta(\lambda - \lambda_a), \quad (2.23)$$

the probability distribution for the eigenvalues can be expressed as,

$$P(\rho) = C_n \exp \left[-\frac{N_f}{4} \left(\int d\lambda \lambda^2 \rho(\lambda) - \left(\int d\lambda \lambda \rho(\lambda) \right)^2 \right) + \frac{N_f^2}{2} \int d\lambda d\lambda' \rho(\lambda) \rho(\lambda') \ln(|\lambda - \lambda'|) \right]. \quad (2.24)$$

The typical distribution of the eigenvalues of the dimensionless Hessian matrix can be found from saddle-point evaluation of equation (2.24). This gives [66],

$$\rho_{sc}(\lambda) = \frac{1}{2\pi N_f} \sqrt{4N_f - (\lambda - \bar{\lambda})^2}. \quad (2.25)$$

For $\bar{\lambda} = 0$, this spectrum is precisely a Wigner semi-circle, i.e. the spectrum of the Gaussian Orthogonal Ensemble (GOE) of random symmetric matrices with independent, Gaussianly distributed entries. For $\bar{\lambda} \neq 0$, the semi-circle is rigidly shifted to be centred at $\bar{\lambda}$ [66].

To properly understand the significance of the shift $\bar{\lambda}$, it is instructive to calculate the conditional probability distribution of the Hessian, given that the potential has a certain value, say $V = V_*$. The Hessian matrix and the value of the potential are correlated, and upon using equation (2.9) for the conditional probability distribution, we find the moments [36, 66],

$$\langle \tilde{V}_{ab} \rangle |_{V=V_*} = -\frac{V_*}{\Lambda_v^4} \delta_{ab}, \quad (2.26)$$

$$\langle \tilde{V}_{ab} \tilde{V}_{cd} \rangle |_{V=V_*} - (\langle \tilde{V}_{ab} \rangle \langle \tilde{V}_{cd} \rangle) |_{V=V_*} = \left(\delta_{ac} \delta_{bd} + \delta_{ad} \delta_{bc} \right). \quad (2.27)$$

According to equation (2.27), every unique element of the Hessian is now statistically independent of the others, and we can write the Hessian as [36],

$$V_{ab} = \frac{\Lambda_v^4}{\Lambda_h^2} \left(-\frac{V_*}{\Lambda_v^4} \delta_{ab} + R_{ab} \right), \quad (2.28)$$

where R_{ab} is a random matrix in the Gaussian Orthogonal Ensemble (GOE). The spectrum of the dimensionless Hessian is then given by,

$$\rho_{sc}(\lambda) = \frac{1}{2\pi N_f} \sqrt{4N_f - (\lambda + V_*/\Lambda_v^4)^2}. \quad (2.29)$$

Clearly, for points with vanishing vacuum energy, $V_* = 0$, the spectrum of the Hessian is precisely that captured by the Wigner semi-circle. For $V_* > 0$, which is the case relevant for

inflation, the typical spectrum is a semi-circle rigidly shifted downwards, making comparatively more eigenvalues tachyonic. However, for $V_\star = \Lambda_v^4$ and $N_f \gg 1$, this shift is small: the endpoints of the semi-circle spectrum of R_{ab} are located at $\pm 2\sqrt{N_f}$, and the spectrum of V_{ab} is a shifted semi-circle with endpoints at $(\pm 2\sqrt{N_f} - 1)\Lambda_v^4/\Lambda_h^2$.

We define the slow-roll η_V parameter as,

$$\eta_V = M_{\text{Pl}}^2 \frac{m_{\text{min}}^2}{V}, \quad (2.30)$$

with m_{min}^2 denoting the smallest eigenvalue of the Hessian matrix. An immediate consequence of equation (2.28) is that η_V tends to be very large and negative for the typical, slightly shifted semi-circle spectrum [36]:

$$\eta_V = -(2\sqrt{N_f} + 1) \left(\frac{M_{\text{Pl}}}{\Lambda_h} \right)^2. \quad (2.31)$$

Smaller magnitudes of η_V can be obtained if the spectrum of the Hessian is in a rare configuration in which no eigenvalue is very tachyonic. Given equation (2.28) for $V = V_\star$, the probability of $|\eta_V|$ being no larger than $|\eta_\star|$ is given by,

$$P \left(|m_{\text{min}}^2| < |\eta_\star| \frac{V_\star}{M_{\text{Pl}}^2} \right) = P_{\text{GOE}} \left(\lambda_{\text{min}} > 1 + \eta_\star \frac{\Lambda_h^2}{M_{\text{Pl}}^2} \right), \quad (2.32)$$

where λ_{min} denotes the smallest eigenvalue of the GOE matrix R , and P_{GOE} denotes its probability distribution. For $N_f \gg 1$, the radius of the typical semi-circle configuration is $2\sqrt{N_f} \gg 1$, so that,

$$P_{\text{GOE}} \left(\lambda_{\text{min}} > 1 + \eta_\star \frac{\Lambda_h^2}{M_{\text{Pl}}^2} \right) \approx P_{\text{GOE}} (\lambda_{\text{min}} > 1) = \exp(-c N_f^2), \quad (2.33)$$

where $c = \frac{1}{108} (35 + 16\sqrt{7} + 27 \ln(18) - 54 \ln(\sqrt{7} - 1)) \approx 1.19$. In the last step we have used the fluctuation probability computed for the subset of ‘fluctuated spectra’ of the GOE with no negative eigenvalue [67]. Hence, small slow-roll parameters are very infrequent in GRF potentials with many fields.

We close this section by noting that the tight connection between our GRF models and random matrix ensembles also has strong implications for the distribution of vacua [36, 66]. Metastability of Minkowski and de Sitter critical points requires $m_{\text{min}}^2 > 0$. According to the RMT analysis, such points are exceedingly rare:

$$P(m_{\text{min}}^2 > 0 | V \geq 0) \leq P_{\text{GOE}}(\lambda_{\text{min}} \geq 0). \quad (2.34)$$

The rarity of metastable de Sitter vacua is a common feature also of other classes of random potentials, such as random supergravity theories [36, 68, 69].

Equation (2.34) implies that the fraction of metastable de Sitter vacua in our GRF potentials is bounded from above by the probability of large fluctuations of one of the simplest random matrix ensembles. As a consequence, the frequency of metastable de Sitter vacua scales with N_f like $\ln(P_{\text{GOE}}) \sim -N_f^2$. Recently however, the authors of [70] (see also [36]) found that vacua in GRF potentials comprise a fraction of $\sim \exp(-\alpha N_f)$ of all critical points of GRFs (for some constant α), which far exceeds the metastability estimate of (2.34). This apparent discrepancy is resolved by noting that the vast majority of the metastable vacua found in [70] are located deep down in the potential, at $V \lesssim -2\sqrt{N_f}\Lambda_v^4$, in our mean-zero

GRF models.⁹ For such large and negative values of the potential, the semi-circle spectrum is rigidly shifted upwards so that metastability is common. Due to the simple relation of equation (2.28) (and its generalisation for other covariance functions), any carefully phrased question about the vacuum statistics in GRF models map into precise questions about the eigenvalue statistics of random matrices.

Cubic and higher-order terms:

GRF potentials have non-trivial, randomly generated interaction terms at cubic and higher orders. At order n , these are of the order of,

$$V_{a_1 \dots a_n} \sim \frac{\Lambda_v^4}{\Lambda_h^n}. \quad (2.35)$$

In particular, each of the cubic order terms are then of the order of,

$$V_{abc} \sim \frac{\Lambda_v^4}{\Lambda_h^3} \sim \frac{H^2 M_{\text{Pl}}^2}{\Lambda_h^3} \sim \left(\frac{\Lambda_v}{\Lambda_h}\right)^2 \left(\frac{M_{\text{Pl}}}{\Lambda_h}\right) H. \quad (2.36)$$

The vertical scale Λ_v factors out of the evolution equations for both the background and the perturbations and only serves as a normalisation factor for the scale of the scalar perturbations. We find in all cases that $(\Lambda_v/\Lambda_h)^2 < \Lambda_h/M_{\text{Pl}}$, and the cubic terms of equation (2.36) tend to be smaller than H in the models that we consider. However, since Λ_v does not affect the field equations, it also does not affect our predictions for the spectral index, its running, or the local non-Gaussianity parameter, f_{NL} . Consequently, the predictions of our models also apply to models in which $V_{abc} \approx H$, but for which the amplitude of the scalar perturbations is larger than the observationally inferred value.¹⁰

2.3.2 GRF potentials and physical effective field theories

Gaussian random fields provide a mathematically convenient construct, but are not directly derived as effective field theories (EFTs) from particle physics or string theory.¹¹ In this section, we discuss how the GRF potentials exhibit some ‘EFT-like’ properties with important consequences for the cosmology. Relatedly, we note that these potential naturally have spread-out mass spectra, and additional tuning is required to construct models with non-trivial multifield dynamics.

In quantum field theory, unprotected dimensionful operators are naturally large. For the UV cutoff Λ , the potential is typically of the order of $V \sim H^2 M_{\text{Pl}}^2 \sim \Lambda^4$, and the scalar masses are of order $m^2 \sim \Lambda^2 \sim H M_{\text{Pl}} \gg H^2$ (cf. equation (1.1)). In the GRF potentials considered in this paper, cf equation (2.7), the scale Λ is replaced by the two parameters Λ_v and Λ_h . The horizontal scale Λ_h sets the coherence length of the potentials, and can be interpreted as the UV-cutoff of the theory. Since all operators are suppressed by the same cut-off scale,

⁹ The analogous result in random supergravities is that most metastable de Sitter vacua realised in the ‘approximately supersymmetric’ regime [36, 68]. Note however, that known constructions of de Sitter string compactifications tend to rely on non-random ‘structures’ to enhance the probability of metastability (see e.g. [71–80]). Thus it is certainly possible that the simple GRF models may capture some rather robust aspects of manyfield inflation in fundamental theory, but fail to accurately describe their vacuum structure.

¹⁰ Another way to achieve a relative enhancement of the cubic terms with respect to the Hubble parameter is to set the zeroth order Taylor coefficient much below its rms value: $\tilde{V} \ll 1$. This however makes the fine-tuning required to achieve small slow-roll parameters more severe.

¹¹ Simple GRFs can under certain assumptions be related to the potentials of multi-axion theories [81].

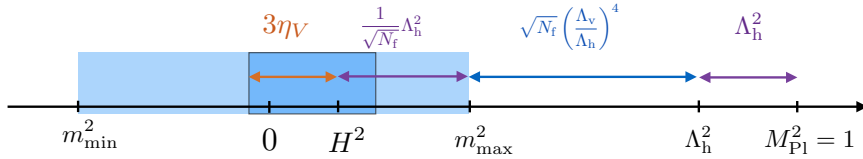


Figure 2: Schematic illustration of the relevant energy scales of the GRF potentials. The light blue shaded region indicates the equilibrium spectrum of the Hessian; the darker region corresponds to our chosen ‘flat spectrum’ initial condition.

sharp features over distances $\ll \Lambda_h$ are very rare. We expect this to be a general feature of models with generic interactions suppressed by a single, common cut-off scale.

The parameter Λ_v sets the natural energy scale of the GRF models. During inflation, a consistent EFT interpretation requires $H^2 \ll \Lambda_h^2$. If reheating proceeds rapidly after the end of inflation, the stronger condition of $V \sim \Lambda_v^4 \sim T_{\text{rh}}^4 \ll \Lambda_h^4$ applies. By taking $\Lambda_v < \Lambda_h$, even the latter condition is generically satisfied. A Wilsonian EFT is obtained by integrating out states more massive than the UV cutoff, leaving only states with $m^2 \leq \Lambda^2$. Consequently, in the context of GRF potentials, we expect the eigenvalues of the Hessian matrix to be no larger than $\sim \Lambda_h^2$. For $\Lambda_v < \Lambda_h$, this condition is satisfied unless N_f is very large:

$$\frac{m_{\text{max}}^2}{\Lambda_h^2} \approx \left(2\sqrt{N_f} - 1\right) \frac{\Lambda_v^4}{\Lambda_h^4}. \quad (2.37)$$

Figure 2 illustrates the relevant energy scales of GRF potentials discussed in this paper.

We now note a serious obstacle for using GRF potentials to study multifield inflation: the mass spectrum is generically spread out over energy scales $\gg H$. This is immediately evident from the width of the (shifted) Wigner semi-circle distribution, which predicts a typical eigenvalue spacing for the Hessian of,

$$\frac{1}{N_f} \frac{(m_{\text{max}}^2 - m_{\text{min}}^2)}{H^2} = 12 \frac{1}{\sqrt{N_f}} \left(\frac{M_{\text{Pl}}}{\Lambda_h}\right)^2. \quad (2.38)$$

For $\Lambda_h < M_{\text{Pl}}$, this then implies that only systems with a very large number of fields, $N_f \gtrsim (M_{\text{Pl}}/\Lambda_h)^4$, can be expected to exhibit non-trivial multiple field effects. This large spread in the masses explains why recent attempts at using GRFs to study multiple-field inflation [55] have only captured single-field dynamics. To use these models to study non-trivial multifield dynamics, one has to further tune the initial conditions.

The particular N_f dependence of equation (2.38) follows from the form of the covariance function, cf. equation (2.6). The width of the eigenvalue distribution may be changed by modifying the covariance function, e.g. to $C(\phi_1 - \phi_2) = N_f \Lambda_v^8 e^{-(\phi_1 - \phi_2)^2/2N_f \Lambda_h^2}$, which gives an N_f independent eigenvalue distribution of the Hessian, and an additional suppression by $1/\sqrt{N_f}$ in equation (2.38). However, such a modified covariance function enhances the effective coherence length of the potential to $\sqrt{N_f} \Lambda_h$, which becomes super-Planckian for large N_f .¹²

¹²This lesson applies somewhat more generally: the width of the mass spectrum relative H^2 is controlled by $C^{(4)}(0)/C(0)$. Compressing the spectrum requires decreasing this ratio, but for many covariance functions $C^{(p)}(0)/C(0) \sim (C^{(4)}(0)/C(0))^{p/4}$, and an overall suppression of these ratios translates directly into an increased coherence length. Compressing the mass scale while keeping the coherence scale associated with the interaction terms fixed then requires covariance functions with multiple scales. We will not consider such modifications further in this paper.

The broad spread in the distribution of masses of GRF potentials is not surprising as these models do not incorporate protective approximate symmetries (e.g. broken supersymmetry, or approximate shift-symmetries), which can lower the natural scale of dimensionful operators, and make inflation less fine-tuned. It would be interesting to extend our method to construct manyfield models of inflation in random supergravity models with spontaneously broken supersymmetry, following the ideas proposed in [36, 68, 69].

2.4 The statistical ensembles of models

As discussed in section 2.1, the hyperparameters of our GRF potentials are:

$$(\tilde{V}, \tilde{V}_a, \tilde{V}_{ab}, N_f, \Lambda_h, \Lambda_v). \quad (2.39)$$

An understanding of pre-inflationary physics in fundamental theory could potentially provide us with prior probability distributions on these parameters. Lacking such priors, we compute the observational predictions for certain ranges of the hyperparameters, and investigate how these predictions change as hyperparameters are varied.

Specifically, we construct ensembles of manyfield models of inflation as follows: First, we set \tilde{V} to its rms value, $\tilde{V} = 1$, so that Λ_v sets the scale of the potential at $\phi = 0$. In slow-roll inflation, the parameter Λ_v has no effect on the equations of motion for either the background field or the perturbations around it. We exploit this by evolving each model with a fiducial value of Λ_v and, for each model yielding a sufficiently long period of inflation, rescale Λ_v at the end of inflation so that the amplitude of the primordial curvature perturbation at the ‘pivot scale’ is consistent with the value determined by the Planck experiment [5].¹³ This fixes Λ_v separately for each model.

To obtain sufficiently flat potentials that support inflation, the gradient and Hessian have to be tuned. We set \tilde{V}_a so that ϵ_v is sufficiently small that models with at least 60 e-folds of inflation are not too infrequent. This leads us to explore values of ϵ_v in the range of 2×10^{-8} to 10^{-11} . We henceforth take,

$$\epsilon_i \equiv \epsilon_v \Big|_{\phi=0}, \quad (2.40)$$

to parameterise the magnitude of the gradient vector. This vector obviously also has a direction, and we explore the effect of its alignment relative to the eigenvectors of \tilde{V}_{ab} , as we now discuss.

We have seen in section 2.3 that the curvature of the potential needs to be tuned to give rise to sustained inflation and multifield dynamics. In particular, the smallest eigenvalue of the Hessian, which we parametrise by,

$$\eta_i \equiv \eta_v \Big|_{\phi=0}, \quad (2.41)$$

must be close to zero. We numerically investigate values of η_i in the range -10^{-1} to -10^{-4} . To explore the non-generic spectra relevant for multifield inflation, we consider two (non-random) initial conditions for the spectrum of V_{ab} :

$$\begin{aligned} \text{Flat spectrum :} & \quad m_a^2 \Big|_{\phi=0} : \text{Uniformly distributed in } (3\eta_i H^2, \frac{9}{4}H^2), \\ \text{Compressed spectrum :} & \quad m_a^2 \Big|_{\phi=0} : \text{Uniformly distributed in } (3\eta_i H^2, -3\eta_i H^2). \end{aligned} \quad (2.42)$$

¹³To identify the precise e-fold at which the pivot scale crossed the horizon during inflation requires a detailed modelling of the reheating phase (cf. [82] for a review). For the baseline parameters, we find that the pivot scale exited the horizon $58 - N_{\text{rh}}$ e-folds before the end of inflation, where N_{rh} parametrises the expansion between the end of inflation and the onset of the hot big bang. For concreteness, we will assume throughout this paper that the pivot scale crossed the horizon 55 e-folds before the end of inflation.

Field perturbations with an effective squared mass greater than $9/4H^2$ are exponentially suppressed already at horizon exit.¹⁴ This motivates the upper bound of the ‘flat spectrum’. The (extremely) compressed, nearly degenerate spectrum is specifically chosen to maximise the chances of non-trivial multifield effects, and is included for reasons that will become apparent in section 5. We note that these initial spectra will ‘relax’ to the generic spectrum for a GRF over distances of $\sim \mathcal{O}(\Lambda_h)$. During most of inflation, the field is slowly rolling and this relaxation is very slow in e-fold ‘time’, but we will see that towards the end of inflation, multiple fields develop tachyonic masses, $m_a^2 < 0$.

We now return to the question of the relative alignment of V_a with the eigenvectors of V_{ab} . In a Gaussian random field the gradient and Hessian are uncorrelated, $\langle V_a V_{ab} \rangle = 0$, and generically, V_a has support along all eigenvectors of V_{ab} . However, slow-roll inflation makes the field follow the gradient descent along the potential, which tends to quickly align V_a with the smallest eigenvalue direction of the Hessian matrix, which we will denote by ‘1’ (for a more detailed discussion on this, see e.g. [28]). Motivated by this, we consider two classes of orientations of V_a :

$$\begin{aligned} \text{Random :} \quad & V_a|_{\phi=0} \sim \sqrt{2\epsilon_1} \frac{\Lambda_v^4}{M_{\text{Pl}}^4} \text{Uniform}(S^{N_f-1}) , \\ \text{Aligned :} \quad & V_a|_{\phi=0} = \sqrt{2\epsilon_1} \frac{\Lambda_v^4}{M_{\text{Pl}}^4} \delta_{a1} . \end{aligned} \tag{2.43}$$

With the initial conditions $(\tilde{V}, \tilde{V}_a, \tilde{V}_{ab})$ fixed, we generate the higher-order Taylor coefficients randomly using the conditional PDFs derived as discussed in section 2.2.

Finally, we explore the numerically accessible a range of values for the remaining hyperparameters N_f and Λ_h : for N_f very large or Λ_h small, inflation is only supported if the slow-roll parameters are highly tuned, which can cause numerical accuracy problems.¹⁵ A summary of the hyperparameter choices that we explore in this paper can be found in Appendix C. Some of our results are best illustrated for a fixed choice of parameter. We take as our baseline model,

$$\textbf{Baseline: } N_f = 10, \quad \Lambda_h = 0.4M_{\text{Pl}}, \quad \epsilon_1 = 2 \times 10^{-9}, \quad \eta_i = -10^{-4}, \tag{2.44}$$

with the flat spectrum of the Hessian, cf. equation (2.42), and a randomly directed gradient vector. For this choice of hyperparameters, obtaining at least 60 e-folds of inflation is not uncommon, and N_f is sufficiently large for multifield effects to be clearly manifest.

2.5 Method: background

Given a randomly generated multifield potential, we evolve the fields numerically using the coupled Klein-Gordon and Friedmann-Robertson-Walker equations,

$$\ddot{\phi}_a + 3H\dot{\phi}_a = -\partial_a V, \quad H^2 = \frac{\frac{1}{2}\dot{\phi}_a\dot{\phi}_a + V}{3M_{\text{Pl}}^2}. \tag{2.45}$$

In the slow-roll approximation that we use throughout this paper, these equations become,

$$3H\dot{\phi}_a = -\partial_a V, \quad H^2 = \frac{V}{3M_{\text{Pl}}^2}. \tag{2.46}$$

¹⁴More precisely, the effective squared masses of the perturbations are the eigenvalues of the matrix $M_{ab} = V_{ab} - \frac{1}{a^3}\partial_t\left(a^3\frac{\dot{\phi}_a\dot{\phi}_b}{H}\right)$ [83, 84].

¹⁵The computations reported in this paper did not require supercomputer capabilities, but potentials with $N_f \gg 1$ places some restrictions on memory access. Our largest simulations ran on a computing system with 144 CPUs and 516 GB RAM.

Expressed with respect to the number of e-folds, N , the slow-roll Klein-Gordon equation is simply given by,

$$\frac{d\phi_a}{dN} = -\partial_a \ln V. \quad (2.47)$$

Equation (2.47) makes it clear that the vertical scale, Λ_v , has no impact on the background field evolution in slow-roll.

2.6 Method: perturbations

To calculate the observational predictions of the manyfield models of inflation, we use the ‘transport method’ [37–40] (see also [85–89]). This formalism allows us to evolve the two-field and three-field correlators on superhorizon scales from horizon crossing to the end of inflation.¹⁶ Analytic solutions for this method exist for certain potentials, just like in the δN formalism, but the main advantage of it is that it allows for accurate and efficient numerical solutions, regardless of the form of the potential. In this subsection, we briefly review the key elements of the transport method. We furthermore recall how multifield dynamics can cause the curvature perturbation to evolve on superhorizon scales, and we define the isocurvature and curvature correlators. We close this section by briefly reviewing the δN formula for the non-Gaussianity amplitude f_{NL} .

The transport method

In the spatially flat gauge, we can write the perturbations at the end of inflation as an expansions in the perturbations at horizon exit:

$$\delta\phi_a = \Gamma_{ab}\delta\phi_b^* + \frac{1}{2}\Gamma_{abc}\delta\phi_b^*\delta\phi_c^* + \dots \quad (2.48)$$

where the horizon exit perturbations have been marked with a $*$. Using the separate-universe approach [90, 91], we expand the slow-roll equations of motion, equation (2.47), around the background trajectory to obtain evolution equations for $\delta\phi_a$. It is then easy to see that the ‘propagators’ Γ_{ab} and Γ_{abc} must obey the differential equations,

$$\frac{d\Gamma_{ab}}{dN} = u_{ac}\Gamma_{cb}, \quad (2.49)$$

$$\frac{d\Gamma_{abc}}{dN} = u_{ad}\Gamma_{dbc} + u_{ade}\Gamma_{db}\Gamma_{ec}, \quad (2.50)$$

where,

$$u_{ab} = -\partial_a\partial_b \ln V, \quad (2.51)$$

$$u_{abc} = -\partial_a\partial_b\partial_c \ln V, \quad (2.52)$$

with the derivatives evaluated on the background trajectory. These differential equations have the following formal solutions:

$$\Gamma_{ab}(N) = \Gamma_{ab}(N, N^*) = \mathcal{P} \exp \left(\int_{N^*}^N dN' u_{ab}(N') \right), \quad (2.53)$$

$$\Gamma_{abc}(N) = \Gamma_{abc}(N, N^*) = \int_{N^*}^N dN' \Gamma_{a\mu} u_{\mu\nu\rho}(N') \Gamma_{\nu b} \Gamma_{\rho c}, \quad (2.54)$$

¹⁶The transport method can be applied to both slow-roll and non-slow-roll systems, and also on sub-horizon scales [37]. For our purposes, it suffices to consider the superhorizon evolution of the field perturbations during slow-roll inflation.

where \mathcal{P} is a path ordering operator. In equation (2.54), we have used Greek indices as a short-hand for propagators evolving to or from N' , e.g. $\Gamma_{\nu b} = \Gamma_{\nu b}(N', N^*)$.

Once the field perturbations at the end of inflation, $\delta\phi_a^{\text{end}}$, are known, the curvature perturbation is given by a gauge transformation:

$$\zeta = N_a \delta\phi_a^{\text{end}} + \frac{1}{2} N_{ab} \delta\phi_a^{\text{end}} \delta\phi_b^{\text{end}} + \dots, \quad (2.55)$$

where the coefficients N_a and N_{ab} are given by [37],

$$N_a = \frac{1}{\sqrt{2\epsilon}} \frac{V_a}{\sqrt{V_b V_c}}, \quad (2.56)$$

$$N_{ab} = \frac{V V_{ab}}{V_c V_c} + \frac{V_a V_b}{V_c V_c} \left(1 + 2 \frac{V}{(V_e V_e)^2} V_f V_f V_d \right) - \frac{V}{(V_c V_c)^2} (V_a V_{bc} V_c + V_b V_{ac} V_c). \quad (2.57)$$

The curvature perturbation

We write the field two-point correlator as,

$$\langle \delta\phi_a^*(\mathbf{k}_1) \delta\phi_b^*(\mathbf{k}_2) \rangle = (2\pi)^3 \delta^{(3)}(\mathbf{k}_1 + \mathbf{k}_2) \frac{2\pi^2}{k^3} \Sigma_{ab}. \quad (2.58)$$

In slow-roll and with a slowly turning field trajectory at horizon crossing, we can take the initial condition of the field correlators to be given by,

$$\Sigma_{ab}^* = \frac{H^2(N^*)}{4\pi^2} \delta_{ab}. \quad (2.59)$$

In [28], it was show that this approximation works well for manyfield models of approximate saddle-point inflation. The curvature power spectrum at some later time, N , is then given by,

$$P_\zeta(N, k) = N_a(N) N_c(N) \Gamma_{ab}(N, N_\star) \Gamma_{cd}(N, N_\star) \Sigma_{bd}^*. \quad (2.60)$$

Isocurvature perturbations

To linear order in the field perturbations, the curvature perturbation of equation (2.55) is given by field fluctuations along the instantaneous background trajectory,

$$\zeta = \frac{1}{\sqrt{2\epsilon_V}} \delta\phi_{\parallel}, \quad (2.61)$$

where $\delta\phi_{\parallel} = n_a \delta\phi^a$ for $n_a = V_a/|V_b|$. Field perturbations along the $N_f - 1$ perpendicular directions give rise to ‘entropic’ or ‘isocurvature’ perturbations. We can decompose the field fluctuations as,

$$\delta\phi^a \equiv \delta\phi_{\parallel} n^a + \delta\phi_{\perp}^j v_j^a, \quad (2.62)$$

where $v_j^a(N)$ denotes a generic orthonormal frame of basis vectors in directions perpendicular to V_a . Here a is a vector index a and with $j = 1, \dots, N_f - 1$. In analogy to ζ (and just as in [28]), we define the isocurvature \mathcal{S}^i as,

$$\mathcal{S}^i \equiv \frac{1}{\sqrt{2\epsilon_V}} \delta\phi_{\perp}^i. \quad (2.63)$$

In slow-roll and on superhorizon scales, the curvature and isocurvature evolve as [28, 92],

$$\zeta' = 2 \left(n^a \frac{V_{ab}}{V} v_i^b \right) \mathcal{S}^i, \quad (2.64)$$

$$(\mathcal{S}^i)' = (n^a \frac{V_{ab}}{V} n^b - 2\epsilon_V) \mathcal{S}^i - v_i^a \frac{V_{ab}}{V} v_k^b \mathcal{S}^k. \quad (2.65)$$

Equations (2.64) and (2.65) reflect the well-known fact that isocurvature can source superhorizon evolution of the curvature perturbation ζ , but the curvature perturbation does not source isocurvature [93, 94].

The isocurvature correlations are then given by,

$$\langle \mathcal{S}^i(\mathbf{k}_1) \mathcal{S}^j(\mathbf{k}_2) \rangle = (2\pi)^3 \delta^{(3)}(\mathbf{k}_1 + \mathbf{k}_2) \frac{k^3}{2\pi^2} P_{\text{iso}}^{ij}(N), \quad (2.66)$$

with,

$$P_{\text{iso}}^{ij}(N) = \frac{1}{2\epsilon_V} v_i^a \Sigma^{ab} v_j^b. \quad (2.67)$$

We refer to the isocurvature power spectrum (without indices) as,

$$P_{\text{iso}} = \delta_{ij} P_{\text{iso}}^{ij} = \frac{1}{2\epsilon_V} v_i^a \Sigma^{ab} v_i^b. \quad (2.68)$$

Non-Gaussianity

Equation (2.55) is related to the commonly used ‘ δN ’ formulas, which involve the field perturbation at horizon crossing, by,

$$N_a^{\delta N} = N_b \Gamma_{ba}, \quad (2.69)$$

$$N_{ab}^{\delta N} = N_c \Gamma_{cab} + N_{cd} \Gamma_{ca} \Gamma_{db}. \quad (2.70)$$

To compute the parameter f_{NL} , we use the δN -formalism expression, which is given by [15],¹⁷

$$-\frac{6}{5} f_{\text{NL}} = \frac{r}{16} (1 + f) + \frac{N_a^{\delta N} N_b^{\delta N} N_{ab}^{\delta N}}{(N_c^{\delta N} N_c^{\delta N})^2}, \quad (2.71)$$

where $0 \leq f \leq 5/6$ is momentum dependent, and r is the tensor-scalar ratio. In the small-field inflation models studied in this paper, $r \ll 10^{-3}$, and the first term is negligible.

While the calculation of the power spectrum typically is insensitive to small numerical errors, f_{NL} is not. The dominant, second term of equation (2.71) can itself be expressed as the sum of two terms,

$$-\frac{6}{5} f_{\text{NL}} = \frac{N_a^{\delta N} N_b^{\delta N} N_{ab}^{\delta N}}{(N_c^{\delta N} N_c^{\delta N})^2} = \frac{N_c \Gamma_{ca} N_d \Gamma_{db} (N_e \Gamma_{ea} \Gamma_{fb} + N_e \Gamma_{cab})}{(N_g \Gamma_{gi} N_h \Gamma_{hi})^2}. \quad (2.72)$$

Quite commonly, both these terms can be large (say $\mathcal{O}(10)$), but cancel each other to a very high degree (say down to $\mathcal{O}(10^{-2})$). This delicate cancellation calls for high precision of the numerical evaluation of the background and the Γ coefficients. We briefly discuss our numerical implementation of the evolution of the perturbations in Appendix B.

¹⁷We adopt the sign convention of [15] for f_{NL} .

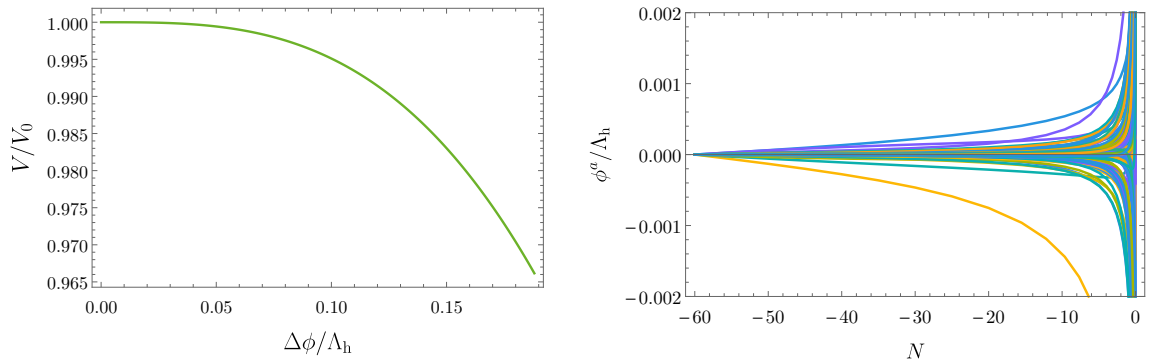


Figure 3: The value of the potential as a function of the field displacement (left), and the evolution of multiple components of the fields (right) in a random 100-field GRF model.

3 Result I: Planck compatibility is not rare, but future experiments may rule out this class of models

We are now ready to discuss the results of our simulations of manyfield models of inflation in random potentials. In this section we focus on observables related to the two-point correlation function, such as the primordial power spectra of curvature and isocurvature perturbations. Our first key result is that despite multifield effects typically being non-negligible, power spectra tend to be very smooth, and observational compatibility is not rare in these models.

This section is organised as follows: we first discuss the evolution of the classical background, and we highlight and explain the particularly strong ‘eigenvalue repulsion’ effect on the smallest eigenvalue of the Hessian in GRF models. We then discuss the primordial perturbations of these models: we validate that the power spectra are well-approximated by approximately scale-invariant power laws over the scales relevant for the CMB. We then note that essentially all models predict small deviations from the strict power-law form, and we compute the predictions for the spectral tilt, n_s and its running, α_s , as functions of the hyperparameters. This leads us to establish a surprisingly robust prediction of these models, which makes it possible to rule them out with future experiments. We furthermore find that multifield effects are typically important, but that, importantly, isocurvature tends to decay during inflation.

Several of the results found in this section are directly analogous to results recently observed in models of manyfield inflation in DBM potentials [28], while others differ substantially. In section 4 we compare these setups in detail.

3.1 Background evolution in GRF inflation

We first briefly discuss some key elements of the evolution of the inflationary background in the GRF potentials. To get an intuition for these models, it is instructive to first consider an example. We here take a randomly generated 100-field model as our case-study. This model was generated from the hyperparameters $\Lambda_h = 0.4$, $\epsilon = 5 \times 10^{-10}$, $\eta_i = -10^{-4}$, a flat spectrum, cf. equation (2.42), and a randomly directed gradient vector at $\phi = 0$. This particular model gives a total number of e-folds $N^{\text{end}} = 80.6$ over a total field displacement of $\Delta\phi = \sqrt{\phi^a \phi^a} = 0.187\Lambda_h$.

The left plot of Figure 3 shows the normalised value of the potential energy as a function of $\Delta\phi$. The potential along the descending inflationary trajectory is very smooth and

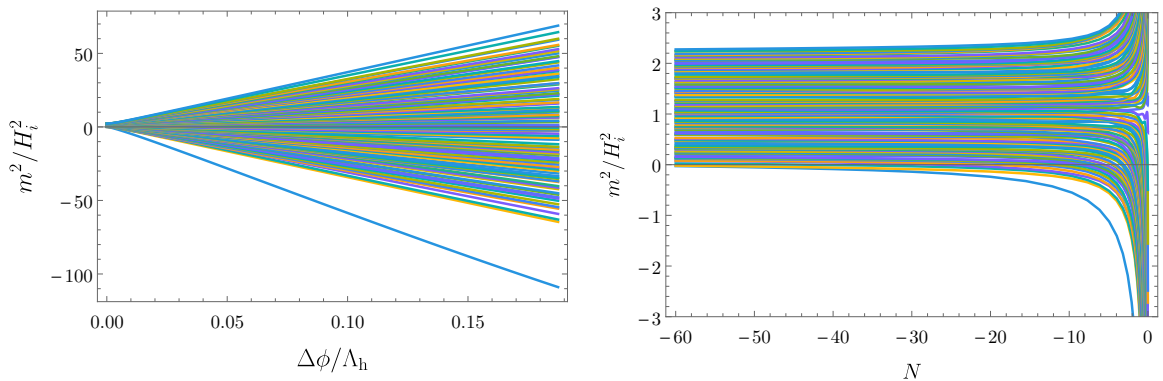


Figure 4: Eigenvalue evolution of the Hessian in a 100-field example, starting from a flat spectrum.

featureless. Since ϵ_V is initially very small and $|\dot{\phi}| = \sqrt{2\epsilon_V}$, the field rolls very slowly initially, but accelerates super-exponentially towards the end of inflation. Figure 3 shows how multiple components of the field evolve during inflation, and indicates that the inflationary trajectory turns as the field descends the potential.

The eigenvalues of the Hessian matrix are not constant in a general inflationary model, and we expect the eigenvalues of the GRF models to relax from the fine-tuned initial configuration to the (slightly off-centred) semi-circle spectrum. Figure 4 shows the evolution of the squared masses as a function of the field displacement during inflation (left plot), and as a function of the number of e-folds (right plot) for our 100-field example. Indeed, as the fields evolve from $\phi = 0$, the spectrum spreads out. Half of the fields, initially heavier than the others, tend to become even more massive during inflation, and are not very important for either the background evolution or the spectrum of the perturbations. By contrast, the lighter half of the fields become even lighter, and many even go tachyonic: with small variations over all the models we have considered, almost precisely half the fields have $m^2 < 0$ at the end of inflation.¹⁸ When plotted as a function of $\Delta\phi$, the bundle of eigenvalues is conical, which is indicative of the dominance of the cubic terms in the potential.

3.1.1 The ‘straying’ smallest mass-squared

Figure 4 also illustrates a curious and important feature of these models: the smallest eigenvalue decreases more rapidly than the others, and ‘strays’ from the conical bundle towards more tachyonic values. This ‘straying’ behaviour of the smallest eigenvalue has to our knowledge not been discussed previously in the literature, but appears for large N_f in essentially all inflationary models that we have studied. In sections 3.4 and 5, we will see that it contributes to some of the most interesting predictions of the inflationary GRF models.

While the rapid evolution of the smallest eigenvalue of the Hessian may appear surprising, it has a simple explanation in terms of the properties of the GRF potentials, and the dynamics of multifield slow-roll inflation. In our inflationary models, the initial values of both the gradient and the Hessian matrix are very small. This means that after a short field excursion, which typically involves some turn, the gradient and Hessian become dominated by the third-order terms. Without loss of generality, we may take the ‘1’-axis to be aligned

¹⁸On approach to the final vacuum configuration after inflation, these eigenvalues will again become positive.

with the field excursion at this point, with $\phi_1 > 0$. We then have,

$$V_a(\phi) \simeq \frac{1}{2}V_{a11}\phi_1^2, \quad V_{ab}(\phi) \simeq \frac{1}{2}V_{ab1}\phi_1. \quad (3.1)$$

With the initial gradient set to be small, the third derivatives are drawn from a distribution with a mean that is very close to zero and variances given by,

$$\text{Var}(\tilde{V}_{abc}) = \begin{cases} 6 & \text{if all indices are equal} \\ 2 & \text{if only two are equal} \\ 1 & \text{if none are equal.} \end{cases} \quad (3.2)$$

We then see that the magnitude of $V_1(\phi)$ is expected to be larger than the other components of the gradient. Furthermore, since $\phi_1 > 0$, we expect that $\dot{\phi}_1 \propto -V_1(\phi) > 0$, in which case V_{111} must be negative. We can therefore expect $V_{11}(\phi) = V_{111}\phi_1$ to be larger than the other elements of the Hessian matrix, and negative. Moreover, since $\text{Var}(V_{a11}) > \text{Var}(V_{ab1})$ for $b \neq 1$ (and $a \neq b$) the off-diagonal row-vector V_{1a} is expected to be larger in magnitude than the other row vectors. This will typically lead to a large negative mass-squared eigenvalue with an eigenvector approximately aligned with the gradient direction. This is precisely what we observe through the ‘straying’ smallest eigenvalue of the Hessian.

This evolution of the squared masses importantly affect the inflationary evolution of the field perturbations (as we will discuss in section 3.4), and also the background dynamics. In slow-roll inflation, the acceleration of the field is given by,

$$\phi_a'' = \sqrt{2\epsilon_V} \left(\frac{V_{ab}n_b}{V} - 2\epsilon_V n_a \right), \quad (3.3)$$

where $n_a = V_a/|V_a|$. We see that if $n_a \approx -\delta_a^1$, the acceleration tends to be large and positive in the ‘1’-direction. This will make the trajectory ‘straighten’ during this phase, and n_a will become closer and closer aligned with the direction of the smallest eigenvalue of the Hessian matrix.

The e-fold distribution of GRF models

An important factor influencing the observables is the distribution of the number of e-folds of inflation. Figure 5 shows the mean values and standard deviations of this distribution for various one-parameter variations from the baseline parameter choice of equation (2.44).

Unsurprisingly, flatter spectra lead to more e-folds of inflation. As the number of fields is increased, the e-fold distribution slowly shift to lower values, but the dependence is not very strong. For a given choice of hyperparameters, the distribution of the number of e-folds typically exhibits a broad peak and a ‘heavy’, polynomially decreasing tail corresponding to models with a large number of e-folds.

3.2 Smooth and simple power spectra from complex inflationary models

We now turn to observables generated by these models, focussing in this section on the power spectrum of the curvature perturbation, $P_\zeta(k)$. While many of the simplest models of single-field or few-field inflation naturally generate very simple, almost scale-invariant power spectra, there is no guarantee that highly complicated and random manyfield models should also do so. Turns of the field trajectory or bumps in the potential could generate strong deviations

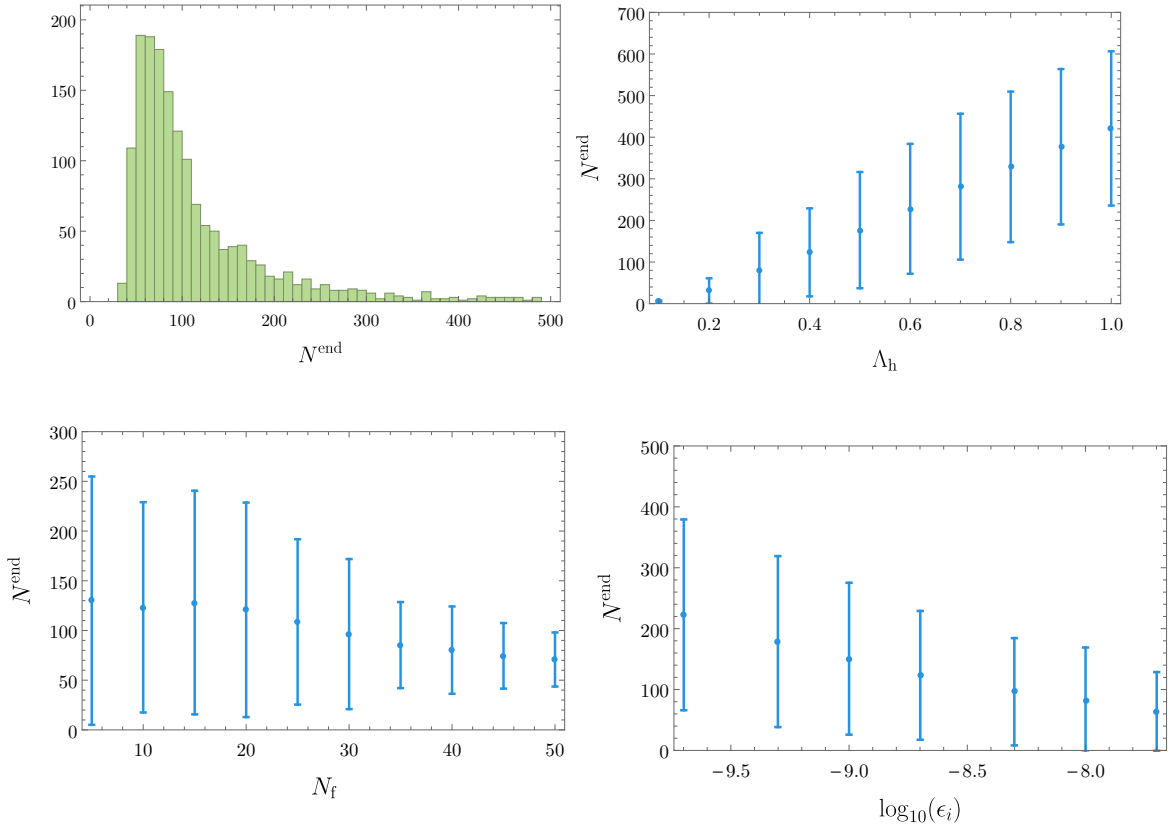


Figure 5: Histogram of the e-fold distribution of the baseline model (cf. equation (2.44)), and the dependence of the mean and standard deviation on the hyperparameters in one-parameter variations from the baseline. Each data point is generated from an ensemble of 2000 inflationary models.

from scale-invariance, and highly featured power spectra. Quite remarkably however, we here find that even random models involving several dozens of fields and millions of interaction terms typically produce extremely smooth and simple power spectra.

A sense of the typical properties of the generated power spectra can be inferred from Figure 6, which shows the power spectra for 15 randomly generated models with 10 (left) and 50 (right) fields. The top row shows the power spectra evaluated over the full range of scales exiting the horizon within the last sixty e-folds of inflation, while the plots of the bottom row zooms in on the 10 e-fold range centred at the ‘pivot scale’ corresponding to modes exiting the horizon 55 e-folds before the end of inflation. All plotted power spectra are evaluated at the end of inflation, $P_{\zeta}(N_{\text{end}}, k) = P_{\zeta}(k)$, and normalised at the pivot scale k_{\star} .

Over the full range of scales spanning 60 e-folds, the power spectra show strong deviations from scale-invariance, with rapidly decreasing power spectra for very small-scale modes. This drop in power is related to the rapid growth of the slow-roll parameter ϵ_V towards the end of inflation, which causes a speed-up of the field and a suppression of the power of the curvature perturbation. On zooming in on the scales most relevant for CMB observations, the generated power-spectra are very simple, and of an approximate power-law form. This simple form of the power spectra is common to all GRF models we have studied, independent of the precise

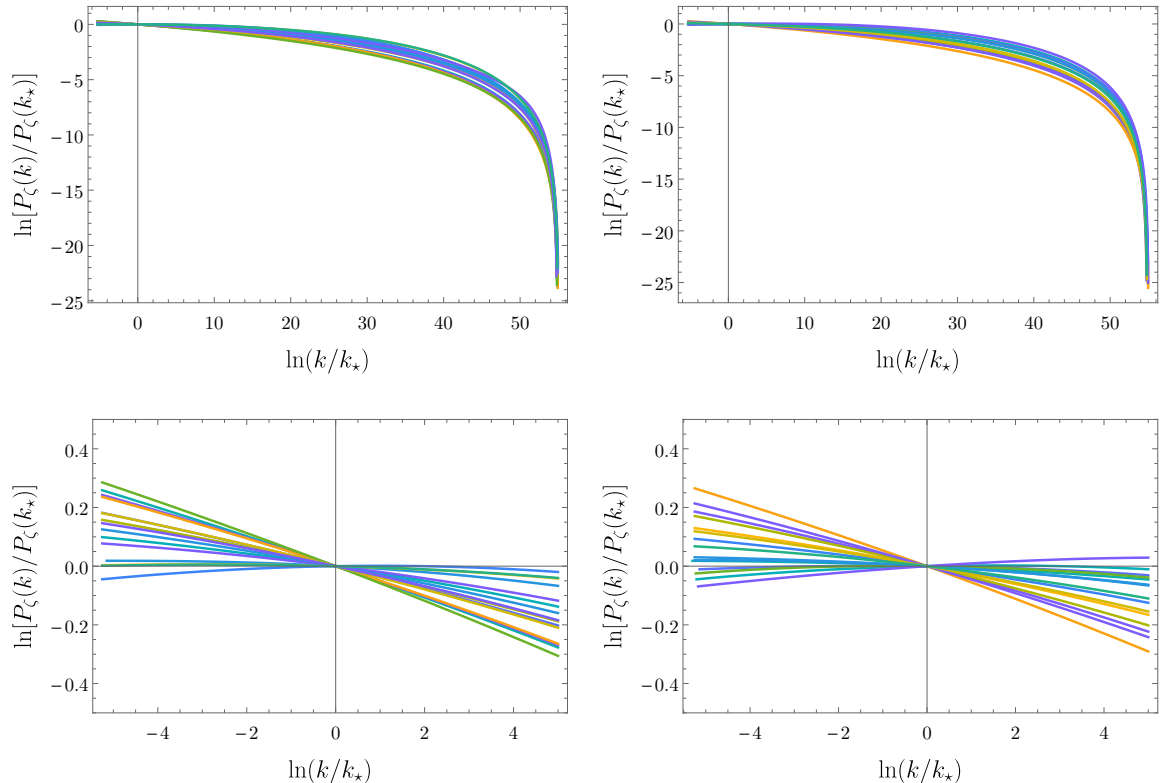


Figure 6: Examples of power spectra from 15 randomly generated models of GRF inflation for $N_f = 10$ (left) and $N_f = 50$ (right). Hyperparameters other than N_f are as in the baseline case, cf. equation (2.44).

choice of hyperparameters. We will now discuss the dependence of the detailed predictions of the models on the hyperparameter choices.

3.3 Distributions of n_s and α_s

The simple form of the power spectra around the pivot scales justifies fitting them by an approximate power-law,

$$P_\zeta(k) = A_s \left(\frac{k}{k_*} \right)^{n_s - 1}, \quad (3.4)$$

where we allow for a non-vanishing running of the spectral index, $\alpha_s = dn_s/d \ln k|_{k=k_*}$.

Figure 7 shows the aggregated values of (n_s, α_s) for 25,000 models of GRF inflation with N_f ranging between 5 and 50, and for varying values of the other hyperparameters.¹⁹ The distribution for n_s indicates that the power spectra are approximately scale-invariant, and that the spectra are more commonly red than blue (around 85% were red). For these values of the hyperparameters, the distribution for n_s is broader than current Planck constraints, but Planck-compatible values are not rare.

The statistical prediction for the running of the spectral index, α_s , is remarkably sharp. A small and negative running is vastly favoured (especially among the models with Planck-

¹⁹This aggregate consists of all models in the tables ‘varying N_f ’ and ‘ $N_f = 50$ ’ in Appendix C.

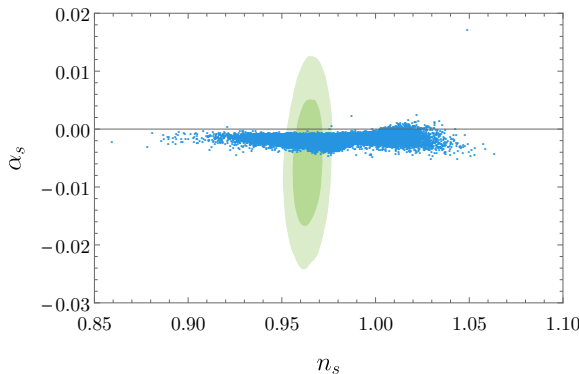


Figure 7: The distribution of n_s and α_s for 25,000 inflation models spanning values of N_{f} between 5 and 50, with the 68% and 95% confidence contours from Planck (TT+TE+lowP+lensing) [5].

compatible spectral indices), and these models could be ruled out should future experiments infer a positive or substantially negative running of the spectral index. Indeed, over 99% of these models, and all of those in the Planck 68% c.l. for n_s , fall in the range $-0.04 < \alpha_s < 0$. For the baseline hyperparameters, cf. equation (2.44), we find $n_s = 0.970 \pm 0.018$ and $\alpha_s = -0.00143 \pm 0.00034$. Normalising the amplitude of scalar perturbations fixes Λ_{v} , for the baseline models we find $\Lambda_{\text{v}} = 9.6 (\pm 1.7) \times 10^{-5}$.

The tensor-to-scalar ratio is very small in all models we have constructed. For the baseline parameters, we find $r = 3.07 (\pm 0.28) \times 10^{-8}$. Since the total field displacement during inflation is $\Delta\phi = 0.36 (\pm 0.04) \Lambda_{\text{h}}$ for these parameters, we see that the ‘Lyth bound’ [95] is far from saturated: in single-field models of inflation,

$$r = 16\epsilon_{\text{V}} < 8 \left(\frac{1}{N_{\text{exit}}} \right)^2 \left(\frac{\Delta\phi}{M_{\text{Pl}}} \right)^2, \quad (3.5)$$

if ϵ_{V} is constant or monotonically increasing, N_{exit} denotes the e-fold when the pivot scale crossed the horizon (in our case $N_{\text{exit}} = 55$), and $\Delta\phi$ denotes the total field displacement during inflation. Thus, for the mean-value base-line parameters, we find the bound $r < 5.5 \times 10^{-5}$. There are two reasons for the non-saturation of the Lyth bound. First, the field initially evolves very slowly, but speeds up super-exponentially towards the end of inflation. Second, we will see in section 3.4 that isocurvature modes tend to enhance the amplitude of the scalar perturbation, but leave the tensor perturbations untouched. This further suppresses the tensor-to-scale ratio r .

Figure 7 shows that manyfield GRF models can be compatible with current observational constraints on the power spectrum, but provide a sharp prediction for its running, and can be ruled out by future experiments. We now investigate how these predictions depend on the hyperparameters.

Figure 8 shows the dependence of n_s and α_s of ϵ_i and Λ_{h} . All data points are based on at least 1000 models except those with $\Lambda_{\text{h}} \leq 0.3$ or $\epsilon_i \geq 10^{-8}$ where fewer models gave sufficient number of e-folds, and the data points are determined from several hundred realisations. We first note that taking Λ_{h} large or ϵ_i small both have the effect of ‘flattening’ the potential, either globally or locally around $\phi = 0$. Figure 8 indicates that such a flattening makes the spectrum more red, and the statistical predictions for n_s and α_s become sharper. For

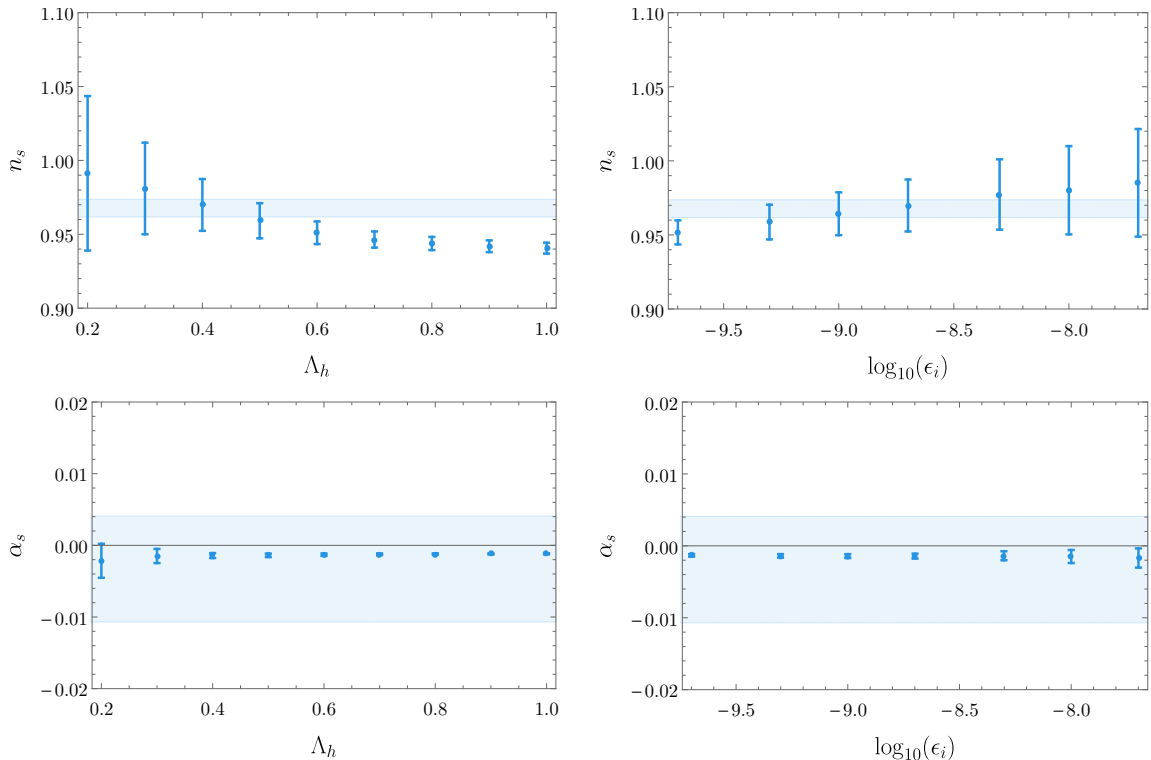


Figure 8: The spectral index and its running as functions of the smoothness of the potential in one-parameter variations from the baseline hyperparameters. The blue regions indicate the 68% c.l. from Planck (TT+lowP+lensing) [5].

large Λ_h , this reddening of the spectra make the models significantly discrepant with current observational bounds on n_s , making it possible to rule out this particular region of hyperparameter space with current observations (however, by increasing ϵ_i , the spectral indices at large Λ_h can be made compatible with Planck again). The distribution of the running of the spectral index is, by comparison, remarkably robust under changes to the hyperparameters. All sampled models are compatible with current constraints on α_s , and the prediction of a small negative running remains sharp as either ϵ_i is decreased or Λ_h is increased.

The observed relation between a flatter potential and a redder spectral index may appear surprising at first, as flatter potentials commonly give rise to more scale-invariant spectra. There is however a rather simple explanation of this empirical relation. The spectral index of the perturbations depends not only on the flatness of the potential, but also on its curvature. In a general multifield model,²⁰ the spectral index at the end of inflation is given by [85],

$$n_s - 1 = -2(\epsilon^* + e_a u_{ab}^* e_b) = 2 \frac{e_a V_{ab}^* e_b}{V^*} - 2 \left(\epsilon^* + \frac{e_a V_a^* V_b^* e_b}{V^*} \right), \quad (3.6)$$

where the \star subscript denotes quantities evaluated at horizon crossing, the symmetric tensor u_{ab} is defined as in equation (2.51), and the unit vector e_a , which encodes the possible

²⁰Assuming that at horizon crossing $\Sigma_{ab} = \delta_{ab} H_\star^2/2$, as we do throughout this paper.

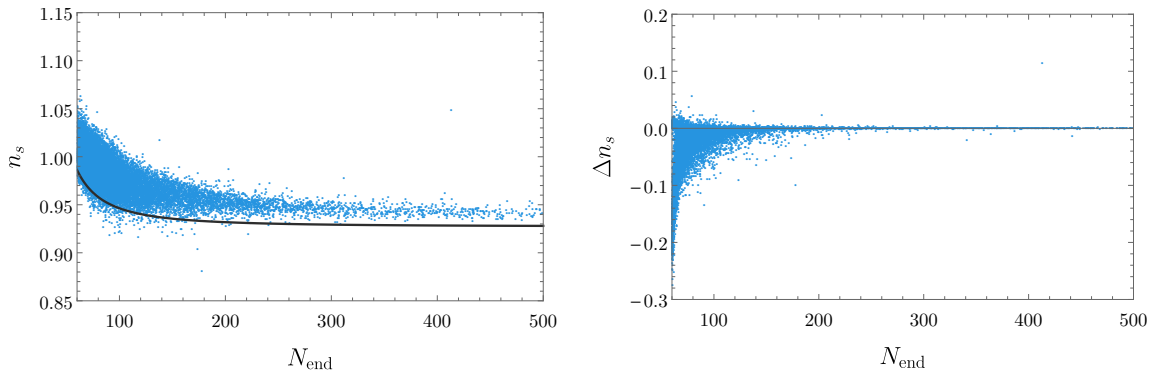


Figure 9: The distribution of (N^{end}, n_s) at the end of inflation (left) and the change of the spectral index on superhorizon scales, $\Delta n_s = n_s^{\text{end}} - n_s^*$, (right), for about 19,000 inflation models with uniform mass spectra, again spread over values of N_f varying between 5 and 50 (the same models as in Figure 7, but without the compressed spectra models). The black curve in the left graph shows the prediction of the single-field model discussed in Appendix D.

superhorizon evolution of the spectral index, is defined as,

$$e_a = \frac{N_b \Gamma_{ba}}{|N_c \Gamma_{cd}|}. \quad (3.7)$$

Physically, it relates the adiabatic perturbation at the end of inflation to field perturbations at horizon crossing. If there is no superhorizon evolution, e^a is aligned with the tangent vector of the field trajectory at N^* (i.e. $e_a \propto \partial_a V(\phi_*)$). However, if the spectral index evolves on superhorizon scales, e^a becomes misaligned, typically towards the most tachyonic directions.

In the approximate saddle-point models that we consider, the potentials need to be very flat around $\phi = 0$ in order to support sufficiently long periods of inflation, cf. Figure (5). The spectral index will therefore be dominated by the term involving the Hessian.

In inflationary realisations giving not much more than 60 e-folds of inflation, the pivot scale exits the horizon relatively early during inflation. At this point, the masses will not have had time to spread out much, and the gradient will in general not be aligned with the most tachyonic direction. The curvature perturbation will then typically undergo some evolution on superhorizon scales, and the vector e_a will develop components in both the adiabatic direction (at N^*) and the more tachyonic directions.²¹ A wide distribution of the spectral index is therefore expected in this case.

By contrast, in models supporting $\gg 60$ e-folds of inflation, the pivot scale typically exits the horizon when the gradient is dominated by the third-order coefficient in the Taylor series. In this case, the masses will have spread out more and both the gradient vector at N^* and e_a will, to good approximations, be aligned with the direction of the smallest eigenvalue of the Hessian. This results in a redder power spectrum, since the smallest mass eigenvalue has had time to decrease further. Moreover, the variance of the spectral index is smaller in these models, since the direction of e_a is much less random. These effects are visible in Figure 9.

²¹This also explains why the spectral index becomes redder due to superhorizon evolution, cf. Figure 9.

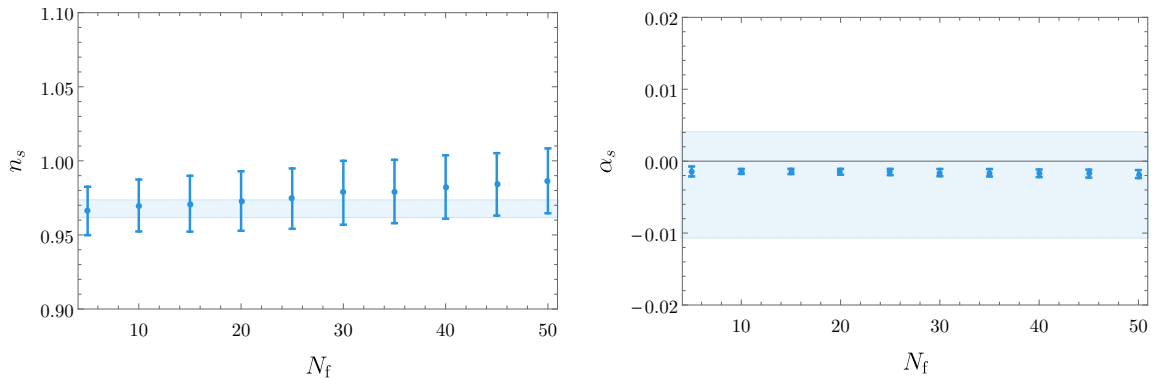


Figure 10: The spectral index and its running as a function of N_f in one-parameter variations from the baseline together with the 68% c.l. from Planck [5].

The relation between flatter potentials and redder power spectra is now easy to understand. With all else the same, a flatter potential generates more e-folds of inflation so that the horizon crossing of the pivot scale, 55 e-folds before the end of inflation, happens correspondingly later (in e-fold time) after the field has left $\phi = 0$. As per the discussion above, we then expect to see redder power spectra with smaller variances, which is precisely what we see when ϵ_i is decreased or Λ_h is increased.

We now turn to the effects of the number of fields, N_f , on the power spectrum. Figure 10 shows how the mean values and standard deviations of n_s and α_s are weakly dependent on N_f . First, we note that as N_f is increased, the spectra become less red and the variance of the spectral index also increases, albeit slowly. This may again be explained by the correlation between n_s and the total number of e-folds of inflation: as the number of fields is increased, the models tend to give fewer e-folds of inflation, cf. Figure 5, which leads to e_a developing non-vanishing components along multiple directions in field space.

In sum, we have found that the distribution for the spectral index in our GRF models tends to favour red, approximately scale-invariant spectra. Some regions of the parameter space lead to sharp predictions of excessively red spectra, and can be ruled out already with current observations. However, large regions of hyperparameter space are compatible with current constraints from the Planck experiment. More importantly, we have found that these models predict, sharply and robustly, a small negative running of the spectral index. The Planck experiment has constrained the running of the spectral index to $\alpha_s = -0.0033 \pm 0.0074$, but future experiments may reach a sensitivity of $\sigma(\alpha_s) = 10^{-3}$ [96]. A future observation of $\alpha_s \gtrsim 0$ or $\alpha_s \lesssim -0.004$ would rule out all Planck-compatible models that we have constructed.

3.4 Substantial superhorizon evolution, but also decaying isocurvature

We have seen in section 3.3 that the predictions from the random GRF models are remarkably simple, despite the underlying potentials being highly non-trivial functions of many fields. Indeed, the prediction of an approximate scale-invariant power spectrum with a small running of the spectral index agree with two of the ‘generic’ predictions of *single-field* models of slow-roll inflation. In this section, we investigate to what extent multifield dynamics is important for the predictions of the manyfield GRF models.

We begin by considering the superhorizon evolution of the pivot-scale modes exiting the horizon 55 e-folds before the end of inflation. We first recall that to linear order in the field

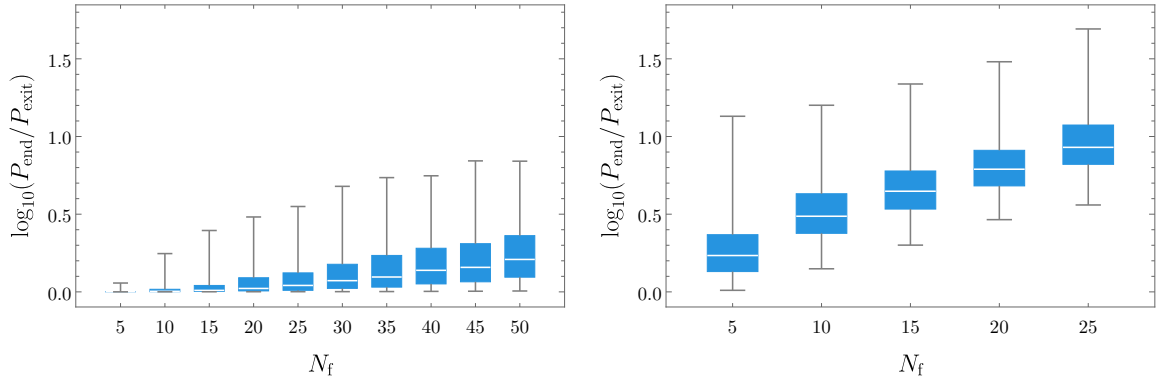


Figure 11: Superhorizon evolution of the mode exiting the horizon 55 e-folds before the end of inflation for the flat initial spectrum (left) and the compressed spectrum (right), cf. equation (2.42). Boxes indicate first and third quartile, together with the median; ‘whiskers’ indicate 1st and 99th percentile. The left graph shows a one-parameter variation from the baseline; the right shows models with $\Lambda_h = 0.4$, $\epsilon_i = 10^{-10}$ and $\eta_i = -10^{-4}$.

perturbations (and upon suppressing the k dependence), the modes at the end of inflation are related to the modes at horizon exit by the transfer equation [97–99],

$$\begin{pmatrix} \zeta \\ \mathcal{S}^i \end{pmatrix}_{\text{end}} = \begin{pmatrix} 1 & T_{\zeta \mathcal{S}^j} \\ 0 & T_{\mathcal{S}^i \mathcal{S}^j} \end{pmatrix} \begin{pmatrix} \zeta \\ \mathcal{S}^j \end{pmatrix}_{\star}. \quad (3.8)$$

For $\Sigma_{ab}^* \propto \delta_{ab}$ (as we assume in this paper, cf. equation (2.59)), the superhorizon evolution of the curvature perturbation is given by,

$$\frac{P_{\zeta}(N_{\text{end}}, k)}{P_{\zeta}(N_{\star}, k)} = 1 + \sum_{i=1}^{N_f-1} T_{\zeta \mathcal{S}^i}^2, \quad (3.9)$$

so that, under these assumptions, superhorizon evolution can only lead to a net increase in the power of the curvature perturbation. If $P_{\zeta}(N_{\text{end}}, k)/P_{\zeta}(N_{\star}, k) - 1 \lesssim 10^{-3}$ for a range of k modes, the observational predictions of the model can be regarded as safely independent of multifield effects, and the horizon crossing power spectrum determines the observational predictions for e.g. n_s and α_s . This rarely happens in manyfield models of inflation in GRF potentials.

The box plots in Figure 11 show the effects of varying N_f on the distributions of $\log_{10}(P_{\zeta}(N_{\text{end}}, k_{\star})/P_{\zeta}(N_{\star}, k_{\star}))$ for both the flat (left) and compressed (right) spectra. Each box is generated from over 1000 inflationary models, except for $N_f = 20$ and 25 for the compressed spectrum, which were generated from 600 and 200 models, respectively. Unsurprisingly, models with more fields and more compressed initial spectra exhibit larger superhorizon evolution. However, even for the flat spectrum, models with more than 5 fields tend to evolve substantially on superhorizon scales, so that the predictions at horizon crossing do not automatically give the predictions for observables at the end of inflation. Evidently, multi-field effects are important in manyfield inflation in GRF potentials.

In multifield models of inflation, the curvature perturbation may evolve well past the end of inflation, through the reheating phase. In many models of multifield inflation in the literature, this problem is dealt with by ensuring that the fields enter an approximately

single-field ‘adiabatic limit’ in which all but a single mode are very massive (i.e. $m^2 > H^2$) and the isocurvature modes decay exponentially. Once the isocurvature perturbations have decayed, the curvature perturbation ceases to evolve and the predictions are expected to become insensitive to the details of the reheating phase. As illustrated by Figure 4, the spectrum of the Hessian matrix of the GRF models we consider typically contains multiple tachyonic eigenvalues at the end of inflation so that, clearly, no standard adiabatic limit is reached. However, we will now see that isocurvature still becomes exponentially suppressed during inflation.

At horizon crossing, $\Sigma_{ab} \propto \delta_{ab}$ and $P_{\text{iso}}/P_\zeta = (N_f - 1)$, cf. equation (2.68). Figure 12 shows the mean values and standard deviations of the ratio P_{iso}/P_ζ evaluated at the end of inflation in our ensembles of models. Strikingly, the power in the isocurvature mode evolves during inflation from dominating over the curvature perturbation to becoming exponentially suppressed. For the flat initial spectrum and $N_f = 5$, the ratio P_{iso}/P_ζ falls below the numerical accuracy of our simulations. For larger N_f , this ratio typically remains exponentially suppressed. Models with the highly compressed initial spectrum feature larger levels of isocurvature at the end of inflation, but even in this extreme case, the superhorizon evolution suppresses the isocurvature perturbations by several orders of magnitude.

The suppression of the isocurvature despite multiple tachyonic directions can be understood as a consequence of the inflationary slow-roll dynamics, as discussed in [28]. To see this, we may re-express the components of the transfer matrix (3.8) in terms of the transport coefficients $\Gamma_{ab}(N, N_\star)$, using the decomposition of the fluctuations into instantaneous adiabatic and entropic fluctuations, cf. equation (2.62):

$$1 = \left(\frac{\epsilon_\star}{\epsilon_N} \right)^{1/2} n_a(N) \Gamma_{ab} n_b(N_\star), \quad (3.10)$$

$$T_{\zeta \mathcal{S}^i} = \left(\frac{\epsilon_\star}{\epsilon_N} \right)^{1/2} n_a(N) \Gamma_{ab} v_b^i(N_\star), \quad (3.11)$$

$$T_{\mathcal{S}^i \mathcal{S}^j} = \left(\frac{\epsilon_\star}{\epsilon_N} \right)^{1/2} v_a^i(N) \Gamma_{ab} v_b^j(N_\star). \quad (3.12)$$

Here $\epsilon_N = \epsilon(N)$ and equation (3.10) follows from the conservation of ζ in the absence of entropic perturbations. The appearance of multiple negative eigenvalues of the Hessian matrix leads to multiple growing field perturbations (and multiple eigenvalues of $\Gamma^T \Gamma$ that are greater than 1). In slow-roll inflation, the field velocity tends to align with the smallest eigenvalue of the Hessian matrix, cf. equation (3.3). This makes the adiabatic field perturbation grow faster than each of the less tachyonic entropic perturbations. However, from equation (3.10) we see that the growth of the adiabatic field perturbation (in the absence of additional sourcing from entropic modes) is directly related to the growth of $\epsilon(N)$.

For entropic modes that grow slower than the adiabatic perturbation, the decaying prefactor $\sqrt{\epsilon_\star/\epsilon_N}$ cause a net suppression of isocurvature during inflation. This explains why the isocurvature \mathcal{S} can decay during inflation, despite the presence of multiple tachyonic fields.

This discussion also makes it clear that the ‘straying’ behaviour of the smallest eigenvalue of the Hessian, discussed in section 3.1.1, leads to a further suppression of isocurvature modes during inflation. Furthermore, the associated ‘straightening’ of the field trajectory leads to fewer opportunities for the isocurvature to source the curvature perturbation through turns in field space, cf. equation (2.64).

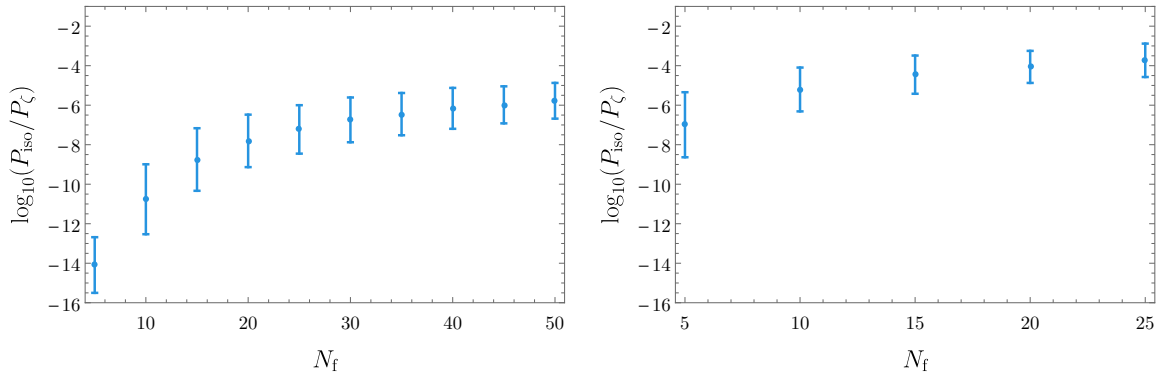


Figure 12: Isocurvature-to-curvature ratio at the end of inflation for flat (left) and compressed (right) initial spectra. Other hyperparameters as in Figure 11.

In sum, in this subsection we have seen that multifield effects are typically important in manyfield inflation, but that entropic perturbations tend to decay. While no single-field ‘adiabatic limit’ is reached during inflation in these models, the large suppression of isocurvature may shield observables from subsequent superhorizon evolution during the post-inflationary reheating phase. It would be interesting to apply our construction of GRF potentials to investigate the evolution of the adiabatic and entropic perturbations in reheating models with many interacting fields in more detail.

4 Result II: At large N_f , GRF and RMT models largely agree

A key motivation behind this work is to use mathematically simple constructions of manyfield systems to search for mechanisms that may drive observables to simple and robust predictions. Identifying such mechanisms could prove very helpful in analysing more complicated manyfield models motivated by fundamental theory. However, even for a given class of mathematically simple models, it can be hard to separate its particularities from the properties that may be more broadly applicable. It is therefore important to test the predictions of any class of models by comparing to the predictions of independent constructions. To make such comparisons useful, the different classes of models should share some rough similarities, but be fundamentally different in their details. For our purposes, we are interested in models of small-field, slow-roll, saddle-point inflation with many interacting fields. Fortunately, our construction of GRF models in this paper and the construction of random DBM potentials of [26, 28] now provide two such classes of theories, thus allowing the first critical tests of possible ‘universal’ predictions of random manyfield models of inflation.

In this section, we first briefly review the differences and similarities between the DBM models and our GRF models in section 4.1. Our discussion highlights the differences in the evolution of the Hessian matrix, but also clarifies the context of recent discussions on the equilibrium spectra of single-field and effectively single-field GRF models [52, 55]. In section 4.2, we then provide a first detailed comparison between the observational predictions of the DBM and GRF models. A brief review of the DBM construction can be found in Appendix E. We refer the reader to references [26, 28] for a more detailed discussion on the properties of DBM potentials.

4.1 Comparison of DBM and GRF potentials

The DBM construction of [26] led to the first explicit studies of models of inflation with many interacting fields in random potentials. As we mentioned in section 1 however, this prescription differs from GRF models in that the cubic and higher-order terms of the potential are regulator-dependent. In this section, we will discuss how some properties the Hessian matrices differ between the GRF and DBM potentials. For the purpose of clarity, we first compare the ‘*equilibrium spectra*’ of the models, i.e. the eigenvalue distribution of the Hessian matrix at some randomly chosen point in field space, and we then turn to the *evolution* of the Hessian, e.g. from a fine-tuned initial configuration to the equilibrium.

The equilibrium spectra of GRF and DBM models

In equation (2.28), we saw that the Hessian matrix in the GRF models consists of a GOE matrix and shift, proportional to the unit matrix times the negative of the value of the potential. We also noted that for $N_f \gg 1$ and typical values of the potential, this shift had a very small effect on the spectrum of the GRF. This way, the spectrum of the simplest GRF models is very similar to that of the simplest DBM model, which omits the shift entirely. In the light of this, it may appear surprising that a recent study claimed that the equilibrium spectrum constitutes a fundamental difference between the GRF and DBM models [55]. We here provide the context for these claims.

First, the variance of the GOE matrix in the simplest GRF model is fixed by the choice of covariance function. For equation (2.6), this leads to a width of the Wigner semi-circle spectrum of $4\sqrt{N_f}$, cf. equation (2.25). In the DBM model, the variance is a free parameter which is typically chosen so that the spectrum has an N_f -independent width. This choice makes it convenient to compare systems with different number of fields within a fixed mass-range, but other choices are possible, and clearly, the width of the equilibrium eigenvalue spectrum can hardly be described as a fundamental difference between the DBM and GRF constructions.

Second, one can try to make the shift of the spectrum more important even during inflation. To do so, one may attempt to inflate near the bottom of the potential, where the semi-circle spectrum is significantly ‘up-shifted’ from the centred Wigner semi-circle law. However, for the mean zero GRF models, any upward shift of spectrum only occurs for negative values of the potential, making inflation impossible. To construct models in which the shift is important, one may add to the mean-zero GRF a large, field-independent cosmological constant of size $\mathcal{O}(2\sqrt{N_f}\Lambda_v^4)$.²² The uplifted potential will then have a typical, 1σ range of $(2\sqrt{N_f} \pm 1)\Lambda_v^4$, as opposed to $\pm\Lambda_v^4$ for the mean-zero GRF. By construction, the equilibrium spectrum for small values of the potential is now a Wigner semi-circle with the left edge shifted to zero, and no tachyonic eigenvalues. We briefly discuss manyfield inflation in this class of potentials in Appendix F.

The substantially shifted spectrum of the Hessian of the modified GRF potential is (by construction) discrepant with the centred Wigner semi-circle, and thereby the equilibrium spectrum of the standard DBM model. This was key to the argument of reference [55], which proposed this discrepancy as a fundamental difference between DBM and GRF models. However, due to the simplicity of equation (2.28), it is straightforward to modify the DBM model

²² The addition of a large field-independent cosmological constant may appear ad-hoc, and to our knowledge, lacks a clear physical motivation. For example, sources of energy density in string compactifications tend to be moduli-dependent in the Einstein frame.

to capture the spectrum of any such modified GRF model.²³ Thus, it appears challenging to use simplistic arguments based on the equilibrium spectra of the DBM and GRF models to identify fundamental differences between these constructions.

The evolution of the Hessian matrix

The *evolution* of the Hessian matrix as the field traverses some path in field space constitutes a fundamental difference between the DBM and GRF constructions, even if the equilibrium spectra coincide. This difference is evident in the relaxation of the eigenvalues of the Hessian from an atypical initial configuration to the equilibrium configuration, as can be seen by comparing the 100-field DBM model of Figure 4 of reference [28] to our 100-field GRF model of Figure 4. The spectra of the GRF models relax in a much more linear, regular fashion. Moreover, in section 3.1.1 we showed that the statistical properties of the cubic terms in GRF potentials lead to ‘straying’ smallest eigenvalues in slow-roll inflation. This phenomenon has no counterpart in DBM models.

In sum, while both DBM and GRF models can be used to describe manyfield inflation, the two constructions are independent and differ substantially in several ways. Thus, by comparing the predictions of these two classes of models, we may search for robust and model-independent signatures of many-field dynamics during inflation.

4.2 Comparison of DBM and GRF predictions

In this section, we assess the robustness of the predictions from manyfield models of inflation by comparing our results derived in this paper to those derived from DBM models in [28]. The results of reference [28] were organised into ‘seven lessons’. We here test each of them.

1. **Manyfield inflation is not single-field inflation.** One immediate aspect of multifield models of inflation is that they typically contain several fields with masses not much larger than the Hubble parameter. Such ‘light’ fields cannot be integrated out, and commonly contribute to multifield effects that impact observables. In this sense, manyfield models of inflation are clearly not identical to single-field models.

In [26] however, it was shown that some aspects of the DBM models at large N_f (such as the distribution of e-folds), could be modelled by a single-field model. Reference [30] elaborated on this single-field model to estimate the spectral index of the large- N_f DBM models, however this single-field estimate was discrepant with the actual distribution computed from the DBM multifield models [27, 28]. Thus, single-field models have had a limited success in describing the properties of manyfield DBM models. Moreover, intrinsically multifield effects such as superhorizon evolution of the curvature perturbation are common in DBM models, which indicates that manyfield inflation differ from single-field inflation.

We have seen that in manyfield GRF models, multifield effects are also common: the field explores multiple directions in field space, isocurvature modes can be important, and the curvature perturbation typically evolves on superhorizon scales. These effects cannot be captured by a single-field model so that, evidently, manyfield inflation is different

²³For example, in direct analogy with equation (2.28), one may take $v_{ab}^{\text{tot}} = v_{ab}^{\text{DBM}} + \delta_{ab} f_{\text{shift}}(v_0)$, where only v_{ab}^{DBM} undergoes Dyson Brownian Motion, and the new term encodes the desired shift of the spectrum.

from single-field inflation.²⁴ It can still be interesting to explore how well a simple single-field model can capture the results of the GRF manyfield models. In Appendix D, we construct such a single-field model and show that its predictions qualitatively (but not quantitatively) agree with the more complicated GRF models.

In conclusion, for both GRF and DBM models, manyfield inflation is different from single-field inflation.

2. The larger the number of fields, the simpler and sharper the predictions.

For small N_f , the power spectra generated by the DBM models are heavily featured, and deviate strongly from scale-invariance. However, as N_f is increased, the predictions of these models become simpler, and the power spectra much more regular [27]. For $N_f \gtrsim 10$, the power spectra tend to be well described by an approximate power law, with a spectral index close to unity, and with a small negative running [27, 28].

By contrast, the GRF models studied here give simple predictions already for small N_f . As N_f is increased, the generated power spectra remain simple, but many of the predictions are only weakly dependent on N_f .

Thus, the DBM and GRF constructions differ in that the predictions of the former become simple as N_f is increased, while those of the latter are simple already for small N_f . At large N_f , both constructions predict simple power spectra.

3. Planck compatibility is not rare, but future experiments may rule out this class of models.

For $N_f \gtrsim 10$ in DBM models, the power spectra tend to be well described by an approximate power law, with a spectral index close to unity, and with a small negative running. These models can easily be compatible with current observational constraints on the power spectrum, and make a rather sharp prediction for a small negative running of the spectral index: $-0.004 \lesssim \alpha_s \lesssim 0$ at 1σ [27, 28].

In section 3.3, we saw that the GRF models predict a spectral index close to unity, and make a sharp prediction of a small negative running. Comparing Figure 7 to Figure 10 of [28], we see that the predictions of the two constructions also qualitatively agree: red spectra tend to be favoured, but (for a wide range of hyperparameters) not so red as to be incompatible with Planck observations. The prediction for the running is in both cases sharper than that for n_s , and the prediction from the GRF model agrees quantitatively with, but is sharper than, the prediction from the DBM models.

We conclude that observational compatibility and the prediction of a small negative running appear to be quite robust predictions of manyfield inflation in random potentials.

4. The smoother the potentials, the sharper the predictions. Reference [28] found that flattening the DBM potential by increasing Λ_h^{DBM} or decreasing ϵ_i led to sharper statistical predictions. In Figure 8, we have seen that the same sharpening occurs also for GRF models.

²⁴ Recently, reference [55] studied a GRF-motivated ‘multifield’ system with one light and many heavy fields, finding that this model gives rise to single-field dynamics. As we are interested in inflation with many dynamically important fields, our assumptions for the initial configuration differ from that of [55], and the question that we explore here – whether manyfield systems can be effectively described as single-field models – also differ significantly from whether an effectively single-field system is well-described by a single-field system.

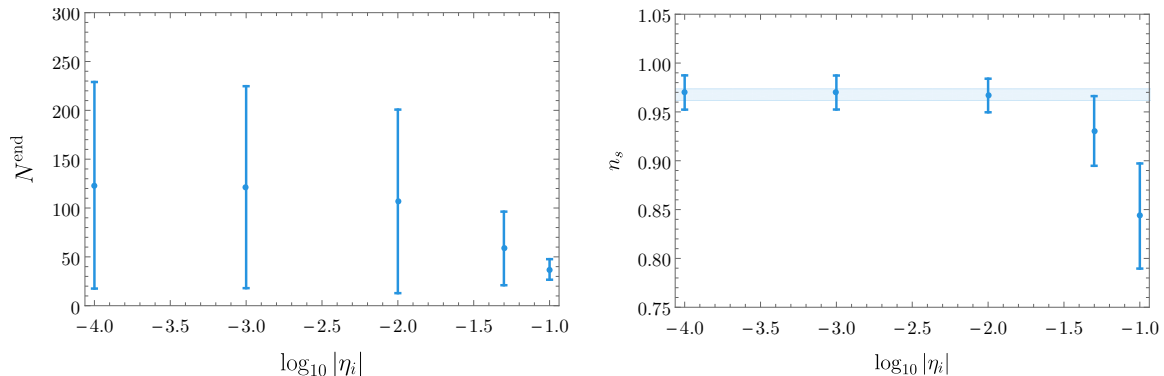


Figure 13: The total number of e-folds and n_s as functions of η_i , with other parameters as in the baseline and together with the 68% c.l. from Planck [5].

5. **Hyperparameters can transition from stiff to sloppy** A key finding of reference [26] was that ‘eigenvalue repulsion’ sharply reduces the duration of inflation near a critical point of the DBM potentials: even if the curvature of the potential is fine-tuned to be small at the critical point, small cross-couplings in the Hessian cause the curvature to grow in the neighbourhood of the critical point. As the field evolves from $\phi = 0$ in DBM models, the eigenvalues of the Hessian matrix relax towards the equilibrium configuration, and quickly spoil any initial fine-tuning of the η_V parameter. As a consequence, it was shown in [26] that the number of e-folds becomes independent of η_i for $|\eta_i| \lesssim 0.01$. Reference [28] furthermore showed that also the spectral index and its running are independent of $|\eta_i|$, if similarly small, and interpreted this behaviour as a ‘stiff-to-sloppy’ transition of the hyperparameter η_i .

As discussed in section 4.1, the evolution of the Hessian matrix in the DBM and GRF models differ significantly, and the η_i -dependence of the predictions of the GRF models provides a non-trivial test of the robustness of the DBM results. This is particularly interesting as reference [55] recently used an effectively single-field system motivated by uplifted GRF potentials to propose that the ‘steepening’ responsible for the η_i independence is absent in GRF models.²⁵

For the GRF models studied in this paper, Figure 13 settles this question. For $-\eta_i \gtrsim 0.01$, the predictions depend strongly on η_i , as the initial curvature of the potential curbs the duration of inflation. By contrast, for $-\eta_i \lesssim 0.01$ the predictions become independent of the precise value of η_i , as the initial fine-tuning of the Hessian matrix is quickly spoiled when the field moves away from the saddle-point. The distribution of the number of e-folds and the predictions for n_s then stabilise, and become independent of η_i . The running, α_s , while not plotted, is independent of η_i whenever n_s is. Thus, while the evolution of the Hessian matrix differ between GRF and DBM models, the prediction of η_i independence holds for both constructions. This strongly suggests that in models in which the eigenvalue spectrum relaxes from an initial, fine-tuned spectrum to a more generic spectrum that includes some tachyonic eigenvalues, the predictions become independent of the initial curvature of the potential for small $|\eta_i|$.

²⁵The authors of references [52, 55] also state that this ‘steepening’ leads to strong deviations from scale-invariance in DBM models of inflation, but the power spectra of these models are commonly consistent with small deviations from scale invariance [27, 28].

6. **Despite tachyons, isocurvature can decay.** In section 3.4, we found that despite the presence of multiple tachyons, isocurvature tends to decay during inflation in GRF models. This suppression of isocurvature was previously observed in DBM models in [28], and was there similarly explained as a dynamical consequence of multi-field slow-roll inflation. Comparing our Figure 12 to Figure 17 of [28], we see that dependence of the end-of-inflation values of $P_{\text{iso}}(k_*)/P_\zeta(k_*)$ on N_f qualitatively agree between DBM and GRF models: for small N_f , the suppression is most severe, but it remains exponential for large N_f .

Our work provides suggestive evidence for a rather model-independent suppression of isocurvature perturbations in small-field slow-roll inflation. This is non-trivial, as no single-field ‘adiabatic limit’ is reached in these models, which typically contain many tachyons.

7. **Eigenvalue repulsion drives the predictions.** In DBM models, several of the predictions at large N_f can be explained by eigenvalue repulsion [26–28]. In particular, the non-generic spectrum in the initial patch quickly relaxes towards the Wigner semi-circle distribution as a consequence of eigenvalue repulsion. This relaxation explains the independence on η_i , the tendency towards red spectral indices, the negative running, and the observed regularity of the power spectra for large N_f .

In GRF models, the eigenvalues of the Hessian repel in a linear fashion over small field-space distances, leading to the cone of eigenvalue trajectories observed in Figure 4. In section 3.1.1, we showed that the statistical properties of the cubic terms of GRF potentials lead to a ‘straying’ behaviour of the smallest eigenvalue in slow-roll inflation, which is then repelled to tachyonic values at a faster rate than other eigenvalues. Also for the GRF models, we have been able to relate the predictions of the model to properties of the relaxation of the spectrum from a fine-tuned initial configuration to the (slightly shifted) semi-circle. Thus, also for the GRF models, eigenvalue repulsion drives the predictions.

In sum, six out of the seven ‘lessons’ from manyfield inflation in DBM potentials derived in [28] apply also to manyfield inflation in GRF potentials. The single lesson for which the predictions differ involves the properties of the models for small N_f , in which the details of the constructions evidently are very important. For $N_f \gg 1$, the predictions of these very different constructions agree, which may be indicative of an emergent limit of inflation in which disparate classes of potentials make the same ‘universal’ predictions.

5 Result III: $f_{\text{NL}} \sim \mathcal{O}(1)$ is very rare in manyfield inflation

We are now ready to discuss the main result of this paper: the levels of primordial non-Gaussianities (NGs) generated in models of manyfield inflation with random potentials. Upcoming cosmological experiments are set to target $f_{\text{NL}} \equiv f_{\text{NL}}^{\text{local}}$, and are expected to reach a sensitivity of $\sigma(f_{\text{NL}}) \sim \mathcal{O}(1)$ over the next few years [7–13]. The results presented in this section provide important insights into what we can realistically hope to learn from these experiments.

In inflationary models with multiple canonically normalised fields, the level of non-Gaussianity at horizon exit is commonly very small [15, 16]. Substantial amplitudes of local NG, i.e. $f_{\text{NL}} \sim \mathcal{O}(1)$, can be generated through superhorizon evolution of the curvature

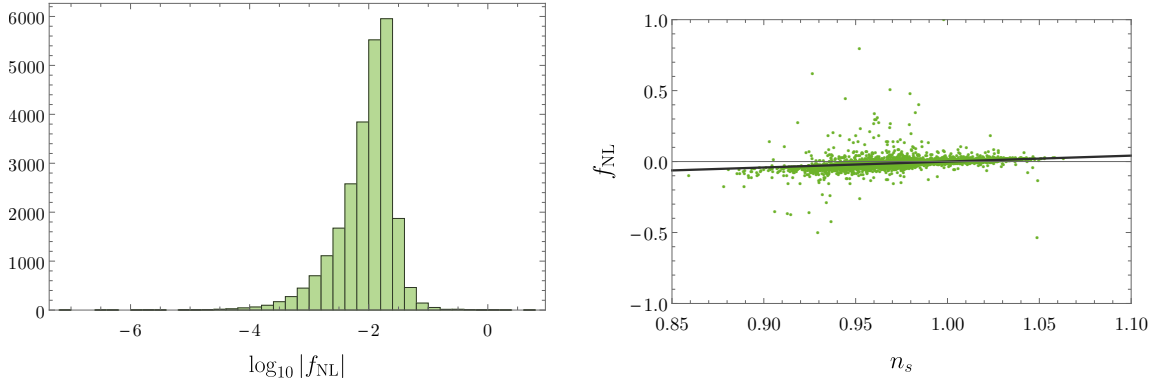


Figure 14: Values for f_{NL} and n_s for 25,000 random inflation models, spanning values of N_f between 5 and 50 (the same as in Figure 7). The black line in the right plot indicates the single-field consistency condition: $f_{\text{NL}} = \frac{5}{12}(n_s - 1)$. NB: the graph on the right excludes six points with $|f_{\text{NL}}| > 1$.

perturbation, either during inflation or after the end of inflation (cf. e.g. [15, 16, 100–105] and [14] for a review). In this section, we use the transport method and δN formalism to compute f_{NL} in our ensembles of randomly generated models of manyfield inflation.

The main result of this section is illustrated by Figure 14: here n_s and f_{NL} are plotted for an aggregate of 25,000 random inflation models, spanning values of N_f between 5 and 50, with both flat and compressed initial mass spectra, cf. equation (2.42). The levels of non-Gaussianity is generally very small for these models, with the vast majority having $f_{\text{NL}} \sim \mathcal{O}(0.01)$. Out of the 25,000 models, only six had values of $|f_{\text{NL}}| > 1$ (these fall outside the boundaries of the right plot of Figure 14). Moreover, most realisations even approximately follow the single-field consistency condition between f_{NL} and n_s . For the baseline ensemble of 1000 models (with parameters as in equation (2.44)), we find $f_{\text{NL}} = -0.012 \pm 0.008$ (at 68% confidence level).

Single-field inflation generates only small levels of NG, and multifield effects are necessary for large f_{NL} . However, multifield effects do not suffice to ensure $|f_{\text{NL}}| \sim \mathcal{O}(1)$. The left plot of Figure 15 shows the relation between f_{NL} and the superhorizon evolution, as given by $\log_{10}(P_\zeta(N_{\text{end}})/P_\zeta(N_\star))$, for these 25,000 models of inflation. Large values of f_{NL} are only observed in models with some level of superhorizon evolution, but many models with a large ratio of $P_\zeta(N_{\text{end}})/P_\zeta(N_\star)$ produce low levels of non-Gaussianity.

There is however a stronger relation between large f_{NL} and the amount of surviving power in the isocurvature modes at the end of inflation, as the right plot of Figure 15 shows. All the cases with large f_{NL} have a ratio of isocurvature modes to adiabatic modes (at $k = k_\star$) of at least $\mathcal{O}(0.01)$. In these models, the curvature perturbation may continue to evolve after the end of inflation, and it is necessary to model the reheating phase to determine the final value of f_{NL} relevant for CMB and Large Scale Structure (LSS) experiments. Only in a handful instances with the highly compressed initial mass spectrum did f_{NL} increase to $\mathcal{O}(1)$ during inflation, but decrease again by the end of it. In Appendix F, we provide case studies of a typical 100-field model (with small f_{NL}) and one of the rare cases of a 25-field model yielding $f_{\text{NL}} \sim \mathcal{O}(1)$.

The statistical prediction of small f_{NL} is robust under changes to the hyperparameters. The number of fields, N_f , has no noticeable effect on f_{NL} : large NGs are rare for all values

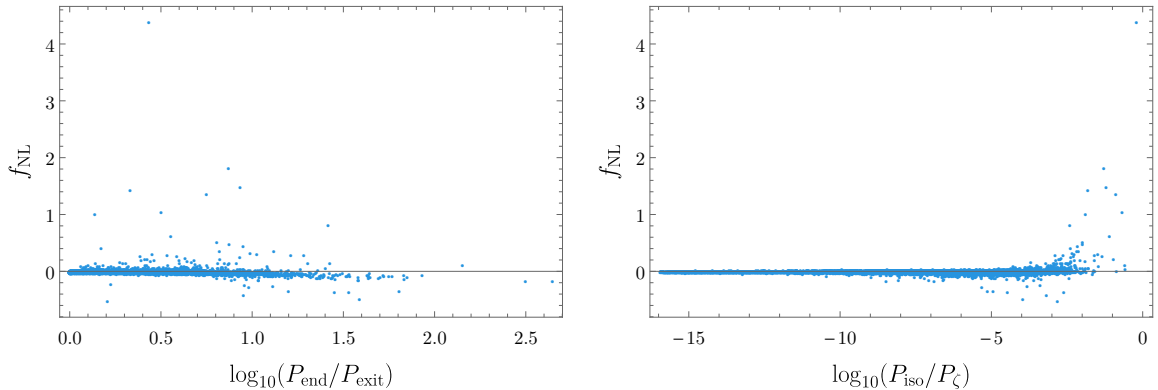


Figure 15: Superhorizon evolution and surviving isocurvature for the same models as in Figure 14.

we have considered. We find a weak dependence on the flatness of the potential: when the potential becomes very flat and the superhorizon evolution decreases (cf. our discussion in section 3.3), the values of f_{NL} follow the single-field consistency relation very closely, and large values of f_{NL} become more rare. We find that f_{NL} is independent of $|\eta_i|$, except the largest values of $|\eta_i|$ we investigate, for which large values of f_{NL} become slightly more common.

The initial mass spectrum at $\phi = 0$ does however have a clear impact on the levels of f_{NL} generated. For the flat spectrum with the eigenvalues of the Hessian uniformly distributed between $3\eta H^2$ and $9H^2/4$, large values of f_{NL} are exceedingly rare: in 19,000 examples with values of N_f varying between 5 and 50 we found only one model with large f_{NL} (see Appendix F). By contrast, with the (rather extremely) compressed initial spectrum where the masses are spread between $3\eta H^2$ and $-3\eta H^2$, we saw 5 in a sample of around 6,000. Thus, while large values of f_{NL} are still rare, near-degenerate initial spectra appear to make large NGs more frequent.

5.1 Why so small?

We have found that in randomly generated models of inflation involving many coupled fields, large values of f_{NL} are very rare. In this section, we discuss the main reasons for this suppression of non-Gaussianities.

The smallness of f_{NL} in our class of models resonates with previous results on the generation of non-Gaussianity through non-derivative interactions during multifield inflation. Reference [16] derived an analytic formula for f_{NL} in multifield models of inflation with sum-separable potentials (thereby generalising the two-field result of [15]), and found that large non-Gaussianities are very rare in slow-roll models with N_f free fields. In particular, f_{NL} was found not to be enhanced as N_f was increased, consistent with our findings. Moreover, two-field models generating large non-Gaussianities during inflation tend to require substantial levels of fine-tuning, cf. [14, 18, 106–108].

To understand the smallness of f_{NL} in these random manyfield models, it is illuminating to consider the re-expression of the δN formula for f_{NL} derived in [18, 19]. In our notation, generating large f_{NL} in slow-roll, slow-turn models of multifield inflation requires a large

contribution from the term,

$$f_{\text{NL}} \supset \frac{5}{6} \sqrt{2\epsilon_\star} \frac{T_{\zeta\mathcal{S}}^2}{(1 + T_{\zeta\mathcal{S}}^2)^2} h^j \partial_j^* T_{\zeta\mathcal{S}}. \quad (5.1)$$

Here $T_{\zeta\mathcal{S}} \equiv \left(\sum_i T_{\zeta\mathcal{S}_i}^2\right)^{1/2}$, and $h^i = e_b v_b^i(N^*)/|e_c v_c^j(N^*)|$, cf. equations (2.62), (3.7) and (3.11). Here also, ∂_j^* denotes a derivative with respect to the field-space position of the trajectory at horizon crossing in an entropic direction. Equation (5.1) has two important consequences: first, to generate large NG, some superhorizon evolution of the curvature perturbation is necessary ($T_{\zeta\mathcal{S}} \neq 0$). However, too much superhorizon evolution suppresses f_{NL} . Second, large f_{NL} is only possible if the level of superhorizon evolution of P_ζ is a very sensitive function of the initial conditions, so that $|h^j \partial_j^* T_{\zeta\mathcal{S}}| \gtrsim \mathcal{O}(1/\sqrt{\epsilon_\star})$.

In our GRF models, $T_{\zeta\mathcal{S}}$ is commonly $\mathcal{O}(1)$, and the factor $T_{\zeta\mathcal{S}}^2/(1 + T_{\zeta\mathcal{S}}^2)^2$ does not strongly suppress f_{NL} . However, the amount of superhorizon evolution is rarely a highly sensitive function of the initial conditions: trajectories separated by some small, initial perturbations $|\delta\phi_\perp^*| \ll \Lambda_h$ tend to follow very similar paths in field space, and do not generate drastically different $T_{\zeta\mathcal{S}}$. Consequently, $|h^j \partial_j^* T_{\zeta\mathcal{S}}|$ is typically not large enough to generate appreciable levels of NGs.

The decay of isocurvature in multifield, saddle-point models of inflation (cf. our discussion in section 3.4) contributes to the typical smallness of f_{NL} . When the entropic perturbations \mathcal{S}^i have decayed sufficiently, $T_{\zeta\mathcal{S}}$ ceases to be sourced, and no additional initial condition dependence is induced. This way, the decay of \mathcal{S}^i limits the period during which large NGs could be generated. We also note that $T_{\zeta\mathcal{S}}$ tends to be sensitive to the initial conditions precisely when entropic, off-trajectory perturbations are important. This provides a heuristic explanation for why the isocurvature tends to be large in the few examples we found with $f_{\text{NL}} \sim \mathcal{O}(1)$.

We close this section by noting how large f_{NL} may be more frequent in modifications of our construction. Models with very sharp turns or in which nearby classical background trajectories rapidly diverge can lead to substantial non-Gaussianities (see e.g. [109, 110]). In our construction of the potentials, cf. equation (2.7), all terms in the potential are suppressed by the same ‘UV cutoff scale’ Λ_h , which makes features or sharp turns on scales $\ll \Lambda_h$ very rare, even if the interaction terms are random. Large f_{NL} may be more common in multi-scale potentials with features on small scales, at least if these appear along the trajectory before the isocurvature has decayed.

Finally, our results do not preclude large values of f_{NL} being generated after inflation, during the reheating phase, as is the case in many ‘spectator’ models, cf. [111–115]. However, in models with general interactions and exponentially suppressed isocurvature at the end of inflation, generating large f_{NL} through reheating dynamics may remain challenging.

To get a rough sense of the reheating dynamics required in order for isocurvature to become relevant during reheating, we consider a modified version of the curvaton scenario [112] with two fields: the inflaton, ϕ , and the curvaton, σ . For simplicity, we assume that the fields are free, without mutual interactions, and decay instantaneously at $H(t_\phi) = \Gamma_\phi$ and $H(t_\sigma) = \Gamma_\sigma < \Gamma_\phi$, respectively. The inflaton is assumed to decay into radiation, which initially dominates the energy density, while σ oscillates around the vacuum, with an energy density that red-shifts like matter. At the time t_σ , the curvaton is assumed to have come to dominate the energy density. The total energy density during the period $t_\phi < t < t_\sigma$ is given

by,

$$\rho = \rho_r + \rho_\sigma = \rho_r(t_\phi) \left(\frac{a(t_\phi)}{a(t)} \right)^4 + \rho_\sigma(t_\phi) \left(\frac{a(t_\phi)}{a(t)} \right)^3. \quad (5.2)$$

With these assumptions, the total curvature perturbation is given by [112],

$$\zeta = \frac{4\zeta_r + 3\frac{\rho_\sigma}{\rho_r}\zeta_\sigma}{4 + 3\frac{\rho_\sigma}{\rho_r}}, \quad (5.3)$$

where ζ_r and ζ_σ are separately conserved and respectively correspond to the curvature perturbations induced by ϕ and σ . Highly suppressed isocurvature at the end of inflation corresponds to $\zeta_r \gg \zeta_\sigma$ (this assumption differs from those of the curvaton scenario in which ζ_r is taken to be negligibly small). The curvaton will become important during reheating if,

$$\frac{\rho_\sigma(t_\sigma)}{\rho_r(t_\sigma)} \gtrsim \frac{\zeta_r}{\zeta_\sigma}. \quad (5.4)$$

Using equation (5.2), we may write this condition as,

$$\left(\frac{\rho_\sigma(t_\phi)}{\rho_r(t_\phi)} \right) \left(\frac{\rho_\sigma(t_\phi)}{3\Gamma_\sigma^2 M_{\text{Pl}}^2} \right)^{1/3} \gtrsim \frac{\zeta_r}{\zeta_\sigma}. \quad (5.5)$$

Writing $\rho_\sigma(t_\phi) = \beta \rho_r(t_\phi)$ for $\beta \ll 1$, this equation can be written as a simple condition on the decay rates,

$$\frac{\Gamma_\phi}{\Gamma_\sigma} \gtrsim \frac{1}{\beta^2} \left(\frac{\zeta_r}{\zeta_\sigma} \right)^{3/2}. \quad (5.6)$$

This indicates that an exponential hierarchy of decay rates is necessary for initially suppressed isocurvature to become important during reheating. We note in closing that this argument is simplified and relies on assumptions that are not expected to hold for GRF potentials (e.g. the absence of interactions). We expect to return to the question of manyfield reheating in more detail in future work (see also [116–119] for some recent studies of this and related questions).

6 Conclusions

In this paper, we have studied inflation in models with multiple fields subject to randomly generated interaction terms. We have used Gaussian random fields (GRFs) with a Gaussian covariance function to model the scalar potentials locally around an approximate saddle-point in field space. These potentials admit an interpretation as proxies for physical effective field theories, and exhibit structure over field space distances of $\Lambda_h < M_{\text{Pl}}$. By identifying and systematically applying algebraic simplifications to the covariance matrix of the Taylor coefficients, we have for the first time been able to use this method to construct explicit scalar potentials with many interacting fields. Our examples include 100-field models involving 97 million independent, randomly generated couplings.

We used these potentials to construct models of slow-roll inflation with many dynamically important fields, i.e. models of manyfield inflation. By using the transport method and the δN formalism, we computed the primordial perturbations generated during inflation, including the curvature and isocurvature modes, and the amplitude of local non-Gaussianity, f_{NL} . These studies led to several novel results.

Summary of findings

As the fields evolve from the approximate saddle-point where the mass spectrum is fine-tuned, the eigenvalues of the Hessian ‘relax’ towards a shifted semi-circle distribution. This relaxation is, over short distances, driven by the cubic terms in the potential. We have shown that a combination of the statistical properties of Gaussian random fields and the dynamics of multifield slow-roll inflation leads to a particularly fast relaxation of the smallest eigenvalue of the Hessian, making it ‘stray’ from the other eigenvalues. This ‘straying’ has important consequences for the observational predictions of the models.

The generated power spectra of the GRF models are very simple, close to scale-invariant and well-described by an approximate power law. We have shown that large regions of the (hyper-)parameter space are compatible with current observational constraints on the spectral index. However, some regions, in particular those describing very flat potentials, are already ruled out by the Planck experiment.

These models make a robust prediction for the running of the spectral index. A small negative running is vastly preferred, and a future observation of α_s outside the range $-0.004 \leq \alpha_s \leq 0$ would, together with existing Planck constraints, rule out all models that we have constructed. For our baseline 10-field model (cf. equation (2.44)), we find $\alpha_s = -0.00143 \pm 0.00034$ (at 68% confidence level).

A striking aspect of these models is that while several fields go tachyonic during inflation and the curvature perturbation commonly evolves significantly on superhorizon scales, the power in the isocurvature modes decays during inflation. We have explained this phenomenon, also observed in [28], as a consequence of multifield slow-roll dynamics, in which the adiabatic mode tends to align with the most rapidly growing field perturbation. The suppression is further enhanced by the ‘straying’ of the smallest eigenvalue of the Hessian matrix. The exponential suppression of isocurvature during multifield slow-roll inflation makes the predictions less sensitive to the details of the reheating phase, and could make models involving large numbers of dynamically important fields comfortably compatible with CMB constraints on isocurvature.

We have furthermore critically assessed the similarities and differences between our models and those recently constructed using the random matrix theory ‘DBM’ technique [26–28]. We have argued that these constructions provide fundamentally different descriptions for the evolution of the eigenvalues of the Hessian matrix,²⁶ yet strikingly, six out of the seven ‘lessons’ from manyfield inflation in DBM potentials found in reference [28] also hold for our GRF models, with the only difference being related to properties of the models at small N_f . This suggests that, at large N_f , these very different constructions may fall in the same ‘universality class’ of inflationary models.

Finally, we computed the level of local non-Gaussianity (NG) generated by multifield effects on superhorizon scales and found that, typically, it is very small, with $|f_{\text{NL}}| \ll 1$. For the baseline parameters we found $f_{\text{NL}} = -0.012 \pm 0.008$ (at 68% confidence level). The smallness of f_{NL} is largely independent of the choice of hyperparameters, and constitutes a robust statistical prediction of these models. We found that f_{NL} is typically small even in models in which multifield effects are important and in which the superhorizon evolution of the perturbations is substantial. In a handful of models, we found $f_{\text{NL}} \sim \mathcal{O}(1)$. However, all models with large f_{NL} that we found also have comparatively large levels of isocurvature

²⁶By contrast, the equilibrium spectra of these models only differ superficially, and are easily rendered compatible. Our discussion in sections 2.3 and 4 may be useful for readers interested in the context of some recent results comparing GRF and RMT models [52, 55, 70].

remaining at the end of inflation, which may affect the predictions of the models through the reheating phase. We have argued that the suppression of f_{NL} is a consequence of the robustness of the multifield evolution to small modifications of the initial conditions, and the decay of isocurvature during inflation.

Our results indicate that multifield models of inflation do not generically predict $f_{\text{NL}} \sim \mathcal{O}(1)$, and that large classes of models including the slow-roll, saddle-point GRF models we have constructed, typically yield $|f_{\text{NL}}| \ll 1$. This suggests that a future detection of f_{NL} of order unity would point to rather special, non-random inflationary dynamics.

Future directions

There are a number of possible extensions to this work. We anticipate that our method can be varied and applied to other scenarios involving GRF potentials. Our focus in this paper has been on inflation for typical values of the potential in the simplest mean-zero GRFs, and we have only briefly discussed some variations involving a field-independent cosmological constant in Appendix F. There, we found a remarkable agreement of the predictions between saddle-point models of inflation for the mean-zero and the ‘uplifted’ GRF models. It would be interesting to obtain a broader understanding of the possible range of multifield inflationary scenarios that can be investigated through GRF potentials. Moreover, our choices for the initial conditions at the approximate saddle point have been motivated by simplicity, and could be generalised.

In section 2.3.2, we noted that our class of potentials share many properties with physical effective field theories valid below the cutoff scale Λ_{h} . Features on scales $\ll \Lambda_{\text{h}}$ are very rare in such models. It would be interesting to investigate multiple-scale extensions of this construction, in which such sharp features would be more common. Relatedly, it would be interesting to apply our methods to theories in which the mass-scale of the fields is naturally of the order of the Hubble parameter, for example by constructing supergravity theories with randomly generated superpotentials [36]. Such a description could also make it possible to tighten the connection between mathematically simple models of manyfield inflation and fundamental physics.

By truncating the potential at a very high order, $n_{\text{max}} \gg 1$, it is also possible to use our method to describe large potential ‘landscapes’ for models with a few fields (cf. Figure 1). This can be applied to study manyfield dynamics in the post-inflationary reheating phase, which may lead to further insights into the evolution and fate of isocurvature perturbations and non-Gaussianities. With a larger landscape it becomes possible to follow both the fields and their perturbations through the inflationary phase and then down to the vacuum. This has however has been left for future work. These high-order, low-dimensional potentials can also be large enough to include false vacua, inflationary regions, and ‘final’ vacua with small cosmological constants, and may serve as testing grounds for various other theoretical ideas.

Finally, we have limited our studies to geometrically flat field spaces ($\phi \in \mathbb{R}^{N_{\text{f}}}$), and it would be very interesting to include derivative interactions and non-trivial field space geometries. Highly curved field spaces can have strong impact on the background dynamics (see e.g. [110, 120–124]), but already weak interactions can lead to bispectrum signals beyond the local shape. For example, interactions between a single, light, self-interacting isocurvature field, Σ , and the inflaton, Φ , of the form,

$$\mathcal{L}_{\text{mix}} = -\frac{1}{2} \frac{\Sigma}{\Lambda} (\partial\Phi)^2, \quad (6.1)$$

can lead to large amplitude non-Gaussianities, even if $\Lambda \gg H$ [125, 126]. Finally, these models could be extended to include non-minimal couplings of the fields to gravity, cf. e.g. [127–131].

In closing, we note that the method developed in this paper opens a new window towards general models of inflation with many fields subject to non-trivial interactions. Our findings speak for the robustness of the inflationary paradigm: adiabatic, approximate scale-invariant and nearly Gaussian perturbations are commonly regarded as the ‘generic predictions’ of single-field slow-roll inflation. In this paper, we have shown that even highly complex models of manyfield inflation produce very similar predictions. We anticipate that these results can be useful in interpreting the outcomes of future cosmological observations.

Acknowledgements

We are very grateful to Mustafa Amin, Tobias Baldauf, Daniel Baumann, James Fergusson, Bogdan Ganchev, Alan Guth, Liam McAllister, Christopher Moore, Sonia Paban, Enrico Pajer and Paul Shellard for stimulating discussions. We would in particular like to thank Thomas Bachlechner, Mafalda Dias and Jonathan Frazer for interesting discussions and valuable comments on a draft of this paper. TB is funded by an STFC studentship at DAMTP, University of Cambridge. DM is funded by Stephen Hawking Advanced Fellowship from the Centre for Theoretical Cosmology, DAMTP, University of Cambridge.

A Formulae for the covariance matrices

Once all the lower-order Taylor coefficients of the same type have been fixed, the covariance matrix is a diagonal matrix where the entries are given by a simple combinatorial factor. This factor is the product of the factorials of the number of times each number appears in the set of indices. Equivalently, this is just the number of ways one can pair up numbers of the same values from two identical sets of indices.

Every time we fix some Taylor coefficients, we need to shift the expectation values of the higher-order Taylor coefficients, as shown in equation 2.9. Let us for convenience denote the matrix corresponding to $\Sigma_{21}\Sigma_{11}^{-1}$ by $E_{\alpha\beta}$, where β corresponds to some set of indices at the order that was just fixed and α corresponds to some higher-order indices. For $E_{\alpha\beta}$ to be non-zero it must be possible to simultaneously pair up every index in β with an identical index in α . For a given sets of indices α and β , the value of the component $E_{\alpha\beta}$ is determined as follows:

1. Multiply the number of ways the indices in α can be paired with identical indices in β by the number of ways the remaining indices in α can be paired up with each other (again, indices can only be paired up with others of the same value).
2. There is an overall minus sign if the orders differ by an odd multiple of two.
3. Finally divide by the above-mentioned combinatorial factor for β .

These matrices are generally sparse, and remain easy to use and store even as the number of fields becomes large.

B Numerical method

Background evolution

Equation (2.47) comprises a set of N_f coupled, non-linear first-order ordinary differential equations, and its general solution is not known. For large N_f , solving it numerically can also be challenging: the right hand side may involve many of millions of terms encoding the various interactions between the fields. We now discuss our method for evolving the fields.

To solve equation (2.47), we approximate the full potential in very small regions around the trajectory to quadratic order, and solve the evolution of the background in a step-by-step manner with a multiderivative method. More precisely, for some small e-fold step ΔN , we write the solution as,

$$\Delta\phi_a(\Delta N) = \Delta\phi_a^{(1)}\Delta N + \frac{1}{2}\Delta\phi_a^{(2)}\Delta N^2 + \mathcal{O}(\Delta N^3). \quad (\text{B.1})$$

Substituting this Ansatz into the slow-roll equations and matching order-by-order in ΔN , we find,

$$\Delta\phi_a^{(1)} = -\frac{V_a}{V}, \quad (\text{B.2})$$

$$\Delta\phi_a^{(2)} = \frac{V_{ab}V_b}{V^2} - \frac{V_aV_bV_b}{V^3}. \quad (\text{B.3})$$

When implementing this solution, it is of course important to make sure that the second order term in the solution is much smaller than the first-order term; otherwise the series is not a good approximation to the solution. The number of small patches needed depends on the individual realisation, and on hyperparameters such as the initial spectrum, and the number of fields. For 50 fields, we typically find that breaking up the inflationary trajectory to around 2000 small patches suffices to keep the step-size small enough for this method to be numerically accurate.

When working with potentials with many millions of interaction terms, finding the local values of the Taylor coefficients in each patch can be come computationally intensive. To ameliorate this problem, we approximate the fifth order Taylor expanded potential in moderately small regions by lower order Taylor series involving fewer terms. For 50 fields, we may approximate the potential to fourth order in around 60 such moderately small regions for each inflationary realisation. We then use this lower order potential to compute the second order Taylor coefficients in the very small local patches used in the solution of equation (2.47). We note however that the calculations of non-Gaussianity are very sensitive to numerical errors, so care is needed to ensure that the computation is sufficiently accurate.

Perturbations

As first pointed out in [27, 28], the transport method is easily implemented in a patch-by-patch manner. The propagator Γ_{ab} transports the perturbation between spatially flat hypersurfaces and satisfies the chain rule,

$$\Gamma_{ab}(N_3, N_1) = \Gamma_{ac}(N_3, N_2)\Gamma_{cb}(N_2, N_1). \quad (\text{B.4})$$

In a sufficiently small patch, say $N_2 - N_1 = \Delta N \ll 1$ the propagator (2.53) simplifies to,

$$\Gamma_{ab}(N_2, N_1) = \exp(\Delta N u_{ab}), \quad (\text{B.5})$$

where $u_{ab} = u_{ab}(N_1 + \Delta N/2) \approx u_{ab}(N_1) \approx u_{ab}(N_2)$. The full propagator from horizon crossing to the end of inflation is then obtained by left-multiplication of all subsequent propagators [27, 28], i.e.

$$\Gamma_{ab}^{\text{tot}}(N_{\text{end}}, N^*) = \Gamma_{ac_p}(N_{\text{end}}, N_p) \Gamma_{c_p c_{p-1}}(N_p, N_{p-1}) \dots \Gamma_{c_2 c_1}(N_2, N_1) \Gamma_{c_1 b}(N_1, N^*). \quad (\text{B.6})$$

Similarly, Γ_{abc} can be simplified by splitting up the integral (2.54) into many parts,

$$\Gamma_{def}(N_{i+1}, N_i) = \int_{N^i}^{N^{i+1}} dN' \Gamma_{d\mu}(N_{i+1}, N') u_{\mu\nu\rho}(N') \Gamma_{\nu e}(N', N_i) \Gamma_{\rho f}(N', N_i), \quad (\text{B.7})$$

$$\Gamma_{abc}(N, N^*) = \sum_{i=0}^p \Gamma_{ad}(N, N_{i+1}) \Gamma_{def}(N_{i+1}, N_i) \Gamma_{eb}(N_i, N^*) \Gamma_{fc}(N_i, N^*), \quad (\text{B.8})$$

where $N_0 = N^*$ and $N_{p+1} = N$. Assuming the step size is sufficiently small, we can with good accuracy evaluate $\Gamma_{def}(N_{i+1}, N_i)$ as,

$$\Gamma_{def}(N_{i+1}, N_i) \simeq \int_{N^i}^{N^{i+1}} dN' e^{[(N^{i+1}-N')u_{d\mu}]} u_{\mu\nu\rho}(N') e^{[(N'-N^i)u_{\nu e}]} e^{[(N'-N^i)u_{\rho f}]}, \quad (\text{B.9})$$

which is easily evaluated numerically. Once the $\Gamma_{ab}(N_{i+1}, N_i)$ and $\Gamma_{def}(N_{i+1}, N_i)$ have been calculated for all steps, they can be used to calculate power spectrum and f_{NL} modes crossing the horizon at any point during inflation. Moreover, by doing the gauge transformation to a constant energy density surface (cf. equations (2.56), and (2.57)) at any point during inflation, we can follow the evolution of the power spectrum and f_{NL} on superhorizon scales.

C Ensembles of models

For each of the initial conditions below we ran 2,000 simulations, giving us more than 1,000 successful inflation models ($N \geq 60$) for all ICs except near certain fringes of the parameter space (e.g. very small Λ_h or large ϵ_i). The analysis of the perturbations was only done for the models which gave at least 60 e-folds of inflation.

Varying N_f

Λ_h	Mass spectrum	Gradient direction	ϵ_i	η_i	N_f
0.4	Uniform	Random	$2 \cdot 10^{-9}$	-10^{-4}	5, 10, 15, 20, 25, 30, 35, 40, 45, 50
0.4	Compressed	Random	$1 \cdot 10^{-10}$	-10^{-4}	5, 10, 15, 20, 25
0.4	Uniform	Aligned	$5 \cdot 10^{-10}$	-10^{-4}	5, 10, 15, 20, 25, 30
0.4	Uniform, uplifted	Random	$2 \cdot 10^{-9}$	-10^{-4}	5, 10, 15, 20, 25
0.4	Compressed, uplifted	Random	$1 \cdot 10^{-10}$	-10^{-4}	5, 10, 15, 20

Varying Λ_h

N_f	Mass spectrum	Gradient direction	ϵ_i	η_i	Λ_h
10	Uniform	Random	$2 \cdot 10^{-9}$	-10^{-4}	0.1, 0.2, 0.3, 0.4, 0.5, 0.6, 0.7, 0.8, 0.9, 1.0
10	Compressed	Random	$1 \cdot 10^{-10}$	-10^{-4}	0.1, 0.2, 0.3, 0.4, 0.5, 0.6, 0.7, 0.8, 0.9, 1.0
10	Uniform	Aligned	$5 \cdot 10^{-10}$	-10^{-4}	0.1, 0.2, 0.3, 0.4, 0.5, 0.6, 0.7, 0.8, 0.9, 1.0

50-field runs

N_f	Λ_h	Mass spectrum	Gradient direction	ϵ_i	η_i
50	0.4	Uniform	Random	$2 \cdot 10^{-9}$	-10^{-4}
50	0.4	Compressed	Random	$2 \cdot 10^{-11}$	-10^{-4}
50	0.4	Uniform	Aligned	$1 \cdot 10^{-10}$	-10^{-4}

Varying ϵ_i

N_f	Λ_h	Mass spectrum	Gradient direction	η_i	ϵ_i
10	0.4	Uniform	Random	-10^{-4}	$2 \cdot 10^{-10}, 5 \cdot 10^{-10}, 1 \cdot 10^{-9},$ $2 \cdot 10^{-9}, 5 \cdot 10^{-9}, 1 \cdot 10^{-8},$ $2 \cdot 10^{-8}$
10	0.4	Compressed	Random	-10^{-4}	$1 \cdot 10^{-11}, 2 \cdot 10^{-11}, 5 \cdot 10^{-11},$ $1 \cdot 10^{-10}, 2 \cdot 10^{-10}, 5 \cdot 10^{-10},$ $1 \cdot 10^{-9}$

Varying η_i

N_f	Λ_h	Mass spectrum	Gradient direction	ϵ_i	η_i
10	0.4	Uniform	Random	$2 \cdot 10^{-9}$	$-10^{-4}, -10^{-3}, -10^{-2}, -5 \cdot$ $10^{-2}, -10^{-1}$
10	0.4	Compressed	Random	$2 \cdot 10^{-11}$	$-10^{-4}, -10^{-3}, -10^{-2}, -5 \cdot$ $10^{-2}, -10^{-1}$

D A single-field toy model

We have seen in section 3.3 that the observational predictions of manyfield models of inflation coincide with some of the ‘generic predictions’ of single-field slow-roll inflation: an approximately scale-invariant power spectrum over observable scales, with a small running of the spectral index. While we have also seen in section 3.4 that multifield are typically important in the full manyfield models, it is interesting to investigate the extent to which our results can be understood through simpler single-field models. Such models may capture the most important aspects of the more complicated manyfield models, but are simple enough to admit an analytic treatment. In this section, we construct such simple class of single-field models, and discuss how its predictions compare against our numerical simulations of the full manyfield models.

We expand the single-field potential to cubic order around the approximate critical point at $\phi = 0$,

$$V(\phi) = V_0 \left(1 - c_1 \phi - \frac{c_3}{3!} \phi^3 \right). \quad (\text{D.1})$$

where the c_i all are positive. We have here set the second order term at $\phi = 0$ to zero, since, as we will justify below, this term is overwhelmed by the third order term already for small field displacements. We furthermore assume that the potential remain approximately constant during inflation, $V \approx V_0$, which simplifies the analytic expressions for the slow-roll parameters in this model:

$$\epsilon_V \simeq M_{\text{Pl}}^2 \frac{(c_1 + c_3 \phi^2/2)^2}{2}, \quad \eta_V \simeq -M_{\text{Pl}}^2 c_3 \phi. \quad (\text{D.2})$$

We will now use this model to compute the expected total number of e-folds generated during inflation and the predictions for the spectral index and its running. We first note that inflation ends when $\epsilon_V \approx -\dot{H}/H^2 = 1$, which happens when the value of the field is,

$$\phi^{\text{end}} \equiv \frac{2^{3/4}}{\sqrt{(c_3 M_{\text{Pl}})}}. \quad (\text{D.3})$$

The number of e-folds generated as the field travel from $\phi = 0$ to some value ϕ is given by,

$$N(\phi) = \int_0^\phi \frac{d\phi'}{M_{\text{Pl}}\sqrt{2\epsilon_V}} = \frac{\tan^{-1}(\sqrt{c_3/2c_1}\phi)}{M_{\text{Pl}}^2\sqrt{c_1 c_3/2}}. \quad (\text{D.4})$$

Upon evaluating equation (D.4) for $\phi = \phi^{\text{end}}$, we see that the argument of the inverse tangent function becomes very large so that $\tan^{-1}(\sqrt{c_3/2c_1}\phi^{\text{end}}) \approx \pi/2$, and the total number of e-folds is approximately given by,

$$N^{\text{end}} \approx N^{\text{max}} \equiv \frac{\pi}{M_{\text{Pl}}^2\sqrt{2c_1 c_3}}. \quad (\text{D.5})$$

Inflation ends before N becomes exactly N^{max} , but for the initial conditions we are interested in, it is a good approximation.

We can of course also invert equation (D.4) to give ϕ as a function of N :

$$\phi(N) = \sqrt{\frac{2c_1}{c_3}} \tan\left(\frac{\pi N}{2N^{\text{max}}}\right), \quad (\text{D.6})$$

which is valid for $N \leq N^{\text{end}} < N^{\text{max}}$. Using equation (D.6), it is straightforward to compute the spectral index and its running analytically for this toy model. For the models we are interested in, $|\eta_V| \gg \epsilon_V$, and the spectral index is given by,

$$n_s - 1 = 2\eta_V - 6\epsilon_V \simeq -2M_{\text{Pl}}^2 c_3 \phi_\star = -\frac{2\pi}{N^{\text{max}}} \cot\left(\frac{\pi \Delta N}{2N^{\text{max}}}\right), \quad (\text{D.7})$$

where we defined $\Delta N = N^{\text{max}} - N_\star$ (in our multifield simulations, we take $\Delta N = 55$). For $N^{\text{max}} \geq \Delta N$, the spectrum is red and n_s has the limit $1 - 4/\Delta N$ as $N^{\text{max}} \rightarrow \infty$, and it is easy to see that this is a lower bound. Using $d \ln k \simeq dN_\star$, we find that the running is given by,

$$\alpha_s = \frac{dn_s}{dN_\star} = -\left(\frac{\pi}{N^{\text{max}}}\right)^2 \csc^2\left(\frac{\pi \Delta N}{2N^{\text{max}}}\right), \quad (\text{D.8})$$

which is manifestly negative and has the limit $-4/\Delta N^2$ as $N^{\text{max}} \rightarrow \infty$, which is an upper limit.

We are now interested in comparing this class of single-field models to the full multifield models with potential (2.7). To do so, we identify $V_0 = \Lambda_v^4$ and $c_1 = \sqrt{2\epsilon_i} M_{\text{Pl}}^{-1}$. A non-vanishing second-order term could be identified with $c_2 = |\eta_i| M_{\text{Pl}}^{-2}$. The coefficient c_3 then corresponds to a randomly generated third-order derivative, which, as we will detail below, we take to be of $\mathcal{O}(\Lambda_h^{-3})$. Already for small field displacements, $\Delta\phi/\Lambda_h \gtrsim |\eta_i|(\Lambda_h/M_{\text{Pl}})^2$, the third derivative comes to dominate over the second order term. This justifies dropping the second order term from the potential. To see roughly how N^{end} scales with the various parameters, we fix c_3 to,

$$c_3 = \frac{\sqrt{\sum_a \langle V_{a11}^2 \rangle}}{\Lambda_v^4} \approx \sqrt{2N_f} \frac{1}{\Lambda_h^3}, \quad (\text{D.9})$$

where we have denoted the initial gradient direction by ‘1’.²⁷ Since we are using the rms value of the third order coefficients in the multifield model to fix c_3 , we expect that predictions made from the single-field model may capture the mean values of N^{end} (up to some $\mathcal{O}(1)$ coefficient), which in turn tells us how the mean values of n_s and α_s will scale.²⁸

Plugging our expressions for c_1 and c_3 into equation (D.4), we see that the total number of e-folds of the single field model is given by,

$$N^{\text{end}} \approx \frac{\pi}{2} \frac{1}{(N_f \epsilon_i)^{1/4}} \left(\frac{\Lambda_h}{M_{\text{Pl}}} \right)^{3/2}. \quad (\text{D.10})$$

By comparing equation (D.10) to the results of the numerical simulations plotted in Figure 5, we see that the scaling of N^{end} with Λ_h , N_f and ϵ_i are not followed very closely. However, in the more special cases when we start with the gradient aligned with the smallest eigenvalue or when we use the compressed spectrum, these scalings are reasonably accurate (but the $\mathcal{O}(1)$ coefficient is incorrect).

Figure 9 shows the single-field prediction of equation (D.7) together with the numerical simulations from the full GRF models. Qualitatively, the single-field model is in good agreement, and captures both the decrease of n_s for N^{end} not too large, and its asymptotical constancy for $N^{\text{end}} \gg 60$. However, the precise predictions for n_s are inaccurate. The single-field limit for α_s is quite close to value we observe for the multi-field models. For $\Delta N = 55$, the value is $\alpha_s = -0.00132$, which agrees with the baseline model prediction, $\alpha_s = -0.00143 \pm 0.00034$.

Altogether, we see that the single-field toy model captures several of the qualitative features of the multifield models, but does not produce quantitatively accurate predictions. This is not surprising, since the single-field model neither takes into account turns of the trajectory nor the superhorizon evolution of the power spectra. To make accurate predictions, the full multifield treatment is needed.

E The DBM construction of random manyfield potentials

In this subsection, we briefly review the construction of random scalar field potentials using non-equilibrium random matrix theory, and we discuss the most relevant properties and predictions of these models.

A key motivation for the construction of [26] is that inflation is only sensitive to the scalar potential in the vicinity of the field trajectory, while being independent of its properties elsewhere in field space. One may take advantage of this fact by generating the scalar potential only along the dynamically determined field trajectory by gluing together nearby patches in which the potential is locally defined up to some fixed, low order. This method avoids the steep computational cost that limited early studies of multifield inflation in GRF potentials to only involving a few fields, with structure only over super-Planckian field-space distances [34].

²⁷ The approximation comes from taking the contribution from $a = 1$, $\langle (V_{111}^i)^2 \rangle = 6\Lambda_v^8 \Lambda_v^{-6}$, to be the same as for $a \neq 1$, $\langle (V_{a11}^i)^2 \rangle = 2\Lambda_v^8 \Lambda_v^{-6}$. Note that since V_a is already fixed to be very small, the (conditional) mean of V_{abc} is zero to a very good approximation.

²⁸Of course, to find the mean values of all these quantities, one should write them as functions of the V_{a11} and integrate over the PDF. Since our single-field model makes several approximations, however, there is no need to work with such precision (but we did check that for N^{end} the answer is very close).

The starting point of the ‘DBM construction’ is the scalar potential defined up to quadratic order around the point p_0 ,

$$V = (\Lambda_v^{\text{DBM}})^4 \sqrt{N_f} \left(v_0 + v_a \frac{\phi^a}{\Lambda_h^{\text{DBM}}} + \frac{1}{2} v_{ab} \frac{\phi^a}{\Lambda_h^{\text{DBM}}} \frac{\phi^b}{\Lambda_h^{\text{DBM}}} \right). \quad (\text{E.1})$$

Here, Λ_v^{DBM} sets the vertical scale of the potential, the convention for the prefactor $\sqrt{N_f}$ is explained in [26, 28], and Λ_h^{DBM} sets the horizontal scale of the potential (we will shortly return to the interpretation of this parameter). At a nearby point in field space, say p_1 separated from p_0 by $\delta\phi^a$, the potential admits a local Taylor expansion in which the coefficients v_0 , v_a , and v_{ab} only differ from those at p_0 by a small amount:

$$\begin{aligned} v_0|_{p_1} &= v_0|_{p_0} + v_a|_{p_0} \frac{\delta\phi^a}{\Lambda_h^{\text{DBM}}}, & v_a|_{p_1} &= v_a|_{p_0} + v_{ab}|_{p_0} \frac{\delta\phi^b}{\Lambda_h^{\text{DBM}}}, \\ v_{ab}|_{p_1} &= v_{ab}|_{p_0} + \delta v_{ab}|_{p_0 \rightarrow p_1}. \end{aligned} \quad (\text{E.2})$$

Here δv_{ab} captures the effects of cubic (and higher-order) terms on the second derivatives of the potential. Clearly, by stipulating the rules for how δv_{ab} is generated, any potential may be locally generated in this fashion. In a given small patch, the slow-roll equations for the background and the evolution equations for the perturbations are easily solved, making it possible to follow the evolution of the system along a string of points, p_0, p_1, p_2 , etcetera, on the dynamically determined inflationary trajectory. By repeating the procedure of (E.2), the potential is ‘charted’ as the field evolves.

The prescription for constructing δv_{ab} determines the generated potential. To study multifield inflation with randomly interacting fields, reference [26] considered a stochastic evolution law for δv_{ab} , leading to an ensemble of random scalar potentials for each initial choice of parameters. In [26], the law governing the generation of δv_{ab} was then chosen so that, over large distances, v_{ab} samples the Gaussian Orthogonal Ensemble of random symmetric matrices. A simple example of such a law is to take the independent matrix elements of v_{ab} evolve with the Brownian motion of independent harmonic oscillators. More precisely, the independent elements of δv_{ab} are generated as Gaussian random numbers with the first two moments given by,

$$\begin{aligned} \langle \delta v_{ab}|_{p_i \rightarrow p_{i+1}} \rangle &= -v_{ab}|_{p_i} \frac{|\delta\phi^a|}{\Lambda_h^{\text{DBM}}}, \\ \langle \delta v_{ab}^2|_{p_i \rightarrow p_{i+1}} \rangle &= \sigma^2 (1 + \delta_{ab}) \frac{|\delta\phi^a|}{\Lambda_h^{\text{DBM}}}. \end{aligned} \quad (\text{E.3})$$

This is ‘Dyson Brownian motion’ (DBM), originally proposed as an out-of-equilibrium extension of the ‘Coulomb gas’ statistical picture of random matrix theory. Given any initial configuration of $v_{ab}(0)$ at p_0 , the DBM evolution continuously relaxes the Hessian matrix to a random sample of the GOE. The probability distribution of v_{ab} then becomes a function of the path length, s , in units of Λ_h^{DBM} [132, 133],

$$P(v_{ab}(s)) \sim \exp \left[-\frac{\text{tr}((v_{ab}(s) - qv_{ab}(0))^2)}{2\sigma^2(1 - q^2)} \right] \xrightarrow{s \gg 1} \exp \left[-\frac{\text{tr}(v_{ab}(s)^2)}{2\sigma^2} \right], \quad (\text{E.4})$$

where $q = \exp(-s)$. Thus, Λ_h^{DBM} has the interpretation of the coherence length over which the Hessian randomises, the corresponding eigenvectors ‘delocalise’, and the potential exhibit significant random structure.

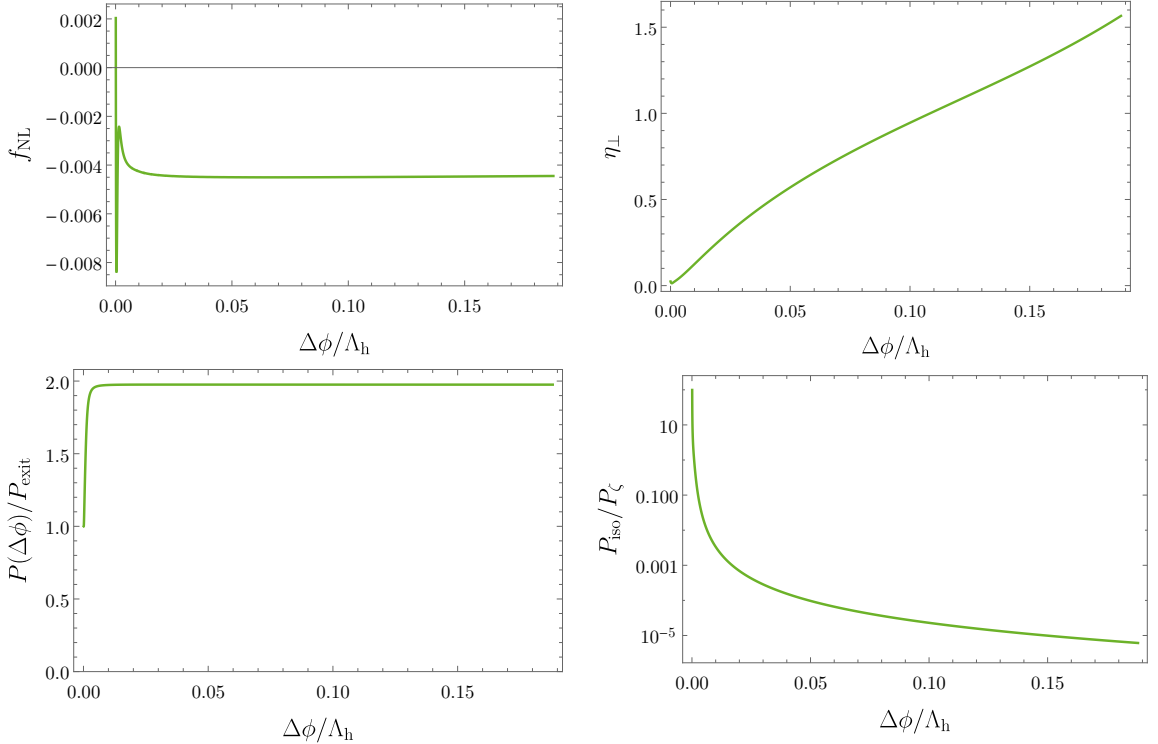


Figure 16: Multifield aspects of the 100-field example.

In [26], the DBM construction was used to gain access to inflation in scalar potentials with multiple interacting fields, and in [27, 28], these were used to, for the first time, study the observational predictions of manyfield models of inflation. Some modifications and extensions of this prescription were discussed in [29, 31, 32], and in [30] the predictions of a single-field approximation to the large- N_f DBM models was elaborated on. (Note however that the observational predictions of this single-field model were already falsified in [27], as subsequently discussed in [28].)

F Case studies and a modified GRF potential

In the main body of this paper, we focussed on the statistical predictions of ensembles of manyfield models. In this appendix, we discuss two particular examples of randomly generated inflation models that highlight the general results discussed in this paper. We furthermore discuss the case of ‘uplifted’ potentials mentioned in section 4.1.

The first inflation model we look at is a 100-field model which, despite significant super-horizon evolution of the power spectrum, gives little non-Gaussianity. The second case is a 25-field model which is one of the rare examples with significant non-Gaussianity at the end of inflation. It is in fact the only model with the uniform mass spectrum that we found to produce large non-Gaussianity, and we will highlight what distinguishes this model from the others.

F.1 A 100-field model

The spectrum of the random 100-field models that we discuss in this section is shown in Figure 4, and its background evolution is further illustrated by Figure 3. Recall that the initial conditions for this model are $\Lambda_h = 0.4$, $\epsilon_i = 5 \times 10^{-10}$, mass-squareds evenly distributed between $\eta_i V_0 M_{\text{Pl}}^{-2}$ and $(3H/2)^2$ with $\eta_i = -10^{-4}$.

The spectral index of this model is $n_s = 0.978$, and its running is given by $\alpha_s = -0.0018$. The amplitude of local non-Gaussianity at the end of inflation is given by $f_{\text{NL}} = -0.004$.

While the observables produced by this model are simple, the superhorizon dynamics of the perturbations is not. Figure 16 shows that the scalar power at the pivot scale doubles after horizon crossing, and that for several e-folds, the isocurvature-to-curvature ratio is greater than one (recall that almost all the field-space movement happens towards the end of inflation). Nevertheless, by the end of inflation the isocurvature becomes heavily suppressed, the power spectrum freezes out, and f_{NL} remains small.

To further understand the multifield aspects of this model, we define the vector,

$$\eta_{\perp i} = \frac{n_a V_{ab} v_b^i}{V}, \quad (\text{F.1})$$

so that, according to equation (2.64), $\zeta' = 2\eta_{\perp i} \mathcal{S}^i$. Thus, the norm $\eta_{\perp} \equiv |\eta_{\perp i}|$ determines the strength of the isocurvature-to-curvature sourcing. Figure 16 shows that η_{\perp} increases during inflation in the 100 field model, and becomes $\mathcal{O}(1)$ towards the end of inflation. However, at this point the isocurvature has decayed exponentially, so that ζ remains essentially constant.

F.2 A 25-field model giving large non-Gaussianity

In rare cases, we found randomly generated manyfield models with substantially non-Gaussian perturbations. A particular example of this is a 25-field model with the uniform initial mass spectrum, $\Lambda_h = 0.4$, $\epsilon_i = 2 \times 10^{-9}$ and $\eta_i = -10^{-4}$. The final spectral index is $n_s = 0.978$ with running $\alpha_s = -0.0014$. The fractional increase of the power spectrum is 2.15, and the final ratio of the isocurvature and curvature power spectra is 0.015. The amplitude of local non-Gaussianities is given by $f_{\text{NL}} = 1.42$, far above the typical values encountered.

What sets this model apart from other models is that the two smallest eigenvalues of the Hessian remain close to each other throughout most of the trajectory, and even ‘bounce off’ each other relatively early on during inflation. The evolution of the spectrum of the Hessian is given by the top panel of Figure 17. When the two eigenvalues are near each other there is significant power in the isocurvature modes and we see a drastic increase in f_{NL} . The generation of f_{NL} in this model is consistent with equation (5.1): as the two eigenvalues of the Hessian come very close to each other, slightly perturbed classical trajectories can become widely separated and experience drastically different levels of superhorizon evolution. We note that η_{\perp} grows during inflation and the isocurvature decays rather slowly. The predictions of this model are likely to be sensitive to the physics of the post-inflationary era.

F.3 Manyfield inflation in uplifted potentials

For Gaussian random fields with zero mean, the minima of the potential typically appear at lower and lower values as the number of fields is increased, and the radius of the Wigner semi-circle grows. As we live in a vacuum with a small, positive cosmological constant, it may therefore be interesting to consider GRF potentials which have been uplifted so that minima typically occur around $V = 0$, cf. our discussion in section 4.1. From equation (2.29), we

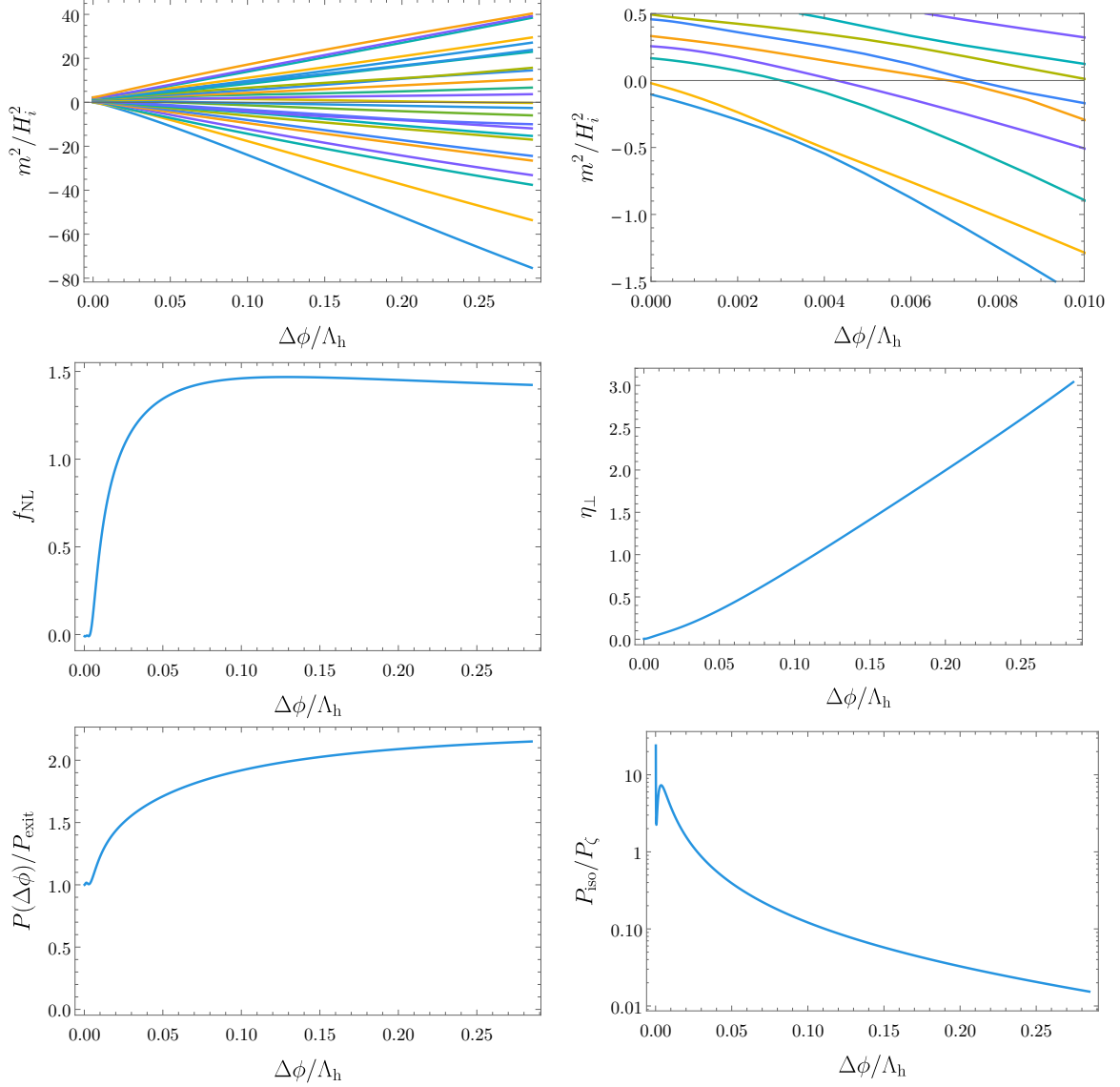


Figure 17: Multifield effects in the 25-field model with large non-Gaussianity.

see that the lower edge of the semi-circle will be at zero at $V = 0$ if we lift the potential by $\sqrt{2}N_f\Lambda_v^4$.

The typical spectrum of these models is still too broad to make them useful tools to study multifield inflation, and we again consider the uniform initial spectrum of equation (2.42). The evolution of the eigenvalues of the Hessian of these models behave somewhat differently from those of the simplest, mean-zero GRFs. An example of this is shown in Figure 18: while the dominant effect for small field values is still the eigenvalue repulsion and roughly conical spread of the eigenvalues, for larger values of the field, the smallest eigenvalue tends upwards, towards the lower edge of the equilibrium spectrum.

The upturning behaviour is most clearly visible for small N_f , which is as expected, as for large N_f , eigenvalue repulsion dominates. The predictions of these models for n_s do not differ appreciably from the mean-zero GRF models with similar initial spectra, as shown in

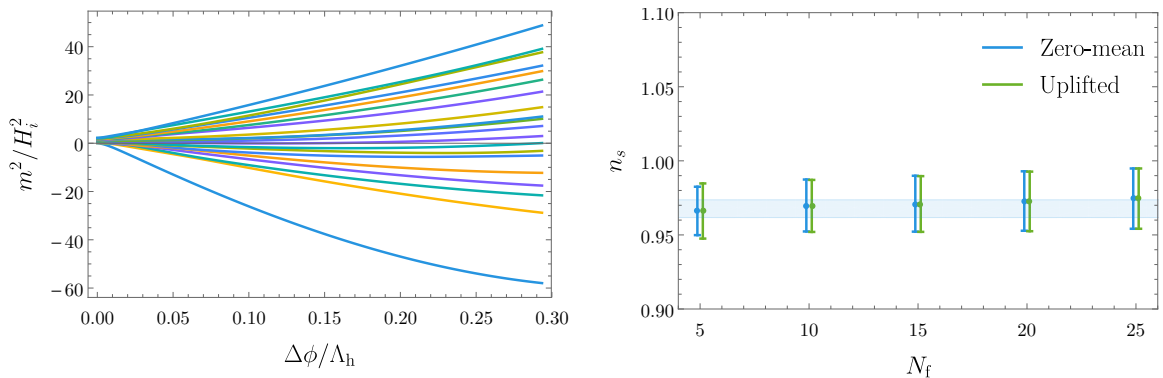


Figure 18: Eigenvalue evolution for a 20-field model with uplifted potential (left) and comparison of predictions for spectral index computed from ensembles of 1000 models (right).

Figure 18. The uplifted models were generated with the same random seeds as the zero-mean ones, and have identical odd-order Taylor coefficients (the even-order Taylor coefficients differ however). The striking similarities in the predictions of these models can be understood as a consequence of the dominance of the cubic terms in the potential during a large fraction of the inflationary evolution.

Clearly, there are many ways to use GRFs to construct inflationary models. We expect that the findings of this paper will extend also to other constructions of small-field, saddle-point inflation in which the spectrum relaxes during inflation (with some eigenvalues taking tachyonic values). However, other, substantially different constructions (e.g. large-field models or other variants of uplifted models) can certainly lead to different predictions.

References

- [1] J. M. Maldacena, *Non-Gaussian features of primordial fluctuations in single field inflationary models*, *JHEP* **05** (2003) 013, [[astro-ph/0210603](#)].
- [2] P. Creminelli and M. Zaldarriaga, *Single field consistency relation for the 3-point function*, *JCAP* **0410** (2004) 006, [[astro-ph/0407059](#)].
- [3] X. Chen, H. Firouzjahi, M. H. Namjoo and M. Sasaki, *A Single Field Inflation Model with Large Local Non-Gaussianity*, *EPL* **102** (2013) 59001, [[1301.5699](#)].
- [4] S. Mooij and G. A. Palma, *Consistently violating the non-Gaussian consistency relation*, *JCAP* **1511** (2015) 025, [[1502.03458](#)].
- [5] PLANCK collaboration, P. A. R. Ade et al., *Planck 2015 results. XX. Constraints on inflation*, *Astron. Astrophys.* **594** (2016) A20, [[1502.02114](#)].
- [6] PLANCK collaboration, P. A. R. Ade et al., *Planck 2015 results. XVII. Constraints on primordial non-Gaussianity*, *Astron. Astrophys.* **594** (2016) A17, [[1502.01592](#)].
- [7] N. Dalal, O. Dore, D. Huterer and A. Shirokov, *The imprints of primordial non-gaussianities on large-scale structure: scale dependent bias and abundance of virialized objects*, *Phys. Rev. D* **77** (2008) 123514, [[0710.4560](#)].
- [8] S. Matarrese and L. Verde, *The effect of primordial non-Gaussianity on halo bias*, *Astrophys. J.* **677** (2008) L77–L80, [[0801.4826](#)].
- [9] A. Slosar, C. Hirata, U. Seljak, S. Ho and N. Padmanabhan, *Constraints on local primordial non-Gaussianity from large scale structure*, *JCAP* **0808** (2008) 031, [[0805.3580](#)].

- [10] V. Desjacques and U. Seljak, *Primordial non-Gaussianity from the large scale structure*, *Class. Quant. Grav.* **27** (2010) 124011, [[1003.5020](#)].
- [11] M. Alvarez et al., *Testing Inflation with Large Scale Structure: Connecting Hopes with Reality*, [1412.4671](#).
- [12] S. Ferraro and K. M. Smith, *Using large scale structure to measure f_{NL} , g_{NL} and τ_{NL}* , *Phys. Rev.* **D91** (2015) 043506, [[1408.3126](#)].
- [13] T. Baldauf, M. Mirbabayi, M. Simonovic and M. Zaldarriaga, *LSS constraints with controlled theoretical uncertainties*, [1602.00674](#).
- [14] C. T. Byrnes and K.-Y. Choi, *Review of local non-Gaussianity from multi-field inflation*, *Adv. Astron.* **2010** (2010) 724525, [[1002.3110](#)].
- [15] F. Vernizzi and D. Wands, *Non-gaussianities in two-field inflation*, *JCAP* **0605** (2006) 019, [[astro-ph/0603799](#)].
- [16] T. Battefeld and R. Easther, *Non-Gaussianities in Multi-field Inflation*, *JCAP* **0703** (2007) 020, [[astro-ph/0610296](#)].
- [17] L. Senatore and M. Zaldarriaga, *The Effective Field Theory of Multifield Inflation*, *JHEP* **04** (2012) 024, [[1009.2093](#)].
- [18] C. M. Peterson and M. Tegmark, *Non-Gaussianity in Two-Field Inflation*, *Phys. Rev.* **D84** (2011) 023520, [[1011.6675](#)].
- [19] C. M. Peterson and M. Tegmark, *Testing multifield inflation: A geometric approach*, *Phys. Rev.* **D87** (2013) 103507, [[1111.0927](#)].
- [20] R. Easther, J. Frazer, H. V. Peiris and L. C. Price, *Simple predictions from multifield inflationary models*, *Phys. Rev. Lett.* **112** (2014) 161302, [[1312.4035](#)].
- [21] L. C. Price, H. V. Peiris, J. Frazer and R. Easther, *Designing and testing inflationary models with Bayesian networks*, *JCAP* **1602** (2016) 049, [[1511.00029](#)].
- [22] E. P. Wigner, *On the statistical distribution of the widths and spacings of nuclear resonance levels*, *Mathematical Proceedings of the Cambridge Philosophical Society* **47** (1951) 790 – 798.
- [23] A. B. J. Kuijlaars, *Universality*, *The Oxford Handbook on Random Matrix Theory*, (G. Akemann, J. Baik, and P. Di Francesco, eds.), Oxford University Press (2011) 103–134, [[1103.5922](#)].
- [24] P. Deift, *Universality for mathematical and physical systems*, *ArXiv Mathematical Physics e-prints* (Mar., 2006) , [[math-ph/0603038](#)].
- [25] L. Erdos, *Universality for random matrices and log-gases*, *ArXiv e-prints* (Dec., 2012) , [[1212.0839](#)].
- [26] M. C. D. Marsh, L. McAllister, E. Pajer and T. Wrase, *Charting an Inflationary Landscape with Random Matrix Theory*, *JCAP* **1311** (2013) 040, [[1307.3559](#)].
- [27] M. Dias, J. Frazer and M. C. D. Marsh, *Simple emergent power spectra from complex inflationary physics*, *Phys. Rev. Lett.* **117** (2016) 141303, [[1604.05970](#)].
- [28] M. Dias, J. Frazer and M. D. Marsh, *Seven Lessons from Manyfield Inflation in Random Potentials*, [1706.03774](#).
- [29] T. Battefeld and C. Modi, *Local random potentials of high differentiability to model the Landscape*, *JCAP* **1503** (2015) 010, [[1409.5135](#)].
- [30] B. Freivogel, R. Gobbetti, E. Pajer and I.-S. Yang, *Inflation on a Slippery Slope*, [1608.00041](#).
- [31] F. G. Pedro and A. Westphal, *Inflation with a graceful exit in a random landscape*, *JHEP* **03** (2017) 163, [[1611.07059](#)].

- [32] G. Wang and T. Battefeld, *Random Functions via Dyson Brownian Motion: Progress and Problems*, *JCAP* **1609** (2016) 008, [[1607.02514](#)].
- [33] J. Frazer and A. R. Liddle, *Exploring a string-like landscape*, *JCAP* **1102** (2011) 026, [[1101.1619](#)].
- [34] J. Frazer and A. R. Liddle, *Multi-field inflation with random potentials: field dimension, feature scale and non-Gaussianity*, *JCAP* **1202** (2012) 039, [[1111.6646](#)].
- [35] M. Tegmark, *What does inflation really predict?*, *JCAP* **0504** (2005) 001, [[astro-ph/0410281](#)].
- [36] T. C. Bachlechner, *On Gaussian Random Supergravity*, *JHEP* **04** (2014) 054, [[1401.6187](#)].
- [37] D. J. Mulryne, *Transporting non-Gaussianity from sub to super-horizon scales*, *JCAP* **1309** (2013) 010, [[1302.3842](#)].
- [38] D. Seery, D. J. Mulryne, J. Frazer and R. H. Ribeiro, *Inflationary perturbation theory is geometrical optics in phase space*, *JCAP* **1209** (2012) 010, [[1203.2635](#)].
- [39] M. Dias, J. Frazer and D. Seery, *Computing observables in curved multifield models of inflation — A guide (with code) to the transport method*, *JCAP* **1512** (2015) 030, [[1502.03125](#)].
- [40] M. Dias, J. Frazer, D. J. Mulryne and D. Seery, *Numerical evaluation of the bispectrum in multiple field inflation – the transport approach with code*, *JCAP* **1612** (2016) 033, [[1609.00379](#)].
- [41] A. Berera, *Thermal properties of an inflationary universe*, *Phys. Rev.* **D54** (1996) 2519–2534, [[hep-th/9601134](#)].
- [42] A. Aazami and R. Easther, *Cosmology from random multifield potentials*, *JCAP* **0603** (2006) 013, [[hep-th/0512050](#)].
- [43] R. Easther and L. McAllister, *Random matrices and the spectrum of N -flation*, *JCAP* **0605** (2006) 018, [[hep-th/0512102](#)].
- [44] J. March-Russell and F. Riva, *Signals of Inflation in a Friendly String Landscape*, *JHEP* **07** (2006) 033, [[astro-ph/0604254](#)].
- [45] S. H. H. Tye, J. Xu and Y. Zhang, *Multi-field Inflation with a Random Potential*, *JCAP* **0904** (2009) 018, [[0812.1944](#)].
- [46] S. H. H. Tye and J. Xu, *A Meandering Inflaton*, *Phys. Lett.* **B683** (2010) 326–330, [[0910.0849](#)].
- [47] D. Battefeld, T. Battefeld and S. Schulz, *On the Unlikelihood of Multi-Field Inflation: Bounded Random Potentials and our Vacuum*, *JCAP* **1206** (2012) 034, [[1203.3941](#)].
- [48] D. Battefeld and T. Battefeld, *A Smooth Landscape: Ending Saddle Point Inflation Requires Features to be Shallow*, *JCAP* **1307** (2013) 038, [[1304.0461](#)].
- [49] F. G. Pedro and A. Westphal, *The Scale of Inflation in the Landscape*, *Phys. Lett.* **B739** (2014) 439–444, [[1303.3224](#)].
- [50] J. Liu, Y. Wang and S. Zhou, *Nonuniqueness of classical inflationary trajectories on a high-dimensional landscape*, *Phys. Rev.* **D91** (2015) 103525, [[1501.06785](#)].
- [51] A. Linde, *Random Potentials and Cosmological Attractors*, *JCAP* **1702** (2017) 028, [[1612.04505](#)].
- [52] A. Masoumi, A. Vilenkin and M. Yamada, *Inflation in random Gaussian landscapes*, *JCAP* **1705** (2017) 053, [[1612.03960](#)].
- [53] Y.-H. He, V. Jejjala, L. Pontiggia, Y. Xiao and D. Zhou, *Flatness of Minima in Random Inflationary Landscapes*, [1704.08351](#).

- [54] J. Liu, *Artificial Neural Network in Cosmic Landscape*, [1707.02800](#).
- [55] A. Masoumi, A. Vilenkin and M. Yamada, *Inflation in multi-field random Gaussian landscapes*, [1707.03520](#).
- [56] D. Green, *Disorder in the Early Universe*, *JCAP* **1503** (2015) 020, [[1409.6698](#)].
- [57] M. A. Amin and D. Baumann, *From Wires to Cosmology*, *JCAP* **1602** (2016) 045, [[1512.02637](#)].
- [58] M. A. Amin, M. A. G. Garcia, H.-Y. Xie and O. Wen, *Multifield Stochastic Particle Production: Beyond a Maximum Entropy Ansatz*, [1706.02319](#).
- [59] N. Agarwal, R. Bean, L. McAllister and G. Xu, *Universality in D-brane Inflation*, *JCAP* **1109** (2011) 002, [[1103.2775](#)].
- [60] L. McAllister, S. Renaux-Petel and G. Xu, *A Statistical Approach to Multifield Inflation: Many-field Perturbations Beyond Slow Roll*, *JCAP* **1210** (2012) 046, [[1207.0317](#)].
- [61] M. Dias, J. Frazer and A. R. Liddle, *Multifield consequences for D-brane inflation*, *JCAP* **1206** (2012) 020, [[1203.3792](#)].
- [62] A. A. Starobinsky, *Multicomponent de Sitter (Inflationary) Stages and the Generation of Perturbations*, *JETP Lett.* **42** (1985) 152–155.
- [63] M. Sasaki and E. D. Stewart, *A General analytic formula for the spectral index of the density perturbations produced during inflation*, *Prog. Theor. Phys.* **95** (1996) 71–78, [[astro-ph/9507001](#)].
- [64] D. H. Lyth and Y. Rodriguez, *The Inflationary prediction for primordial non-Gaussianity*, *Phys. Rev. Lett.* **95** (2005) 121302, [[astro-ph/0504045](#)].
- [65] T. Bjorkmo and M. D. Marsh, “To appear.”
- [66] A. J. Bray and D. S. Dean, *Statistics of critical points of Gaussian fields on large-dimensional spaces*, *Phys. Rev. Lett.* **98** (2007) 150201.
- [67] D. S. Dean and S. N. Majumdar, *Large deviations of extreme eigenvalues of random matrices*, *Phys. Rev. Lett.* **97** (2006) 160201, [[cond-mat/0609651](#)].
- [68] D. Marsh, L. McAllister and T. Wrase, *The Wasteland of Random Supergravities*, *JHEP* **03** (2012) 102, [[1112.3034](#)].
- [69] T. C. Bachlechner, D. Marsh, L. McAllister and T. Wrase, *Supersymmetric Vacua in Random Supergravity*, *JHEP* **01** (2013) 136, [[1207.2763](#)].
- [70] R. Easther, A. H. Guth and A. Masoumi, *Counting Vacua in Random Landscapes*, [1612.05224](#).
- [71] S. Kachru, R. Kallosh, A. D. Linde and S. P. Trivedi, *De Sitter vacua in string theory*, *Phys. Rev.* **D68** (2003) 046005, [[hep-th/0301240](#)].
- [72] S. Ferrara, R. Kallosh and A. Linde, *Cosmology with Nilpotent Superfields*, *JHEP* **10** (2014) 143, [[1408.4096](#)].
- [73] A. Westphal, *de Sitter string vacua from Kahler uplifting*, *JHEP* **03** (2007) 102, [[hep-th/0611332](#)].
- [74] A. Achucarro, B. de Carlos, J. A. Casas and L. Doplicher, *De Sitter vacua from uplifting D-terms in effective supergravities from realistic strings*, *JHEP* **06** (2006) 014, [[hep-th/0601190](#)].
- [75] E. Dudas and Y. Mambrini, *Moduli stabilization with positive vacuum energy*, *JHEP* **10** (2006) 044, [[hep-th/0607077](#)].

- [76] M. Rummel and Y. Sumitomo, *De Sitter Vacua from a D-term Generated Racetrack Uplift*, *JHEP* **01** (2015) 015, [[1407.7580](#)].
- [77] J. Blaback, U. H. Danielsson, G. Dibitetto and S. C. Vargas, *Universal dS vacua in STU-models*, *JHEP* **10** (2015) 069, [[1505.04283](#)].
- [78] M. Cicoli, F. Quevedo and R. Valandro, *De Sitter from T-branes*, *JHEP* **03** (2016) 141, [[1512.04558](#)].
- [79] M. C. D. Marsh, B. Vercnocke and T. Wrase, *Decoupling and de Sitter Vacua in Approximate No-Scale Supergravities*, *JHEP* **05** (2015) 081, [[1411.6625](#)].
- [80] D. Gallego, M. C. D. Marsh, B. Vercnocke and T. Wrase, *A New Class of de Sitter Vacua in Type IIB Large Volume Compactifications*, [1707.01095](#).
- [81] T. C. Bachlechner, K. Eckerle, O. Janssen and M. Kleban, *Systematics of Aligned Axions*, [1709.01080](#).
- [82] D. H. Lyth and A. Riotto, *Particle physics models of inflation and the cosmological density perturbation*, *Phys. Rept.* **314** (1999) 1–146, [[hep-ph/9807278](#)].
- [83] D. Mulryne, D. Seery and D. Wesley, *Non-Gaussianity constrains hybrid inflation*, [0911.3550](#).
- [84] X. Chen and Y. Wang, *Quasi-Single Field Inflation and Non-Gaussianities*, *JCAP* **1004** (2010) 027, [[0911.3380](#)].
- [85] M. Dias and D. Seery, *Transport equations for the inflationary spectral index*, *Phys. Rev.* **D85** (2012) 043519, [[1111.6544](#)].
- [86] G. J. Anderson, D. J. Mulryne and D. Seery, *Transport equations for the inflationary trispectrum*, *JCAP* **1210** (2012) 019, [[1205.0024](#)].
- [87] D. Seery, *CppTransport: a platform to automate calculation of inflationary correlation functions*, [1609.00380](#).
- [88] D. J. Mulryne and J. W. Ronayne, *PyTransport: A Python package for the calculation of inflationary correlation functions*, [1609.00381](#).
- [89] J. W. Ronayne and D. J. Mulryne, *Numerically evaluating the bispectrum in curved field-space - with PyTransport 2.0*, [1708.07130](#).
- [90] D. H. Lyth, *Large Scale Energy Density Perturbations and Inflation*, *Phys. Rev.* **D31** (1985) 1792–1798.
- [91] D. Wands, K. A. Malik, D. H. Lyth and A. R. Liddle, *A New approach to the evolution of cosmological perturbations on large scales*, *Phys. Rev.* **D62** (2000) 043527, [[astro-ph/0003278](#)].
- [92] S. Groot Nibbelink and B. J. W. van Tent, *Scalar perturbations during multiple field slow-roll inflation*, *Class. Quant. Grav.* **19** (2002) 613–640, [[hep-ph/0107272](#)].
- [93] J. Garcia-Bellido and D. Wands, *Metric perturbations in two field inflation*, *Phys. Rev.* **D53** (1996) 5437–5445, [[astro-ph/9511029](#)].
- [94] C. Gordon, D. Wands, B. A. Bassett and R. Maartens, *Adiabatic and entropy perturbations from inflation*, *Phys. Rev.* **D63** (2001) 023506, [[astro-ph/0009131](#)].
- [95] D. H. Lyth, *What would we learn by detecting a gravitational wave signal in the cosmic microwave background anisotropy?*, *Phys. Rev. Lett.* **78** (1997) 1861–1863, [[hep-ph/9606387](#)].
- [96] A. Pourtsidou, *Synergistic tests of inflation*, [1612.05138](#).
- [97] L. Amendola, C. Gordon, D. Wands and M. Sasaki, *Correlated perturbations from inflation and the cosmic microwave background*, *Phys. Rev. Lett.* **88** (2002) 211302, [[astro-ph/0107089](#)].

- [98] D. Wands, N. Bartolo, S. Matarrese and A. Riotto, *An Observational test of two-field inflation*, *Phys. Rev.* **D66** (2002) 043520, [[astro-ph/0205253](#)].
- [99] C. T. Byrnes and D. Wands, *Curvature and isocurvature perturbations from two-field inflation in a slow-roll expansion*, *Phys. Rev.* **D74** (2006) 043529, [[astro-ph/0605679](#)].
- [100] F. Bernardeau and J.-P. Uzan, *NonGaussianity in multifield inflation*, *Phys. Rev.* **D66** (2002) 103506, [[hep-ph/0207295](#)].
- [101] F. Bernardeau and J.-P. Uzan, *Inflationary models inducing non-Gaussian metric fluctuations*, *Phys. Rev.* **D67** (2003) 121301, [[astro-ph/0209330](#)].
- [102] G. I. Rigopoulos, E. P. S. Shellard and B. J. W. van Tent, *Quantitative bispectra from multifield inflation*, *Phys. Rev.* **D76** (2007) 083512, [[astro-ph/0511041](#)].
- [103] G. I. Rigopoulos, E. P. S. Shellard and B. J. W. van Tent, *Large non-Gaussianity in multiple-field inflation*, *Phys. Rev.* **D73** (2006) 083522, [[astro-ph/0506704](#)].
- [104] N. Bartolo, S. Matarrese and A. Riotto, *Nongaussianity from inflation*, *Phys. Rev.* **D65** (2002) 103505, [[hep-ph/0112261](#)].
- [105] T. Wang, *Note on Non-Gaussianities in Two-field Inflation*, *Phys. Rev.* **D82** (2010) 123515, [[1008.3198](#)].
- [106] C. T. Byrnes, K.-Y. Choi and L. M. H. Hall, *Conditions for large non-Gaussianity in two-field slow-roll inflation*, *JCAP* **0810** (2008) 008, [[0807.1101](#)].
- [107] C. T. Byrnes, K.-Y. Choi and L. M. H. Hall, *Large non-Gaussianity from two-component hybrid inflation*, *JCAP* **0902** (2009) 017, [[0812.0807](#)].
- [108] T. Tanaka, T. Suyama and S. Yokoyama, *Use of delta N formalism - Difficulties in generating large local-type non-Gaussianity during inflation -*, *Class. Quant. Grav.* **27** (2010) 124003, [[1003.5057](#)].
- [109] X. Chen, *Primordial Features as Evidence for Inflation*, *JCAP* **1201** (2012) 038, [[1104.1323](#)].
- [110] A. Achúcarro, J.-O. Gong, S. Hardeman, G. A. Palma and S. P. Patil, *Mass hierarchies and non-decoupling in multi-scalar field dynamics*, *Phys. Rev.* **D84** (2011) 043502, [[1005.3848](#)].
- [111] A. D. Linde and V. F. Mukhanov, *Nongaussian isocurvature perturbations from inflation*, *Phys. Rev.* **D56** (1997) R535–R539, [[astro-ph/9610219](#)].
- [112] D. H. Lyth and D. Wands, *Generating the curvature perturbation without an inflaton*, *Phys. Lett.* **B524** (2002) 5–14, [[hep-ph/0110002](#)].
- [113] T. Moroi and T. Takahashi, *Cosmic density perturbations from late decaying scalar condensations*, *Phys. Rev.* **D66** (2002) 063501, [[hep-ph/0206026](#)].
- [114] D. H. Lyth, C. Ungarelli and D. Wands, *Primordial density perturbation in the curvaton scenario*, *Phys. Rev. D* **67** (Jan, 2003) 023503.
- [115] R. de Putter, J. Gleyzes and O. Doré, *The next non-Gaussianity frontier: what can a measurement with $\sigma(f_{\text{NL}}) \lesssim 1$ tell us about multifield inflation?*, [1612.05248](#).
- [116] G. Leung, E. R. M. Tarrant, C. T. Byrnes and E. J. Copeland, *Reheating, Multifield Inflation and the Fate of the Primordial Observables*, *JCAP* **1209** (2012) 008, [[1206.5196](#)].
- [117] J. Meyers and E. R. M. Tarrant, *Perturbative Reheating After Multiple-Field Inflation: The Impact on Primordial Observables*, *Phys. Rev.* **D89** (2014) 063535, [[1311.3972](#)].
- [118] R. J. Hardwick, V. Vennin, K. Koyama and D. Wands, *Constraining Curvaton Reheating*, *JCAP* **1608** (2016) 042, [[1606.01223](#)].
- [119] S. C. Hotinli, J. Frazer, A. H. Jaffe, J. Meyers, L. C. Price and E. R. M. Tarrant, *Effect of reheating on predictions following multiple-field inflation*, *Phys. Rev.* **D97** (2018) 023511, [[1710.08913](#)].

- [120] E. Silverstein and D. Tong, *Scalar speed limits and cosmology: Acceleration from D-cceleration*, *Phys. Rev.* **D70** (2004) 103505, [[hep-th/0310221](#)].
- [121] S. Renaux-Petel and K. Turzynski, *Geometrical Destabilization of Inflation*, *Phys. Rev. Lett.* **117** (2016) 141301, [[1510.01281](#)].
- [122] S. Renaux-Petel, K. Turzynski and V. Vennin, *Geometrical destabilization, premature end of inflation and Bayesian model selection*, [1706.01835](#).
- [123] A. Linde, *Random Potentials and Cosmological Attractors*, *JCAP* **1702** (2017) 028, [[1612.04505](#)].
- [124] A. R. Brown, *Hyperinflation*, [1705.03023](#).
- [125] D. Green, M. Lewandowski, L. Senatore, E. Silverstein and M. Zaldarriaga, *Anomalous Dimensions and Non-Gaussianity*, *JHEP* **10** (2013) 171, [[1301.2630](#)].
- [126] V. Assassi, D. Baumann, D. Green and L. McAllister, *Planck-Suppressed Operators*, *JCAP* **1401** (2014) 033, [[1304.5226](#)].
- [127] D. I. Kaiser and E. I. Sfakianakis, *Multifield Inflation after Planck: The Case for Nonminimal Couplings*, *Phys. Rev. Lett.* **112** (2014) 011302, [[1304.0363](#)].
- [128] K. Schutz, E. I. Sfakianakis and D. I. Kaiser, *Multifield Inflation after Planck: Isocurvature Modes from Nonminimal Couplings*, *Phys. Rev.* **D89** (2014) 064044, [[1310.8285](#)].
- [129] M. P. DeCross, D. I. Kaiser, A. Prabhu, C. Prescod-Weinstein and E. I. Sfakianakis, *Preheating after Multifield Inflation with Nonminimal Couplings, I: Covariant Formalism and Attractor Behavior*, [1510.08553](#).
- [130] M. P. DeCross, D. I. Kaiser, A. Prabhu, C. Prescod-Weinstein and E. I. Sfakianakis, *Preheating after multifield inflation with nonminimal couplings, II: Resonance Structure*, [1610.08868](#).
- [131] M. P. DeCross, D. I. Kaiser, A. Prabhu, C. Prescod-Weinstein and E. I. Sfakianakis, *Preheating after multifield inflation with nonminimal couplings, III: Dynamical spacetime results*, [1610.08916](#).
- [132] F. J. Dyson, *A Brownian-Motion Model for the Eigenvalues of a Random Matrix*, *Journal of Mathematical Physics* **3** (1962) 1191 – 1198.
- [133] G. Uhlenbeck and L. Ornstein, *On the Theory of the Brownian Motion*, *Phys.Rev.* **36** (1930) 823 – 841.